MAY. 2020- AUG. 2020 • Volume XXI Number II

THE ASEAN JOURNAL OF RADIOLOGY

Highlight

- Original Article
- Case Report
- Pictorial Essay
- ASEAN Movement in Radiology

Official Journal of
The Royal College of Radiologists of Thailand,
ASEAN Association of Radiology, and
Foundation for Orphan and Rare Lung Disease

ISSN 2672-9393

The ASEAN
Journal of Radiology

CONTENTS

03 **From The Editor**

05 **Original Article**

Shielding assessment in two computed tomography facilities in South-South Nigeria: How safe are the personnel and general public from ionizing radiation?
Akintayo Daniel Omojola, M.D.
Funmilayo Ruth Omojola, M.D.
Michael Onoriode Akpochafor, M.D.
Samuel Olaolu Adeneye, M.D.

28 **Abdominal CT radiation dose optimization at Siriraj Hospital**
Piyaporn Apisarnthanarak, M.D.
Chosita Buranont, M.D.
Chulaluck Boonma, B.Sc.
Sureerat Janpanich, RN.
Tarntip Suwatananonthakij, RN.
Atchariya Klinhom, RN.
Kobkun Muangsomboon, M.D.
Wanwarang Teerasamit, M.D.
Voraparee Suvannnarerg, M.D.
Pairash Saiviroonporn, Ph.D.

44 **Case Report**

Imaging findings of spontaneous thymic hemorrhage in infancy: Case report and literature review
Chanunporn Leekumnerdthai, M.D.
Panruethai Trinavarat, M.D.
Darintr Sosothikul, M.D.
Nattinee Leelakanok, M.D.

58 **Atraumatic splenic rupture in chronic pancreatitis with successful embolization**
Anooja Abdul Salam, M.D.
Ben Pearch, M.D.
Lisa Sorger, M.D.

69 **COVID-19 pneumonia: The first two chest CTs in the Bamrasnaradura Infectious Disease Institute**
Panyaros Kongpanya, M.D.
Parichut Vongthawatchai, M.D.
Priyanut Atiburanakul, M.D.
Nayot Panitanum, M.D.
Patama Suttha, M.D.

82 **Clinico-Radiologic-Pathologic Correlation**

Distal common bile duct adenoma
Khanin Khanungwanitkul, M.D.
Tanawat Pattarapuntakul, M.D.
Naruemon Wisedopas, M.D.

90 **Pictorial Essay**

Ultrasound imaging of acute scrotum: Pictorial review with etiological correlation
Anitha Mandava, M.B.B.S., D.M.R.D., D.N.B.
Veeraiah Koppula, M.B.B.S., D.N.B.
Rohit Yalamanchili, M.B.B.S, M.D.
Dilip Yadav, MBBS, D.N.B.
Juluri Rakesh, M.B.B.S, M.D.

110 **ASEAN Movement in Radiology**

Summary of discussions and brainstorming session on imaging guidelines and recommendations on Thailand's COVID-19 situation
By experts in chest medicine and chest imaging
Chayanin Nitiwarangkul, M.D.
Nitra Piyavisetpat, M.D.

From The Editor

The first case infected with COVID-19 outside China was reported in Thailand just a few weeks after an outbreak in Hubei, China. This deadly pathogen spread fast and widely during the Lunar New Year vacation in January 2020, when millions traveled across not only China but the entire Asia. This reflects how close to China ASEAN countries are, not only in the geographical but also cultural senses.

From then to the time of writing this article (August 2020), not a single country all over the world has been safe from this virus. The control of the spreading in Asian countries is more satisfactory than that in Europe and America. Keys to success seem to be government's immediate actions and aggressive responses to the situation, including limited social contact, universal precaution, disease surveillance and contact tracing. It is likely that the governments of these countries learned from the legacy of the Severe Acute Respiratory Syndrome (SARS) in 2003.

Because pneumonia is the main manifestation of Covid-19 infected patients, chest imaging plays an important role in diagnosis and treatment. Radiologists and, especially radiographers are those among the health care workers in the front line who risk their lives while helping patients. Guidelines and recommendations for appropriate usage of chest imaging in surveillance, diagnosis and management of Covid-19 pneumonia have been developed by various organizations. Most of them recommended that radiologic images not be used in detection or confirmation of the Covid-19 pneumonia.

During the past several months of this pandemic, we experienced what we needed to know or change to live and work in this situation.

The editor gave an opening speech in front of cameras in an audiovision studio in Bangkok to almost 1,000 on-line participants of the annual congress of the Royal College of Radiologists of Thailand and the Radiological Society of Thailand.

Thanks to digital networks, enormous new knowledge, findings and even innovations have been reported and shared widely and quickly. We share cases happening in Thailand in the current issue. We are looking forward to hearing about situations or observations in Radiology from other ASEAN countries in the upcoming issue.

Wiwatana Tanomkiat, M.D.
Editor,
The ASEAN Journal of Radiology
Email: aseanjournalradiology@gmail.com

Original Article

Shielding assessment in two computed tomography facilities in South-South Nigeria: How safe are the personnel and general public from ionizing radiation?

Akintayo Daniel Omojola, M.Sc.[(1)]
Funmilayo Ruth Omojola, B.Sc.[(2)]
Michael Onoriode Akpochafor, Ph.D.[(3)]
Samuel Olaolu Adeneye, Ph.D.[(3)]
From [(1)]Department of Radiology, Medical Physics Unit, Federal Medical Centre Asaba, Delta, Nigeria.
[(2)]Department of Applied Zoology, Olabisi Onabanjo University, Ago-Iwoye, Ogun, Nigeria.
[(3)]Department of Radiation Biology, Radiotherapy and Radiodiagnosis, College of Medicine, University of Lagos, Lagos, Nigeria.
Address correspondence to A.D.O. (e-mail: akintayoomojola@gmail.com)

Abstract

Objective: The aims of this study were to estimate the instantaneous dose rate (IDR) and annual dose rate (ADR) to radiation staff and the general public within the controlled and supervised areas, respectively, to determine the shielding design goals (P) of the 2 CT facilities and to determine the average annual dose (AD) to radiographer/operator in the control console during CT scans.

Materials and Methods: The equipment used in this study consisted of two newly installed General Electric (GE) Revolution ACTs CT machines. Technical parameters used were a thoracic/dorsal spine scan, which was rarely done in both facilities. A calibrated Inspector USB (S.E. International, Inc.) survey meter was positioned < 50 cm from each barrier at various points to determine the average shielded air kerma.

Results: The average background radiation in the 2 facilities was 0.11 μSv/hr. The average ADR to the controlled and supervised areas in CT_1 was 0.563±0.25 and 0.369±0.11 mSv/yr, respectively. Also, the average ADR to the controlled and supervised areas in CT_2 were 0.410±0.28 and 0.354±0.04 mSv/yr, respectively. The average shielding design goal to the controlled and supervised areas for CT_1 was 0.00898±0.0041 and 0.0059±0.0028 mSv/Week, respectively. Similarly, the average shielding design goal for the controlled and supervised areas for CT_2 was 0.0066±0.0044 and 0.0057±0.0019 mSv/Week respectively. The estimated average AD to the operator in CT_1 and CT_2 was 2.5 and 1.3 μSv, respectively.

Conclusion: The average ADR and shielding design goals in the controlled and supervised areas from both CTs were within acceptable limits for radiation staff and the public.

Keywords: Controlled areas, Supervised area, Shielding design goal, Radiation staff, Shielding.

Introduction

The use of X-ray as a tool in diagnostic radiology have generally improved patient care and management but the harmful effects of ionizing radiation to patients and exposed staffs have raised much concern over the years[1-3]. Radiation shielding is an important aspect of radiation protection. Several recommendations have been put in place to address patient dose through the principle of "As low as reasonably achievable" (ALARA) and protocol optimization. The use of appropriate protective screens/shielding device and the principle of keeping a distance from the source have been used to address staff dose in diagnostic and interventional procedures. Similarly, access to radiation zones in a diagnostic X-ray facility has been used to restrict the general public to some places. All of these principles are well documented in the International Commission on Radiological Protection (ICRP), the National Council on Radiation Protection and Measurements (NCRP), and the International Atomic Energy Agency (IAEA) standards/recommendations, among others[4-12]. In

order to ensure safety in diagnostic imaging, areas are usually categorized into controlled and supervised areas. A controlled area is a limited access area in which occupationally exposed radiation staff are under the supervision of an individual in charge of radiation protection or is a work area in which the annual radiation doses may exceed 3/10 ths of the annual maximum permissible doses for exposed workers. This implies that access, occupancy and working conditions are controlled for radiation protection purposes. Staff in these areas are the radiologists, radiographers and radiological nurses. Supervised or uncontrolled areas are those occupied by individuals such as patients, visitors to the facility, and employees who do not work routinely with or around radiation sources. Areas adjacent to but not part of the x-ray facility are also uncontrolled areas. The controlled and supervised areas have their respective shielding design goals (P). Shielding Design Goals (P) are practical values, for a single X-ray source or a set of sources, that are evaluated at a reference point beyond a protective barrier[13-15].

Prior to the installation of a CT machine, it is paramount that the CT room size be adequate. Other factors that must be considered is the type of CT, and the type of shielding materials that would be used. In Nigeria today, there are more CTs in privately owned diagnostic centres compared to government hospitals. Studies have shown that most diagnostic X-ray facilities in Nigeria are not purposely built and shielding assessments were hardly done[16, 17].

Assessment of shielding barriers in both facilities has not be investigated; likewise, the adequacy of the use blocks plus lead as barriers have not been determined. The expectation of this study is to find out if the current shielding designs meet internationally recommended standards.

This study aimed to estimate IDR and ADR to radiation staff within the controlled areas and other persons within the supervised areas. Comparison would be made with ICRP recommended limits and it would determine if the shielding design goals (P) in both areas are within the NCRP Report 147 recommended limits. Similarly, this study would determine the average AD to radiographers/operators in the control console during CT scans.

Materials and methods

This study was carried out within six weeks, following the installation of two identical CT units supplied by General Electric (GE) at two different areas in Asaba, Delta state, South-South Nigeria. The technical specifications and protocol for determining the dose rates are represented (Table 1 and 2). Both CT rooms were lead lined, with existing block walls as barriers. It is recommended by the Nigerian Nuclear Regulatory Authority (NNRA) that a CT room be adequate to attenuate scatter radiation to background values based on NCRP Report 147 document. According to NNRA regulation, it is expected that a Medical Physicist /Radiation Safety Officer do an assessment to determine if the barriers are adequate and if the shielding design goals are met. Prior to this assessment, the rooms' dimensions were determined using a measuring tape. All areas were marked and classified based on their occupancy factors. Areas like the control boots, adjacent X-ray room, and the door leading to the CT room were classified as controlled areas, while other locations were taken as supervised areas.

Table 1. *Technical specification for the CT machines.*

	CT_1	CT_2
X-ray model	Revolution ACTs	Revolution ACTs
Model no	5331186	2326492-36
Serial no	42051BG3	60739BG0
Tube current	200 mA equivalent with ASiR	200 mA equivalent with ASiR
Maximum power rating	40 W equivalent with ASiR	40 W equivalent with ASiR
Kv range	80/100/120/140	80/100/120/140
Scan range	1350 mm (with extender)	1350 mm (with extender)
Slice per rotation	4/16*	4/16*
Minimum slice thickness (mm)	0.625	0.625
Date of manufacture	January 2018	October 2019

*AsiR is Adaptive Statistical Iterative Reconstruction algorithm, * the slice per rotation can be above 16-slice.*

Table 2. *Average scan parameters for CT_1 and CT_2.*

Parameters	CT_1	CT_2
Scan type	Helical	Helical
Tube potential	140	140
Tube current	150-200 mA	150-200 mA
Slice thickness	2.5-5 mm	2.5-5 mm
Tilt	0.00	0.00
Start/End	>250 mm	>250 mm

An inspector USB survey meter was used for radiation measurements. Background measurements were made. This was to ascertain if there were any environmental factors that could influence the measurements. The Inspector USB survey meter is a health and safety instrument that is operated to detect low levels of radiation. It is designed to measure Alpha (α) and Beta particles (β), Gamma rays (γ) and X-ray radiation (ionizing radiation only). It has the capacity to work in milliroengens per hour (mR/hr) and counts per minute (CPM) or S.I units' microsievert per hour (μSv/hr) and counts per second (cps) with operating range of 0.001 (1 μR) to 100 mR/hr or 0 to 350,000 CPM (Figure 1). Technical parameters for the worst case scenario were used. These parameters were rarely used. A Helios QA test phantom was positioned at the isocentre to produce scatter radiation in both facility (Figure 2). The survey meter was positioned < 50 cm away from the barrier to take measurement in all designated areas. Also, the unshielded air kerma was obtained by positioning the same meter at < 50 cm before the control console lead glass to estimate the barrier thickness. Three measurements were made per position and the average values were calculated. Measurements were made from a total of 20 points each in both facilities. All measurements were made by setting the survey meter to start measurement within a time frame of 60 seconds. The average time scan time was 30 seconds and the remaining 30 seconds were assumed as background values. To compensate for this error, we determined normal background radiation and deducted it from the value

obtained during scanning. The detector unit of measurements was counts per minute (CPM) and a calibration factor (3340 CPM/mR/hr) was applied to determine the dose rate in mR/hr, which was given as:

$$mR/hr = \frac{x\ CPM}{3340\ \frac{CPM}{mR/hr}} \quad \text{——— [1]}$$

Where x is count recorded by the survey meter in CPM (Figure 1).

The results above in mR/hr can then be converted to μSv/hr or mSv/hr to estimate the IDR. Also, estimated ADR was calculated, by multiplying the IDR by 8 working hours per day and 313 days per year (excluding holidays). The AD was determined by considering 10 scans per week, with each scan taking an average of 30.59 seconds for a thoracic/dorsal spine CT. The lead equivalent thickness of the control console was determined using the transmission factor approach:

$$B = \frac{K_S^1\ (\frac{\mu Sv}{hr})}{K_S^2\ \left(\frac{\mu Sv}{hr}\right)\frac{D1}{D2}} \quad \text{——— [2]}$$

Where
B is Secondary transmission
K_S^1 is Unshielded air kerma just before the console barrier.
K_S^2 is Shielded air kerma 30 cm after the console barrier.
D1 is Distance (m) from source to unshielded area,
D2 is Distance (m) from source to shielded area.

The lead equivalent thicknesses (mm) were determined from the CT transmission factor graph in NCRP 147 report.

Figure 1. *The Inspector USB Survey meter in counts per minute (CPM).*

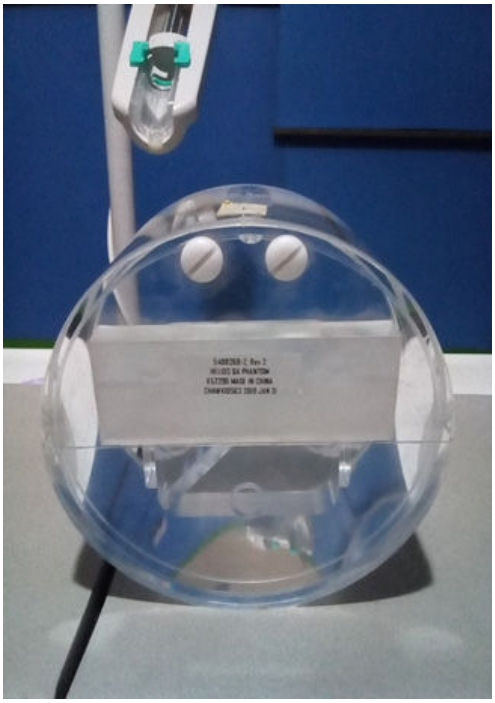

Figure 2. *Test phantom (Helios QA Phantom).*

Results

To begin with, the average background in CT_1 and CT_2 was 0.11 and 0.10 μSv/hr, respectively. The room size for CT_1 was 28.4 m^2 with a height 3.0 m. A total of 20 points located within and outside of the CT room was measured using an Inspector USB survey meter (Figure 1). The average IDR from 4 and 16 points in the controlled and supervised areas was 0.225±0.046 μSv/hr and 0.148±0.102 μSv/hr, respectively (Table 3).

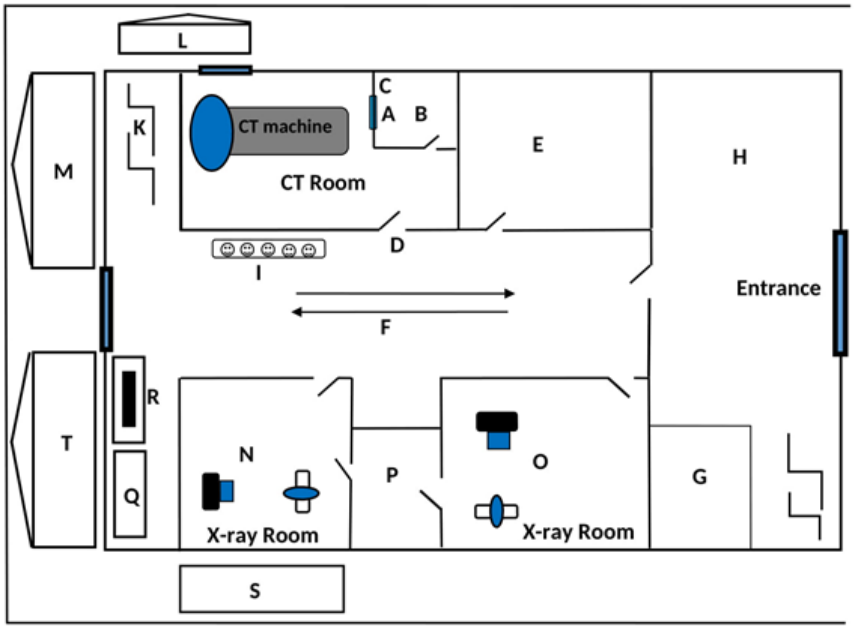

J is Floor above the CT room*

Figure 3. *Schematic diagram of the CT_1 scanner/X-ray facilities and other areas.*

Furthermore, the ADR in CT1 from 4 points of measurements (A-D) in the controlled areas were 0.891, 0.623, 0.308 and 0.428 mSv/yr, respectively. Also, the ADR from 16 points in the supervised areas ranged from 0.193-0.576 mSv/yr (Table 3).

Table 3. *IDR and ADR from 20 points of measurements in and around the CT1.*

Point	Location	IDR (μSv/hr)	ADR (mSv/yr)
A	*Control console (lead glass)	0.356±0.158	0.891
B	*Control console [upper area]	0.249±0.082	0.623
C	*Control console [areas apart from lead glass]	0.123±0.017	0.308
D	*Door [Main entrance to CT room]	0.171±0.093	0.428
E	‡Room behind the control console [unoccupied]	0.135±0.066	0.338
F	‡Walkway	0.156±0.037	0.391
G	‡Receptionist desk	0.110±0.057	0.275
H	‡Patient waiting area [1]	0.145±0.073	0.363
I	‡Patient waiting area [2]	0.216±0.107	0.541
J	Floor above the CT room	0.120±0.006	0.300
K	‡Staircase area behind the CT room	0.209±0.072	0.523
L	‡Kitchen area	0.182±0.091	0.456
M	‡Residential staff area [1]	0.153±0.073	0.383
N	‡X-ray room 1	0.118±0.042	0.295
O	‡X-ray room 2	0.137±0.030	0.343
P	‡Film processing room	0.179±0.082	0.448
Q	‡Toilet area	0.230±0.107	0.576
R	‡UPS area	0.107±0.013	0.268
S	‡Generator area	0.086±0.034	0.215
T	‡Residential staff area [2]	0.077±0.030	0.193

**controlled areas, ‡supervised areas, IDR is Instantaneous Dose Rate, ADR is Annual Dose Rate.*

In addition, the shielding design goals (air kerma) from 4 points were 0.0142, 0.00996, 0.00492 and 0.00684 mGy/wk, respectively in the controlled area. Also, the shielding design goals from 16 points ranged from 0.00308-0.0092 mGy/wk in the supervised area (Figure 4).

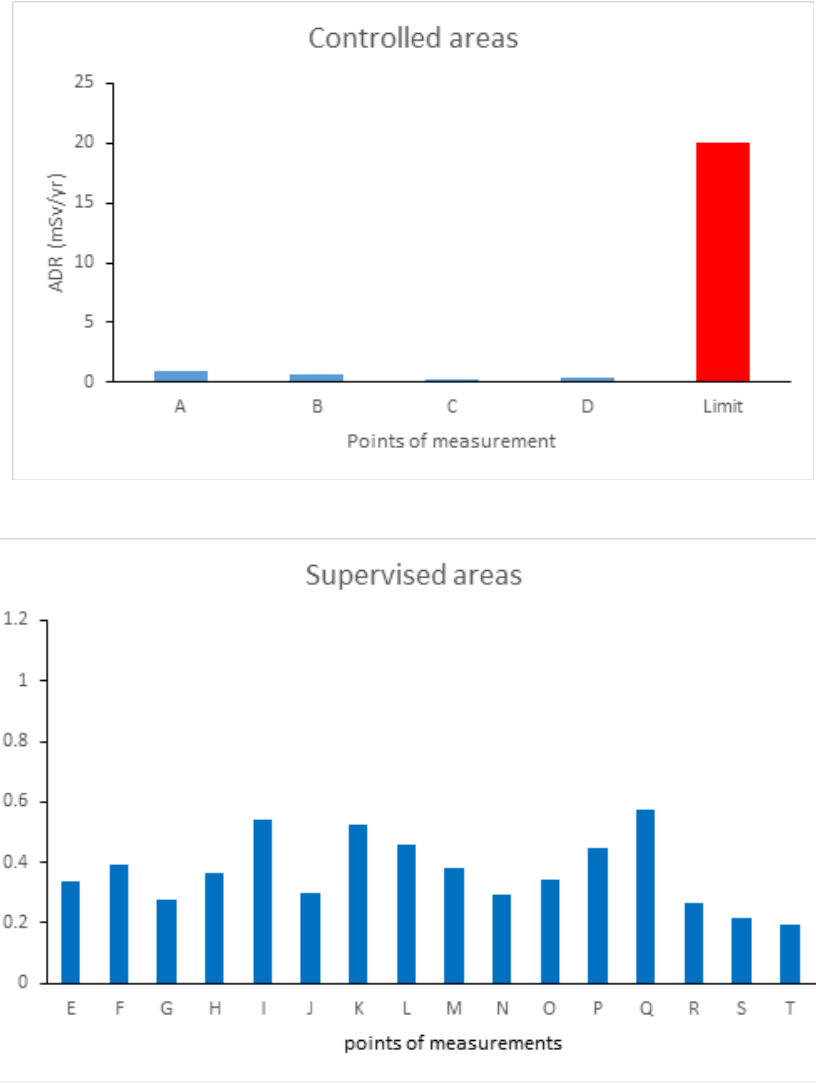

Figure 4. *Comparison of ADR for controlled and supervised areas against ICRP recommended limit for CT₁.*

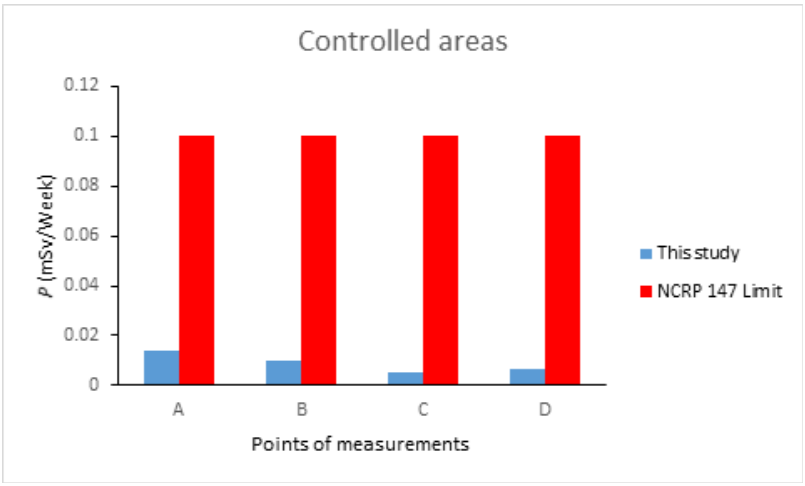

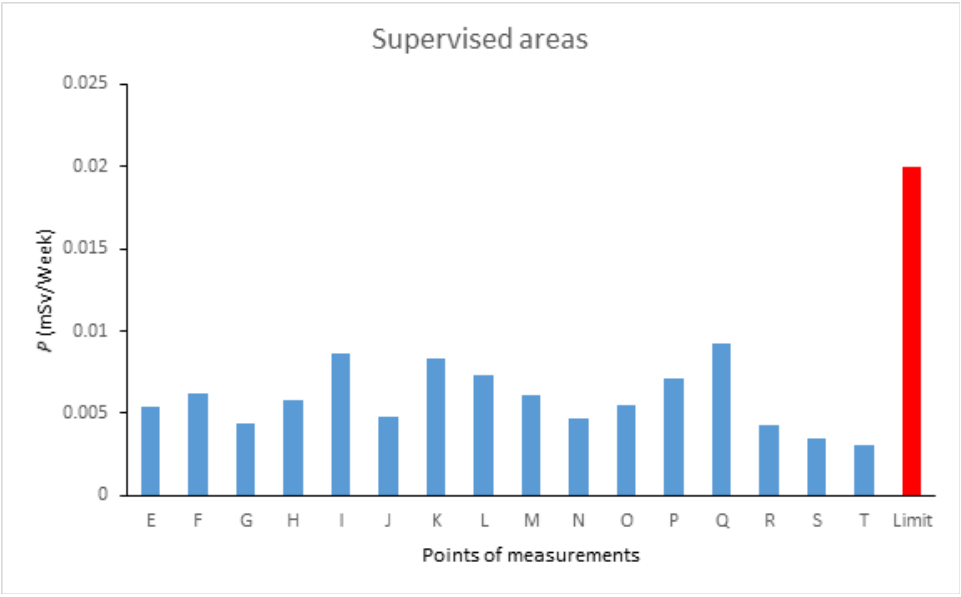

Figure 5. *Comparison of shielding design goal (P) of this study with NCRP 147 recommendations for controlled and supervised areas for CT1.*

The room size for CT_2 was 25.4 m^2 with a height of 2.7 m. A total of 20 points located within and outside the CT room were measured using the same survey meter. The average IDR from 6 and 14 points in the controlled and supervised areas was 0.164±0.111 μSv/hr and 0.141±0.047 μSv/hr (Table 4).

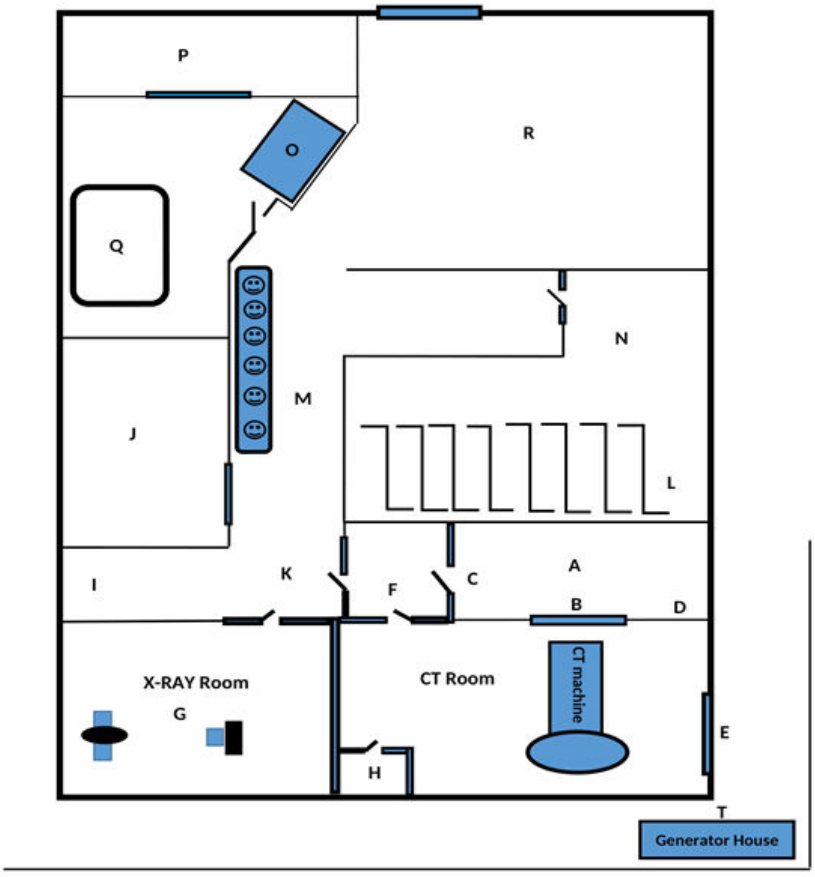

S is Occupied area above the CT & X-ray

Figure 6. *Schematic diagram of the CT_2 scanner/X-ray facilities and other areas.*

Table 4. *IDR and ADR from 20 points of measurements in and around the CT₂.*

Point	Location	IDR (μSv/hr)	ADR (mSv/yr)
A	*Control console	0.100±0.066	0.250
B	*Control console [lead glass]	0.225±0.142	0.563
C	*Control console [right wall]	0.089±0.035	0.223
D	*Control console [left wall]	0.098±0.009	0.245
E	‡Exit door to generator area [1]	0.096±0.007	0.240
F	*Door leading to CT Room	0.365±0.171	0.914
G	*X-ray Room	0.105±0.054	0.263
H	‡Online UPS room (unoccupied area)	0.210±0.097	0.525
I	‡Exit door [2]	0.113±0.035	0.283
J	‡Director's office	0.099±0.022	0.247
K	‡Main door leading to CT Suit	0.269±0.120	0.674
L	‡Walkway leading upstairs	0.120±0.068	0.300
M	‡Walkway leading to radiation areas	0.143±0.011	0.358
N	‡Toilet [1]	0.153±0.062	0.383
O	‡Typing desk	0.105±0.013	0.263
P	‡Laboratory	0.135±0.045	0.338
Q	‡Receptionist desk	0.141±0.015	0.353
R	‡Patient waiting area	0.147±0.070	0.368
S	‡Occupied area above the CT & X-Ray room	0.113±0.034	0.283
T	‡Generator house	0.135±0.080	0.338

**controlled areas, ‡supervised areas, IDR is Instantaneous Dose Rate, ADR is Annual Dose Rate.*

Likewise, the ADR from 6 points of measurements in the controlled areas was 0.250, 0.563, 0.223, 0.245, 0.914 and 0.263 mSv/yr, respectively. Also, the ADR from 14 points of measurements in supervised areas ranged from 0.24-0.674 mSv/yr (Figure 7).

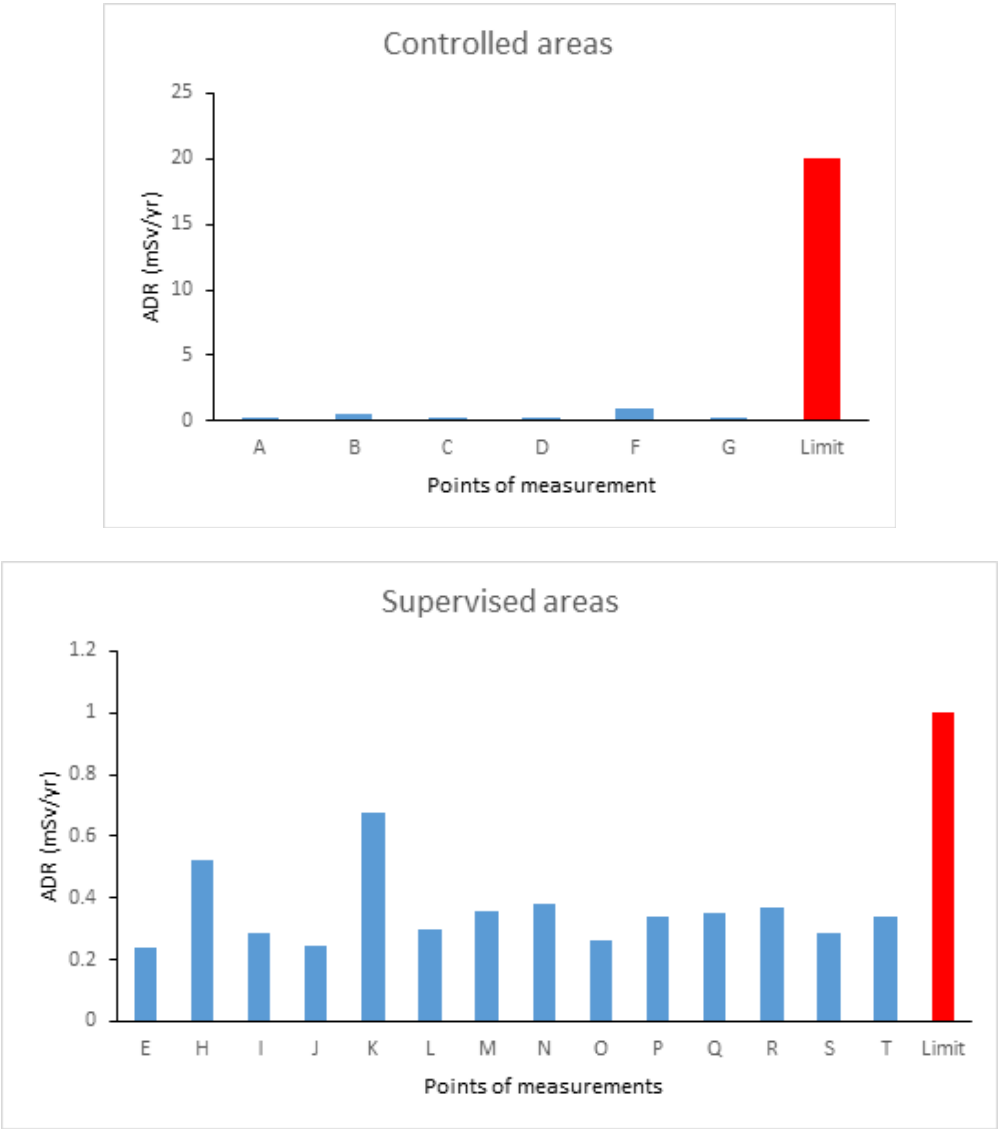

Figure 7. *Comparison of ADR for controlled and supervised areas against the ICRP recommended limit for CT₂.*

Again, the shielding design goals (air kerma) from 6 points were 0.004, 0.009, 0.00356, 0.00392, 0.00146 and 0.0042 mGy/wk, respectively. The shielding design goals from 14 points ranged from 0.00108-0.0084 mGy/wk (Figure 8).

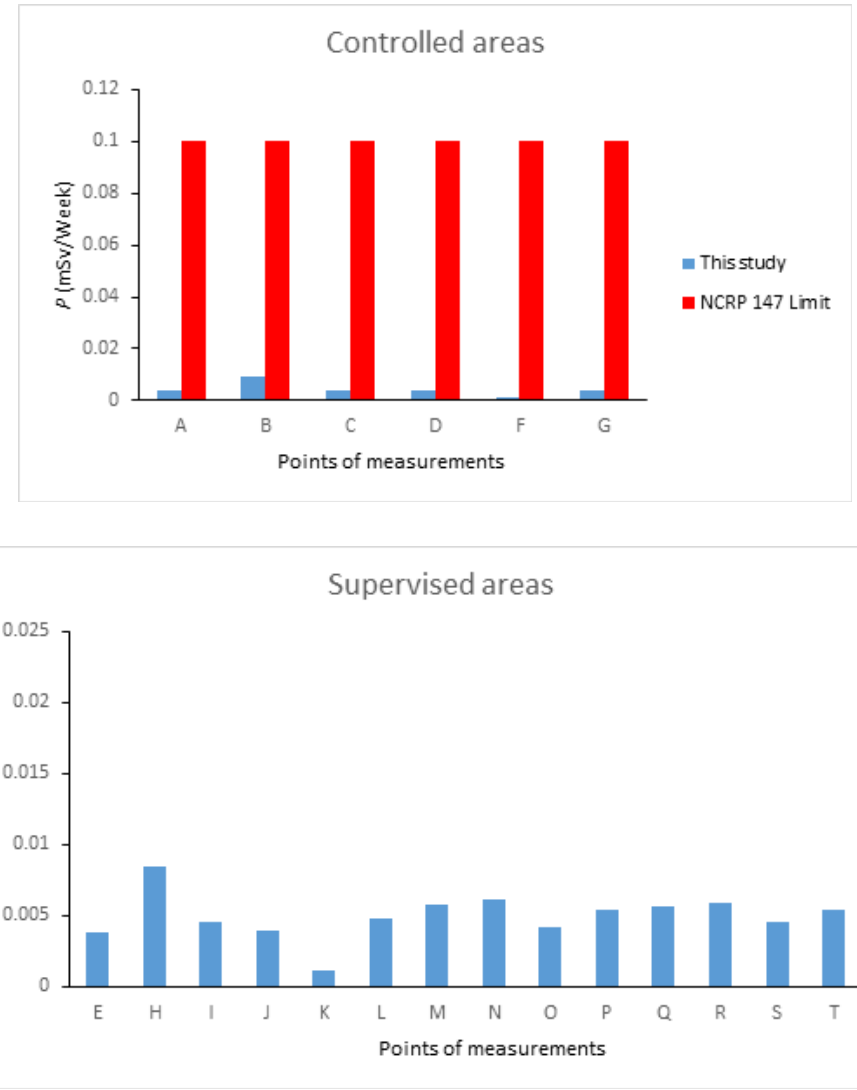

Figure 8. *Comparison of shielding design goal (P) of this study with NCRP 147 recommendations for controlled and supervised areas for CT2.*

Finally, the barrier thickness in CT_1 and CT_2 was 2.1 and 2.6 mm, respectively and AD for the radiographer/operator in CT_1 and CT_2 was 2.5 μSv and 1.3 μSv, which amounted to an overall average dose of 2 μSv (Table 5).

Table 5. *Estimated annual dose to the operator in the control console.*

CT	Location	X-ray source to console (m)	Lead equivalent thickness (mm)	IDR (μSv/hr)	AD (μSv)
CT_1	Control console	3.24	2.1	0.243	2.46
CT_2	Control console	3.25	2.6	0.128	1.29

AD is Annual dose.

Discussion

A study to estimate the IDR, ADR, shielding design goals (P) and AD, within and outside two similar CT machines has been carried out. The ADR with both CTs to the controlled areas were < 20 mSv/yr and the shielding design goals was < 0.1 mSv/wk recommended by NCRP Report 147. Similarly, the ADR with both CTs to the supervised areas were < 1 mSv/yr recommended by ICRP and the shielding design goals were < 0.02 mSv/wk recommended by NCRP Report 147. The estimated ADs to the control console where the radiographer/operator occupy during every CT scan were < 20 mSv ICRP limit.

Deductions from this study shows that 43% and 74% of the measured IDR with CT_1 and CT_2, at the controlled areas were close to background. Similarly, 67% and 78% of the IDR with CT_1 and CT_2, at the supervised areas were close to the background. These results indicate the effectiveness of the walls and the lead materials used for shielding. Over 70% of the IDR at the supervised areas was closer to background values; this was because of the distances and barriers that would be encountered before reaching the CT room. From this study, CT_2 had

thicker barriers compared to CT_1. The background values from this study were similar to the value obtained by Owusu-Banhene et al in Ghana, who conducted a research on dose rate assessment in diagnostic radiology and Joseph et al in a similar study carried out in Nigeria[18, 19].

Furthermore, the shielding design goals in this study were based on NCRP Report 147 document, which was updated from an initial document (NCRP 49). The standards obtained in this document is relevant for all medical imaging facilities, including CTs. In the light of these, the shielding design goal in our study in the controlled areas from both CTs were higher (0.00898 and 0.0066 mSv/wk), compared to a study by Nkubli et al, who used a survey meter similar to ours to determine the shielding design goals from 4 X-ray facilities. His design goals ranged from 0.00152-0.00496 mSv/week. The differences observed were expected because CT systems produce larger scatter radiation compared to conventional X-ray systems[20]. In contrast to this, there was variation in the shielding design goals between our study and a study by Okon et al, who used thermoluminescent dosimeters (TLDs) in Kaduna State Nigeria, with the conventional X-ray system. The shielding design goal from our study was lower compared to Okon's study. Detector responses may have affected the dose rates observed[21].

This study's average IDR for CT_1 and CT_2 in the controlled areas (8.89 and 6.6 μSv/week) was lower compared to a study by Nkansah et al, where the average dose rate in the controlled areas was 18 μSv/week. The aforementioned differences in the controlled areas may be due to the protocol used, the distance of the CT from the console, the position of the detector, the type of the detector used and barrier thickness. Similarly, this study showed an average IDR from both CTs in the supervised areas (5.9 and 5.7 μSv/week) was slightly higher than Nkansah's study which was 3.4 μSv/week[22]. The average IDR in the control console in this study was very low (0.2 μSv/hr) compared to a study by Mohammed et al (7.05 μSv/hr), who also investigated ambient dose rate in the control room in a CT study. Differences observed may be due to factors such as the distance of the CT to the control room, the CT protocol and barrier thickness[23].

Estimation of the control console dose near the lead glass for CT_1 (3.6 μSv) and CT_2 (2.3 μSv) was the highest compared to other areas in the CT room. Dose to personnel at the extreme side, in the control console for CT_1 (1.2 μSv) and CT_2 (0.9 μSv) were the least. This claim proved to be accurate when compared to a study by palm & Nelson, who investigated staff dose in the control console. Their findings show that a dose to areas at the side in the console of the CT had the least dose (0.42 μSv); however, the dose to personnel facing the gantry, through the lead glass was quite higher (96 μSv) than this study[24].

Furthermore, the ADR in the controlled areas between both CTs in this study were close. We observed that the room dimension for CT_1 was larger compared to CT_2, but the shielded air kerma from CT_2 attenuated more of the scatter radiation. Although both CT room dimensions were below the recommended standards of 45 m^2 as required by the International Health Facility Guideline (IHFG); in addition, both CT control console rooms were below 14 m^2 proposed by the iHFG document[25]. In another comparison, the room dimensions in this study met the Uganda Atomic Energy Council (UAEC) guideline, which recommended a total room area of ≥ 25 m^2 (with at least 4 m for each length). The control cubicle for both CTs were approximately 4 m^2 which was below UAEC required area (5 m^2). The control cubicle heights from this study were above the recommended height by UAEC, which was 2.0 m[26].

Conclusion

This study has verified the safety of personnel and the public in and around the CT room during scanning. The estimated ADR from both CTs in the controlled and supervised areas were within an acceptable limit. Similarly, the shielding design goals were within the recommended standards. From this study, the staff working in the control console were safe and the general public who occasionally stay in the patient waiting area were safe. Occasionally, radiation workplace monitoring should be carried out to ensure the general safety of everyone within the facility.

Limitations

1. At longer distances from the control booth to other areas where measurements were taken, it was difficult to communicate with the radiographer when to start exposure and to ascertain when exposure was over.

2. The actual count by the survey meter was challenging to note due to the influence of background count after exposure.

Recommendations

1. Shielding should be done according to the room size, the type of CT system, protective materials and workload. This will ensure that the shielding design goals are properly met.

2. Sensitive survey meter should be used for shielding assessment.

3. Adjoining wall areas should be considered while taken measurements.

References

1. Power SP, Moloney F, Twomey M, James K, O'Connor OJ, Maher MM. Computed tomography and patient risk: facts, perceptions and uncertainties. World J Radiol 2016;8:902-15. doi:10.4329/wjr.v8.i12.902.

2. European Society of Radiology 2009. The future role of radiology in healthcare. Insights Imaging 2010;1:211. doi: 10.1007/s13244-009-0007-x.

3. European Society of Radiology (ESR); European Federation of Radiographer Societies (EFRS). Patient safety in medical imaging: a joint paper of the European Society of Radiology (ESR) and the European Federation of Radiographer Societies (EFRS). Insights Imaging 2019; 10:45. doi: 10.1186/s13244-019-0721-y.

4. International Atomic Energy Agency (IAEA). Radiation protection and safety of radiation sources: international basic safety standards. General safety requirements Part 3. no. GSR Part 3. Vienna (Austria): IAEA Publications; 2014.

5. International Atomic Energy Agency (IAEA). Occupational radiation protection: general safety guide. no. GSG-7. Vienna (Austria): IAEA Publications; 2018.

6. Radiological protection and safety in medicine. a report of the International Commission on Radiological Protection. Ann ICRP 1996;26(2):1-47.

7. General principles for the radiation protection of workers. Ann ICRP 1997;27(1):1-60. doi: 10.1016/s0146-6453(97)88275-9.

8. López PO, Dauer LT, Loose R, Martin CJ, Miller DL, Vañó E, et al. ICRP Publication 139: Occupational Radiological Protection in Interventional Procedures. Ann ICRP 2018;47(2):1-118. doi: 10.1177/0146645317750356.

9. Radiological Protection Institute of Ireland (RPII). The design of diagnostic medical facilities where ionising radiation is used. a code of practice issued by the Radiological Protection Institute of Ireland. Dublin (Ireland): RPII Publication; 2009.

10. Madsen MT, Anderson JA, Halama JR, Kleck J, Simpkin DJ, Votaw JR, et al. AAPM Task Group 108: PET and PET/CT shielding requirements. Med Phys 2006;33:4-15. doi: 10.1118/1.2135911.

11. National Council on Radiation Protection and Measurements (NCRP). NCRP report no. 49: structural shielding design and evaluation for medical use of X-rays and gamma rays of energies up to 10 MeV. Bethesda (MD): NCRP; 1976.

12. International Electrotechnical Commission (IEC). Medical electrical equipment Part 1-3: General requirements for basic safety and essential performance. Collateral standard: radiation protection in diagnostic X-ray equipment. IEC 60601-1-3:2008. Geneva (Switzerland): IEC; 2008.

13. Sutton DG, Williams JR. Radiation shielding for diagnostic X-rays: report of a joint BIR/IPEM working party. London: British Institute of Radiology; 2000.

14. Dixon RL, Simpkin DJ. Primary shielding barriers for diagnostic x-ray facilities: a new model. Health Phys 1998;74:181-9. doi: 10.1097/00004032-199802000-00005.

15. National Council on Radiation Protection (NCRP). NCRP report no. 147: structural shielding design for medical X-ray imaging facilities. Bethesda (MD): NCRP; 2004.

16. Adejoh T, Nwogu BU, Anene NC, Onwujekwe CE, Imo SA, Okolo CJ, et al. Computed tomography scanner distribution and downtimes in southeast Nigeria. J Assoc Rad Niger 2017; 31: 8-15.

17. Akpochafor MO, Omojola AD, Adeneye SO, Ekpo V, Adedewe NA, Adedokun AR et al. Computed tomography dose reference level for noncontrast and contrast examination in 13 CT facilities in South-West Nigeria. PJR 2018;28:285-93.

18. Owusu-Banahene J, Darko EO, Charles DF, Maruf A, Hanan I, Amoako G. Scatter radiation dose assessment in the Radiology Department of Cape Coast Teaching Hospital-Ghana. Open J Radiol 2018;8:299-3. doi: 10.4236/ojrad.2018.84033.

19. Joseph DS, Ibeanu IG, Zakari YI, Joseph DZ. Radiographic room design and layout for radiation protection in some radio-diagnostic facilities in Katsina State, Nigeria. J Assoc Rad Niger 2017;31:16-23.

20. Nkubli FB, Nzotta CC, Nwobi NI, Moi SA, Adejoh T, Luntsi G, et al. A survey of structural design of diagnostic x-ray imaging facilities and compliance to shielding design goals in a limited resource setting. J Glob Radiol 2017;3(1): Article 6. doi: 10.7191/jgr.2017.1041.

21. Okon EE. X-ray shielding barrier estimation: a case study of radiology department, Ahmadu Bello University Teaching Hospital, Shika - Zaria [dissertation]. Zaria (Nigeria): Department Of Physics, Faculty of Science, Ahmadu Bello University; 2007.

22. Nkansah A, Schandorf C, Boadu M, Fletcher JJ. Assessment of the integrity of structural shielding of four computed tomography facilities in the greater Accra region of Ghana. Radiat Prot Dosimetry 2013;155:423-31. doi: 10.1093/rpd/nct021.

23. Mohammed SAH. Ambient dose measurement in some CT department in Khartoum State [dissertation]. Khartoum (Sudan): Atomic Energy Council, Sudan Academy of Science; 2012.

24. Palm F, Nelson F. The importance of medical staff placement in CT examination rooms: a study of the scattered radiation doses in CT examination rooms in Da Nang, Vietnam [dissertation]. Da Nang (Vietnam): School of Health and Welfare, Jonkoping University; 2017.

25. International Health Facility Guidelines (IHFG). Part B Health facility briefing and design: 160 medical imaging unit-general. Version 5. IHFG; 2016.

26. Uganda Atomic Energy Council (UAEC). Guidance on the designs and layout of medical radiology facilities Vol. 1, 2017. Uganda: UAEC; 2017.

Original Article

Abdominal CT radiation dose optimization at Siriraj Hospital

Piyaporn Apisarnthanarak, M.D.
Chosita Buranont, M.D.
Chulaluck Boonma, B.Sc.
Sureerat Janpanich, RN.
Tarntip Suwatananonthakij, RN.
Atchariya Klinhom, RN.
Kobkun Muangsomboon, M.D.
Wanwarang Teerasamit, M.D.
Voraparee Suvannnarerg, M.D.
Pairash Saiviroonporn, Ph.D.
From Department of Radiology, Faculty of Medicine Siriraj Hospital, Mahidol University, Bangkok, Thailand.
Address correspondence to P.A. (e-mail: punpae159@gmail.com)

Abstract

Objective: To compare radiation dose and image quality between standard dose abdominal CT currently performed at our hospital and new low dose abdominal CT using various percentages (0%, 10%, 20%, and 30%) of Adaptive Statistical Iterative Reconstruction (ASiR).

Materials and Methods: We prospectively performed low dose abdominal CT (30% reduction of standard tube current) in 119 participants. The low dose CT images were post processed with four parameters (0%, 10%, 20% and 30%) of ASiR. The volume CT dose index (CTDIvol) of standard and low dose CT were compared. Four experienced abdominal radiologists independently assessed the quality of low dose CT with aforementioned ASiR parameters using a 5-point-scale satisfaction score (1 = unacceptable, 2 = poor, 3 = average, 4 = good, and 5 = excellent image quality) by using prior standard dose CT as a reference of excellent image quality (5). Each reader selected the preferred ASiR parameter for each

participant. The image noise of the liver and the aorta in all 5 (1 prior standard dose and 4 current low dose) image sets was measured.

Results: The mean CTDIvol of low dose CT was significantly lower than of standard dose CT (7.17 ± 0.08 vs 12.02 ±1.61 mGy, p<0.001). The mean satisfaction scores for low dose CT with 0%, 10%, 20% and 30% ASiR were 3.95, 3.99, 3.91 and 3.87, respectively with the ranges of 3 to 5 in all techniques. The preferred ASiR parameters of each participant randomly selected by each reader were varied, depending on the readers' opinions. The mean image noise of the aorta on standard dose CT and low dose CT with 0%, 10%, 20%, and 30% ASiR was 29.07, 36.97, 33.92, 31.49, and 29.11, respectively, while the mean image noise of the liver was 24.60, 30.21, 28.33, 26.25, and 24.32, respectively.

Conclusion: Low dose CT with 30% reduction of standard mA had acceptable image quality with significantly reduced radiation dose. The increment of ASiR was helpful in reducing image noise.

Keywords: Abdominal computed tomography, Abdominal CT, Radiation dose reduction, Iterative reconstruction, IR, Adaptive Statistical Iterative Reconstruction, ASiR.

Introduction

The image quality of abdominal computed tomography (CT) is one of the main factors for accurate CT interpretation. Unfortunately, the quality of CT scan increases in accordance with the high radiation exposure. This problem is a major concern among patients and radiologists worldwide. There were many proposed techniques of radiation dose reduction, such as minimizing the number of CT acquisitions and area coverage as necessary, reducing tube current, and decreasing peak kilovoltage[1,2]. However, increasing image noise and beam-hardening artifacts were the unavoidable consequences. The CT vendors proposed many techniques for optimizing image quality of low dose CT scan. One widely accepted reconstruction technique was iterative reconstruction (IR) which

provided less image noise than the conventional filtered back projection (FBP) reconstruction technique[3-5].

In our hospital, we continued to reduce CT radiation dose for patients' safety. At the same time, we needed to balance image quality for the sake of accurate CT interpretation. We instructed our residents and fellows to protocol each patient for a suitable number of CT acquisitions and area coverage. According to our abdominal CT standard protocol, we used the tube current of 400 and 340 mA for 64-slice and 256-slice CT scanners, respectively. With the new de-noising IR technique (Adaptive Statistical Iterative Reconstruction, ASiR), we recently performed the pilot study of 22 abdominal CT with radiation dose reduction, which achieved acceptable image quality with 30% reduction of our standard tube current, from 400 to be 260 mA on 64-slice CT scanner and from 340 to be 210 mA on 256-slice CT scanner (standard mA multiplied with mA adjustment factor for 30 % dose reduction of 0.66 and 0.63 for 64-slice and 256-slice CT scanners, respectively). This current study with a larger number of study participants were prospectively performed for the purpose of comparing radiation dose and image quality between standard abdominal CT currently performed at our hospital and the new low dose abdominal CT with various parameters of IR techniques.

Materials and methods

Study Designs and Participants

This study was a prospective, single-centered study performed at a 2,200-bed university hospital in central Thailand. This study was approved by our institutional review board with informed consents from all included participants. All participants were aged over 18 years old who were scheduled for contrast enhanced abdominal CT examinations at our department in January 2018. They had prior standard dose contrast enhanced abdominal CT available on our Picture Archiving and Communication System (PACS). One hundred and nineteen patients met the criteria and were recruited as our study population. The demographic data of each participant including gender and age were recorded by one of our investigators (CB).

CT Techniques

Standard Dose Abdominal CT

The prior standard dose abdominal CT of our participants was routinely performed by four General Electric (GE) CT scanners including three 64-slice scanners (one LightSpeed VCT and two Discovery CT750 High Definition, GE Healthcare, Milwaukee, WI, USA) and one 256-slice scanner (Revolution CT, GE healthcare, Milwaukee, WI, USA). The CT of each participant was protocoled for a suitable number of CT acquisitions and area coverage. All participants were advised to hold their breath during the scan. The scan coverage included at least the upper abdominal area. The slice collimation was 1.25 mm (reconstructed at 7.0 mm) for all scanners. There were varieties on the administration of oral and rectal contrasts according to each participant's suitable protocol. All participants underwent precontrast and postcontrast studies, before and after a bolus intravenous injection of nonionic iodinated contrast agent (2 mL per kg body weight), followed by 20 mL of water via a power injector at a rate of 3 mL/second. Each participant had at least a portovenous phase with an 80-second delay for postcontrast study. An additional arterial phase at 35 to 40-second delay or delayed phase at 5 to 10-minute delay were obtained in some participants as necessary. The peak kilovoltage was fixed at 120 kVp for all scanners. The tube current based on our standard protocol was 400 and 340 mA for 64-slice and 256-slice CT scanners, respectively. The rotation time was 0.5 second for all scanners. The pitch was 1.375:1 and 0.992:1 for for 64-slice and 256-slice CT scanners, respectively. All images were reconstructed with the standard FBP techniques and sent to PACS for subsequent reviews.

Low Dose Abdominal CT

The low dose abdominal CT of the study participants were performed by three GE CT scanners including two 64-slice scanners (Discovery CT750 High Definition, GE Healthcare, Milwaukee, WI, USA) and one 256-slice scanner (Revolution CT, GE healthcare, Milwaukee, WI, USA). Our remote 64-slice CT scanner (LightSpeed VCT, GE healthcare, Milwaukee, WI, USA) did not have IR de-noising technique for improving image quality; therefore, it was not included

in the performance of low dose abdominal CT. The CT scanners for standard and low dose CT of each participant were not fixed to be the same scanner. The CT of each participant was protocoled for a suitable number of CT acquisitions and area coverage (at least cover the upper abdominal area). The scan techniques were the same as described in prior standard dose abdominal CT section except for the tube current on the portovenous phase which was reduced for 30%; from 400 to be 260 mA on 64-slice CT scanners and from 340 to 210 mA on 256-slice CT scanner (standard mA multiplied with mA adjustment factor for 30 % dose reduction of 0.66 and 0.63 for 64-slice and 256-slice CT scanners, respectively). The other phases used the standard tube current (400 and 340 mA for 64-slice and 256-slice CT scanners, respectively). We chose to study only the portovenous phase because most abdominal organs had homogeneous enhancement on this phase. It was easy for radiologists to evaluate the CT image quality.

The IR technique specific for our GE CT scanners (Adaptive Statistical Iterative Reconstruction, ASiR) was applied by blending with the conventional FBP on low dose portovenous phase images by post-processing at a CT workstation with the range of 0% ASiR (with 100% FBP), 10% ASiR (with 90% FBP), 20% ASiR (with 80% FBP) and 30% ASiR (with 70% FBP). With these reconstruction techniques, each participant had four sets of low dose CT images on the portovenous phase sent to PACS for subsequent reviews.

For a parameter of radiation dose comparison, we selected volume CT dose index (CTDIvol) instead of the dose length product (DLP). The DLP would depend on the length of scan which varied in the participants due to the difference in area coverage and the number of CT acquisitions.

The details of CT scanners, study dates, and CTDIvol of each participant's prior standard dose abdominal CT and current low dose abdominal CT were recorded by one of our investigators (CB). The time interval between the two studies was calculated.

CT Analysis

For qualitative assessment of low dose abdominal CT, four board-certified, fellowship-trained abdominal radiologists (PA, KM, WT, and VS with 22, 22, 16, and 13 years of experience in abdominal CT evaluation) separately reviewed 5 sets of abdominal CT images (1 set of prior standard dose portovenous phase images; and 4 sets of low dose portovenous phase images with 0%, 10%, 20%, and 30% ASiR) of each participant. All readers were not blinded to the percentage of applied ASiR. They graded the image quality of each low dose CT set by using a 5-point-scale satisfaction score on a visual scale as follows:

1: Unacceptable image quality, unable to interpret
2: Poor image quality, interfering with interpretation
3: Average image quality, possible interpretation
4: Good image quality
5: Excellent image quality

The satisfaction score was given by using each participant's prior standard dose CT images as a reference of excellent image quality (5). The satisfaction score of 3 to 5 were acceptable for CT interpretation. Each reader selected the preferred image set from 4 sets of low dose abdominal CT for each participant.

For quantitative assessment of abdominal CT, the image noise of the aorta and the liver was measured on either routine standard dose CT images or 4 sets of low dose CT images by one of our investigators (CB) on a CT workstation (Advantage workstation AW 4.6, GE healthcare, Milwaukee, WI, USA). The image noise was measured by drawing circular region of interests (ROIs) at 4 locations (one aortic and 3 hepatic regions) on a 1.25-mm slice portovenous image at the same locations and levels of these 5 image sets. For image noise of the aorta, the ROI was drawn at least 1/3 area of aortic lumen (60-90 mm^2 ± 5 mm^2) at the most central part to avoid calcified plaque at the aortic wall. Three hepatic ROIs (100-150 mm^2 ± 5 mm^2) were routinely applied on the left lobe, the anterior right lobe, and the posterior right lobes (Figure 1). In patients with prior hepatic surgery, the ROIs were placed in three different locations in the remaining hepatic areas. The hepatic ROIs were placed at the homogenous enhancing hepatic areas avoiding vessels,

bile ducts, hepatic lesions, calcifications and surgical materials. The mean image noise of each liver was calculated from these 3 hepatic ROIs of image noise.

Statistical Analysis

The demographic data of participants, CT scanners, time interval between CT studies, the image quality (satisfaction scores, readers' preferred ASiR parameters, image noise) and CTDIvol of low dose and standard dose CT were presented as number (%), mean (standard deviation, SD), median, and range. Paired t-test was used to compare mean CTDIvol between standard dose CT and low dose CT. Multivariate analysis with Bonferroni adjustment for a pairwise comparison was applied to compare mean satisfaction scores, mean image noise of the aorta and the liver among different ASiR parameters.

All statistical data analyses were performed by using PASW 18.0 (SPSS Inc., Chicago, IL, USA). A 2-sided p-value of less than or equal to 0.05 was considered a statistical significance.

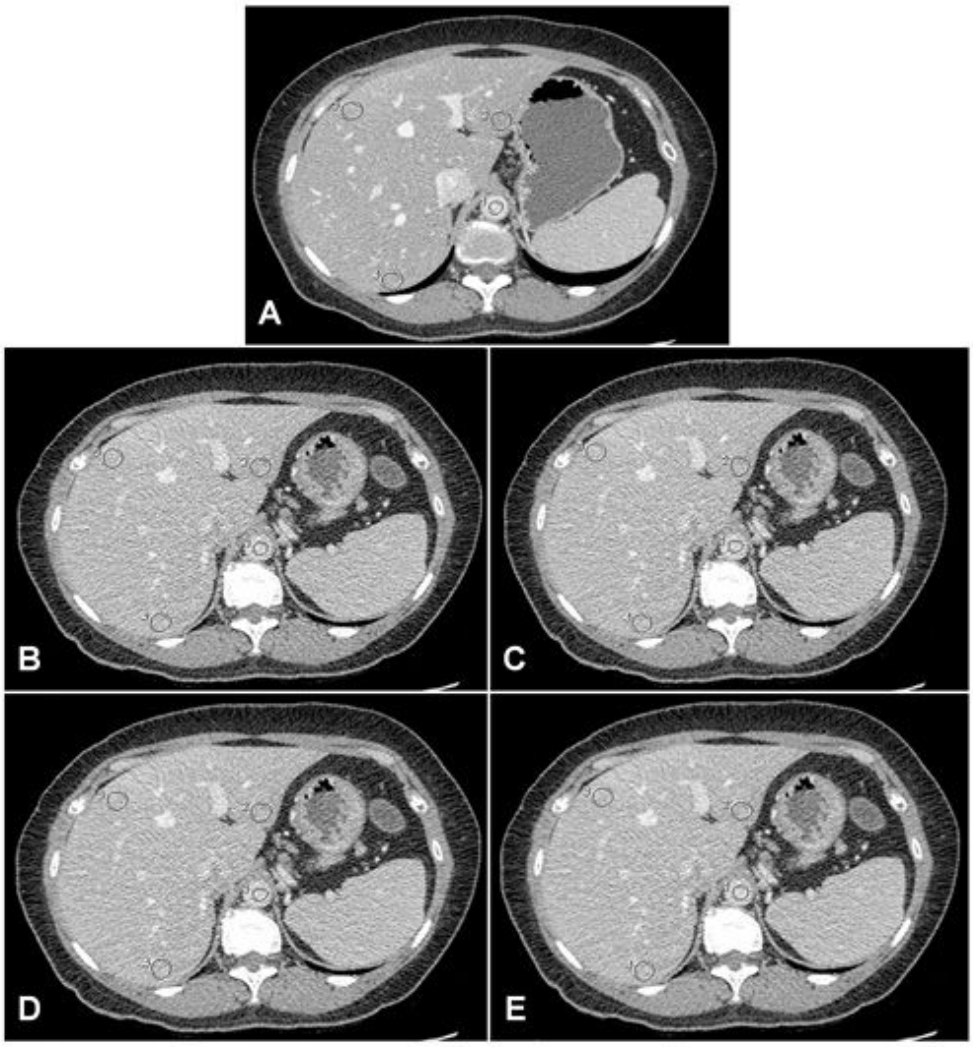

Figure 1. *The image noise measurement of the aorta (1 ROI) and the liver (3 ROIs at the left lobe, the anterior right lobe and the posterior right lobe) on the 5 image sets (A-E)*

A: Prior standard dose abdominal CT,

B-E: The low dose abdominal CT with 0% ASiR (B), 10% ASiR (C), 20% ASiR (D) and 30% ASiR (E).

The ROI were positioned at the same locations and levels for all 5 image sets.

Results

Participants

One hundred and nineteen participants in this study included 50 (42.0%) men and 69 (58.0%) women. The mean age (SD) of the participants at the time of low dose CT scan was 59.2 (14.3) years with the range of 18-88 years.

CT Techniques

The standard dose abdominal CT of 80 (67.2%) and 39 (32.8%) participants were performed by 64-slice and 256-slice scanners, respectively. The low dose abdominal CT of 78 (65.5%) and 41 (34.5%) participants were performed by 64-slice and 256-slice scanners, respectively. The time interval between the two studies ranged from 6 to 422 days (median 161 days).

The mean CTDIvol (SD) of low dose CT was significantly lower than of standard dose CT, 7.17 (0.08) vs 12.02 (1.61) mGy, $p<0.001$.

CT Analysis

For qualitative assessment, the satisfaction score of low dose abdominal CT with 4 ASiR parameters graded by 4 readers ranged from 3 to 5, which were all acceptable for CT interpretation. The mean satisfaction scores of low dose abdominal CT with 4 ASiR parameters were summarized in Table 1. The preferred ASiR parameters applied to low dose CT of each participant randomly selected by each reader were varied, depending on the readers' opinions (Table 2).

For quantitative assessment, the image noise of the aorta and the liver on standard dose CT and low dose CT with 4 ASiR parameters was summarized in Table 3. The image noise of the aorta and the liver was significantly increased on low dose CT with 0% ASiR compared to prior standard dose CT. With the consecutive increment of ASiR, the image noise sequentially decreased. There was no difference between the mean image noise of the aorta and the liver on low dose CT with 30% ASiR compared to prior standard dose CT ($p=1.000$) (Table 4).

Table 1. *The satisfaction scores of low dose abdominal CT with 0%, 10%, 20%, and 30% ASiR parameters by 4 readers.*

	Mean Satisfaction Score (SD) of Low Dose Abdominal CT			
	0% ASiR	10% ASiR	20% ASiR	30% ASiR
Reader 1	4.22 (0.56)	4.39 (0.54)	4.34 (0.48)	4.35 (0.48)
Reader 2	4.01 (0.09)	4.01 (0.09)	4.01 (0.09)	4.01 (0.09)
Reader 3	3.66 (0.68)	3.80 (0.65)	3.82 (0.63)	3.93 (0.55)
Reader 4	3.92 (0.63)	3.76 (0.58)	3.45 (0.52)	3.20 (0.48)
All readers	3.95 (0.37)	3.99 (0.34)	3.91 (0.31)	3.87 (0.28)

Note: There were significant statistical differences between 0% ASiR vs 30% ASiR ($p=0.001$)
10% ASiR vs 20% ASiR ($p<0.001$)
10% ASiR vs 30% ASiR ($p<0.001$)

Table 2. *The preferred ASiR parameters applied to low dose CT selected by 4 readers.*

	Number of The Preferred Low Dose Abdominal CT (%)				
	0% ASiR	10% ASiR	20% ASiR	30% ASiR	Total
Reader 1	42 (35.3)	23 (19.3)	40 (33.6)	14 (11.8)	119 (100.0)
Reader 2	1 (0.8)	2 (1.7)	87 (73.1)	29 (24.4)	119 (100.0)
Reader 3	0 (0.0)	0 (0.0)	0 (0.0)	119 (100.0)	119 (100.0)
Reader 4	110 (92.4)	9 (7.6)	0 (0.0)	0 (0.0)	119 (100.0)

Table 3. *The image noise of the aorta and the liver on standard dose CT and low dose CT with 4 ASiR parameters.*

	Standard Dose CT	Low Dose CT			
		0% ASiR	10% ASiR	20% ASiR	30% ASiR
Aorta					
Mean (SD)	29.07 (7.25)	36.97 (8.60)	33.92 (7.61)	31.49 (7.11)	29.11 (6.80)
Median	28.25	36.14	33.69	31.61	28.41
Min	16.02	19.02	18.07	15.89	14.67
Max	50.58	67.87	59.46	58.63	51.17
Liver					
Mean (SD)	24.60 (5.53)	30.21 (6.11)	28.33 (5.70)	26.25 (5.36)	24.32 (5.01)
Median	23.45	29.89	28.30	26.03	24.06
Min	16.13	17.99	16.62	15.09	13.78
Max	43.53	49.75	45.39	43.09	39.58

Table 4. *The difference of mean image noise of the aorta and the liver on low dose CT with 4 ASiR parameters compared to standard dose CT.*

	Difference (SD) of Mean Image Noise Compared to Standard Dose CT	p-Value	95% CI
Aorta			
0% ASiR	7.90 (0.74)	<0.001	5.79, 10.01
10% ASiR	4.86 (0.66)	<0.001	2.96, 6.76
20% ASiR	2.42 (0.66)	0.004	0.54, 4.30
30% ASiR	0.04 (0.66)	1.000	-1.83, 1.92
Liver			
0% ASiR	5.61 (0.51)	<0.001	4.15, 7.06
10% ASiR	3.73 (0.46)	<0.001	2.41, 5.06
20% ASiR	1.65 (0.46)	0.005	0.34, 2.96
30% ASiR	-0.28 (0.45)	1.000	-1.58, 1.01

Discussion

According to the major concern of CT radiation exposure, the CT vendors proposed several new CT reconstruction techniques to optimize the image quality, allowing the radiologists to continue decreasing CT radiation dose for the patients' safety while still achieving the diagnostic confidence. The IR is one of the new methods of image reconstruction that has been developed in the last decade. Each IR technique is unique for each CT vendor, i.e., ASiR for GE healthcare, adaptive iterative dose reconstruction (AIDR 3D) for Toshiba Medical Systems, iDose for Philips Healthcare, and sinogram-affirmed iterative reconstruction (SAFIRE) for Siemens Healthcare. At our hospital, all CT scanners were GE scanners; therefore, we used ASiR as our IR technique to blend with the conventional FBP technique to optimize the image quality of low dose CT. The objective of this study was to assess the suitable amount of ASiR applied with our low dose CT (30% dose reduction from our standard dose), either the qualitative aspect (radiologists' satisfaction and their preferred ASiR parameter) or the quantitative aspect (image noise).

In our study, low dose CT scan by using 30% mA reduction provided significantly lower radiation dose compared to standard dose CT. The quality of all low dose CT images was acceptable for interpretation. There were many previous studies assessing the imaging quality obtained from low dose CT with IR techniques[6-10], showing that IR technique helped optimize the image quality by reducing image noise and provided similar image quality as standard dose CT. The satisfaction score in our study did not sequentially increase along with the increment of ASiR and the selected preferred ASiR parameters were varied by our radiologists' opinions. We assumed that the images with high percentage of ASiR provided smooth image appearances with less sharp borders. This was the reported major drawback of the IR technique[6]. Some of our radiologists were possibly familiar with a relatively noisy image with sharp borders derived from the conventional FBP technique.

As expected, the image noise of the aorta and the liver was significantly increased on low dose CT with 0% ASiR compared to standard dose CT. With the

consecutive increment of ASiR, the image noise sequentially decreased until there was no difference between low dose CT with 30% ASiR compared to standard dose CT. However, in some participants with cirrhosis, ascites or diffuse subcutaneous edema, the image noise was significantly high despite the addition of 30% ASiR (Figure 2). We postulated that the patients with these conditions were not suitable for low dose CT.

There were several limitations of our study. First, there were variables in our CT scanners. Although they were all GE scanners, most were 64-slice scanners and one was a 256-slice scanner. Of which, some CT parameters (i.e. mA and pitch) were not the same. Plus, the CT scanners for standard and low dose CT of each participant were not necessarily the same scanners. Second, the time interval between prior standard dose CT and subsequent low dose CT ranged from 6 to 422 days (median 161 days). With such a long interval, there would be some changes in patient's conditions which would affect the image quality. The new study with a shorter time interval should be designed. Third, our radiologists were not blinded to the percentage of applied ASiR. Fourth, image noise was measured on a 1.25 mm slice portovenous image of each image set. Actually, image noise should be measured by choosing 3-5 consecutive CT slices and the noise should be average for the statistical accuracy. Finally, we evaluated only the image quality of low dose CT, but did not evaluate the ability to detect lesion or diagnostic performance. To evaluate the diagnostic performances between low dose CT and standard dose CT, these 2 studies need to be performed on the same date and almost the same acquisition phase. These will inevitably increase radiation dose received by the participants.

In conclusion, low dose CT with 30% reduction of standard mA had acceptable image quality with significantly reduced radiation dose. The increment of ASiR technique was helpful in reducing image noise.

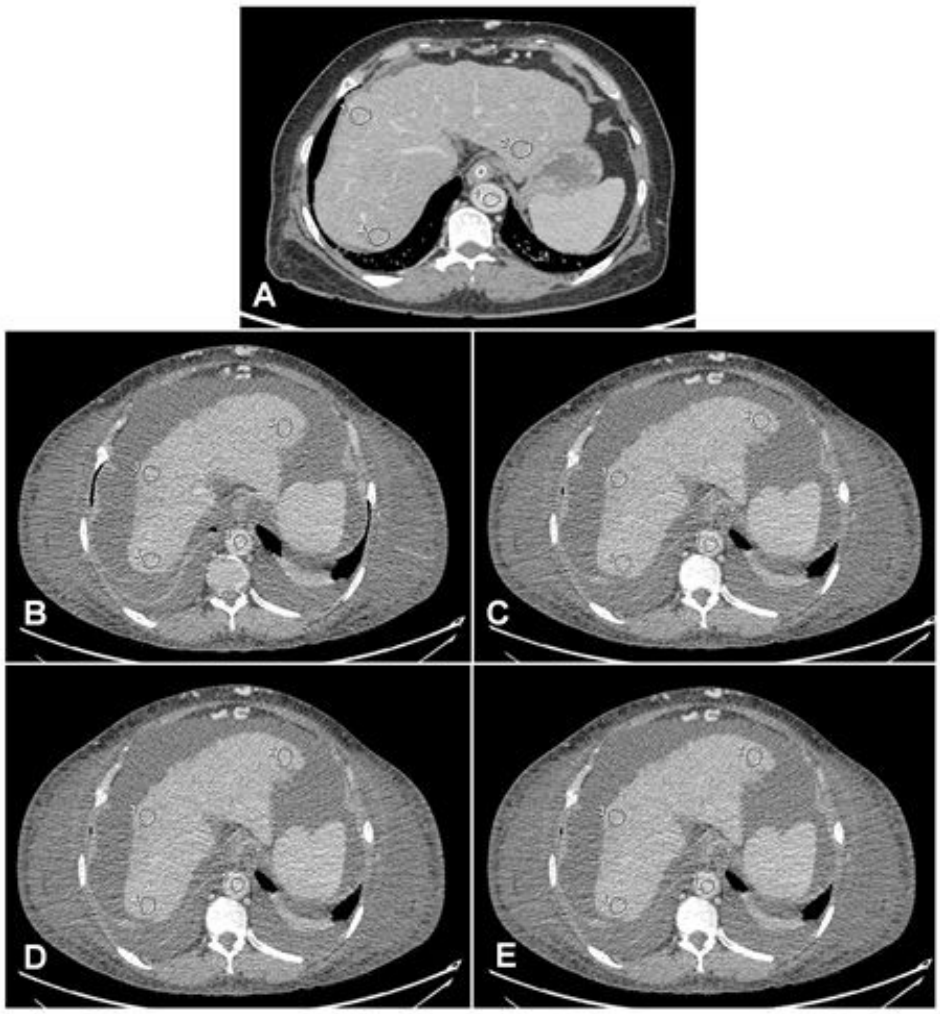

Figure 2. *Poor image quality on low dose abdominal CT due to ascites and subcutaneous edema. Axial portovenous abdominal CT of a 58-year-old female with cirrhosis and portal hypertension (A-E)*

A: Prior standard dose abdominal CT,

B-E: The low dose abdominal CT with 0% ASiR (B), 10% ASiR (C), 20% ASiR (D) and 30% ASiR (E).

The time interval between the two studies was 295 days. The mean satisfaction score for ASiR 0%, 10%, 20% and 30% were 3.5, 3.5, 3.5 and 3.25, respectively. The mean liver image noise for standard dose, ASiR 0%, 10%, 20% and 30% were 19.05, 45.21, 40.10, 38.11 and 35.6, respectively. Note the development of ascites and subcutaneous edema dramatically affected the image quality.

References

1. Hara AK, Wellnitz CV, Paden RG, Pavlicek W, Sahani DV. Reducing body CT radiation dose: beyond just changing the numbers. AJR Am J Roentgenol 2013;201:33-40. doi: 10.2214/AJR.13.10556.

2. Tamm EP, Rong XJ, Cody DD, Ernst RD, Fitzgerald NE, Kundra V. Quality initiatives: CT radiation dose reduction: how to implement change without sacrificing diagnostic quality. RadioGraphics 2011;31:1823-32. doi: 10.1148/rg.317115027.

3. Patino M, Fuentes JM, Singh S, Hahn PF, Sahani DV. Iterative reconstruction techniques in abdominopelvic CT: technical concepts and clinical implementation. AJR Am J Roentgenol 2015;205:W19-31. doi: 10.2214/AJR.14.13402.

4. Willemink MJ, de Jong PA, Leiner T, de Heer LM, Nievelstein RA, Budde RP, et al. Iterative reconstruction techniques for computed tomography Part 1: technical principles. Eur Radiol 2013;23:1623-31. doi: 10.1007/s00330-012-2765-y.

5. Higaki T, Nakamura Y, Fukumoto W, Honda Y, Tatsugami F, Awai K. Clinical application of radiation dose reduction at abdominal CT. Eur J Radiol 2019;111:68-75. doi: 10.1016/j.ejrad.2018.12.018.

6. Mitsumori LM, Shuman WP, Busey JM, Kolokythas O, Koprowicz KM. Adaptive statistical iterative reconstruction versus filtered back projection in the same patient: 64 channel liver CT image quality and patient radiation dose. Eur Radiol 2012;22:138-43. doi: 10.1007/s00330-011-2186-3.

7. Chang W, Lee JM, Lee K, Yoon JH, Yu MH, Han JK, et al. Assessment of a model-based, iterative reconstruction algorithm (MBIR) regarding image quality and dose reduction in liver computed tomography. Invest Radiol 2013;48:598-606. doi: 10.1097/RLI.0b013e3182899104.

8. Singh S, Kalra MK, Gilman MD, Hsieh J, Pien HH, Digumarthy SR, et al. Adaptive statistical iterative reconstruction technique for radiation dose reduction in chest CT: a pilot study. Radiology 2011;259:565-73. doi: 10.1148/radiol.11101450.

9. Gervaise A, Osemont B, Louis M, Lecocq S, Teixeira P, Blum A. Standard dose versus low-dose abdominal and pelvic CT: comparison between filtered back projection versus adaptive iterative dose reduction 3D. Diagn Interv Imaging 2014;95:47-53. doi: 10.1016/j.diii.2013.05.005.

10. Singh S, Kalra MK, Hsieh J, Licato PE, Do S, Pien HH, et al. Abdominal CT: comparison of adaptive statistical iterative and filtered back projection reconstruction techniques. Radiology 2010;257:373-83. doi: 10.1148/radiol.10092212.

Case Report

Imaging findings of spontaneous thymic hemorrhage in infancy: Case report and literature review

Chanunporn Leekumnerdthai, M.D.[(1)]
Panruethai Trinavarat, M.D.[(2)]
Darintr Sosothikul, M.D.[(3)]
Nattinee Leelakanok, M.D.[(4)]
From [(1)]Department of Radiology, Bhumibol Adulyadej Hospital, The Royal Thai Airforce, Bangkok, Thailand.
[(2)]Department of Radiology, Faculty of Medicine, Chulalongkorn University, Bangkok, Thailand.
[(3)]Department of Pediatrics, Faculty of Medicine, Chulalongkorn University, Bangkok, Thailand.
[(4)]Department of Radiology, Faculty of Medicine, Chulalongkorn University and King Chulalongkorn Memorial Hospital, Bangkok, Thailand.
Address correspondence to C.L. (e-mail: chalee507@hotmail.com)

Abstract

The authors report imaging findings of spontaneous thymic hemorrhage, which is a rare entity in infancy, in a 4-month-old boy with congenital factor VII deficiency presented with acute respiratory distress and anemia. Widening of superior mediastinum and left pleural effusion were detected on the chest radiograph. Ultrasound and computed tomography of the chest revealed diffusely enlarged thymus with heterogeneous parenchyma from poorly-defined areas of altered echogenicity or attenuation. Vascular flow was depicted within the abnormal thymus in color-mode sonography. The spontaneous involution of thymic abnormality seen on serial ultrasonography confirmed the diagnosis of thymic hemorrhage, resulting in avoidance of further unnecessary imaging or invasive procedure.

Keywords: Thymic hemorrhage, Spontaneous hemorrhage, Bleeding tendency, Factor 7 deficiency, Infancy, Thymus.

Introduction

A normal thymus gland in children may occupy a large proportion of mediastinum, seen on a chest radiograph without causing symptoms. Normal thymus from ultrasonography shows rather homogeneous medium-echogenicity with some high-echogenic dots and short strands, and minimal internal vascular flow[1]. Normal thymus from CT reveals homogeneous density with mean attenuation value of about 36 HU on unenhanced phase, and homogeneous enhancement after intravenous contrast media injection[2]. Spontaneous thymic hemorrhage is very rare in pediatrics, and even rarer in adults, but it could be a life-threatening condition. The etiology of thymic hemorrhage is usually unidentified, but bleeding diathesis particular from vitamin K deficiency is mostly believed to be the cause in neonates and young infants. Due to its rarity, there are not many reports of its imaging findings. To our knowledge, there were eight reported cases of spontaneous hemorrhage in normal thymus with presence of imaging findings in perinatal and infantile period[3-9], and only three reports in adults[10-12] in English literature. The authors report a 4-month-old boy with thymic hemorrhage from congenital factor VII deficiency and describe imaging findings of his thymus.

Case report

A 4-month-old boy was presented with fever, irritability and poor feeding for 3 days. He was first admitted to the hospital at age of 4-day old due to acute subdural hemorrhage and had been diagnosed with congenital factor VII deficiency. His blood tests at that time showed anemia (hemoglobin 7.4 g/dl), a low level of platelet count (134,000/mcL), isolated prolonged prothrombin time and a low level of factor VII (<1%). The duration of the first admission was 31 days. The treatment after discharge was regular fresh frozen plasma (FFP) 10 mg/kg intravenously, three times a week.

This time was his second admission. His blood tests showed anemia (hemoglobin 7 g/dl), a mildly elevated white blood count (10,370/mcL) and a

normal platelet count (397,000/mcL). A 2-mm-thick acute subdural hematoma at the right parietal convexity was detected from the CT scan of the brain. On the next day, he developed tachypnea with a respiratory rate of 60/min, with subcostal retraction and a decreased breath sound of the left lung. His chest radiograph showed a widened left side of superior mediastinum, partial atelectasis of the left upper lobe, and the left pleural effusion with obscuration of the left hemidiaphragm. These abnormalities were not seen on his chest radiograph during his first admission (Figure 1). The cause of the mediastinal widening was uncertain, and the differential diagnoses were mediastinal hemorrhage, mediastinal mass, and rebound thymic hyperplasia.

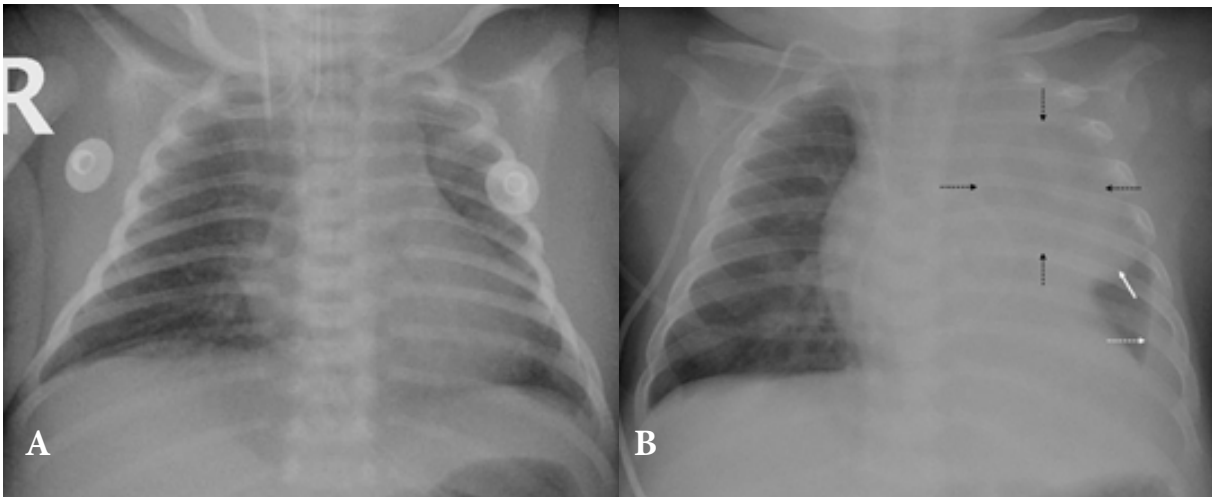

Figure 1. *The chest radiograph of the 11-day old (A) from the first admission showed a normal cardiac size, small thymic shadow, and clear lungs. The chest radiograph on the second admission at the age of 4 months (B) showed a widened left side of the mediastinum reaching the lateral chest wall with an inferior bulging contour (white arrow). There was partial atelectasis of the left upper lobe with a small area of aerated lungs (black dashed arrows) superimposed on the lesion. There was the left pleural effusion (white dashed arrow) causing obliteration of the left hemidiaphragm and the left costophrenic angle.*

Chest ultrasonography on the same day revealed a large heterogeneously-echogenic mass in the left thymic lobe, with a few vascular flows within that thymic lesion (Figure 2).

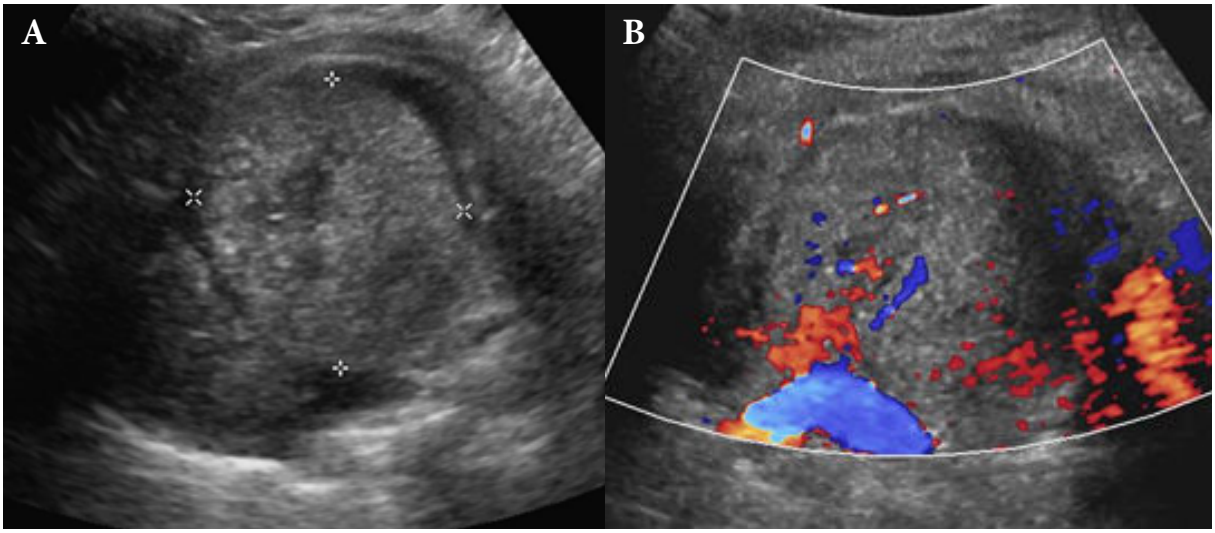

Figure 2. *The ultrasonography of the chest (A) showed a 4.7x4.4 cm heterogeneous hyperechoic mass-like lesion in the location of the left thymic lobe. (B) There were a few foci of vascular flow within the lesion in color-mode sonography.*

The single-venous-phased CT scan of the chest on the same day showed an enlarged thymus gland with preservation of a thymic shape, but had heterogeneous parenchymal enhancement with multifocal poorly-defined areas of hypodensity (Figure 3). The attenuation values of the areas of hypodensity and hyperdensity were 57 HU (probably a recent hemorrhage) and 89 HU (probably an enhanced thymic tissue), respectively. Complete atelectasis of the left lung and the left pleural effusion were spotted.

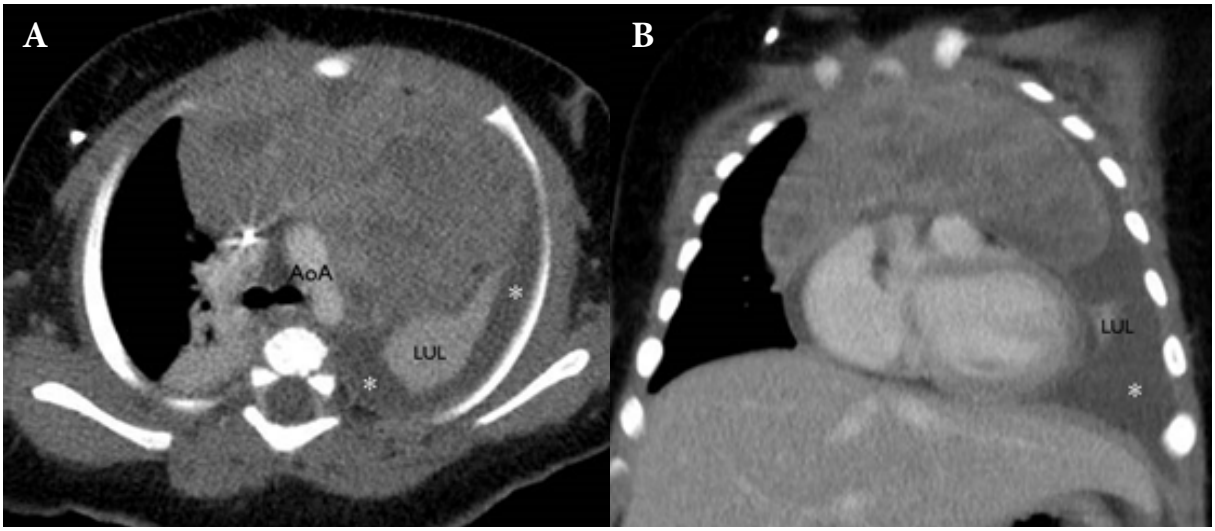

Figure 3. *The venous-phased chest CT in axial (A) and coronal planes (B) revealed an enlarged thymus, particularly the left lobe, with preservation of a thymic shape. Measured in axial plane, transverse diameter = 79 mm (normal = 39.6±5.5 mm in 4-5 months of age), right lobe thickness = 34 mm (normal = 19.5±5.7 mm) and left lobe thickness = 51 mm (normal = 22.5±3.8 mm) [13]. Poorly-defined multifocal areas of hypodensity (57 HU) were noted within the relatively more enhanced areas (89 HU). The left pleural effusion (*) and atelectasis of the left upper lobe (LUL) were also presented (AoA = aortic arch).*

According to a new acute subdural hematoma, anemia, and his underlying factor VII deficiency, the thymic abnormality was suggested to be thymic hemorrhage. The patient was treated with intravenous FFP 10 mg/kg/dose every 6 hours. There was a concern of minimal demonstrable vascular flow within the thymic lesion from the ultrasound, whether there was an infiltrative thymic tumor that may need thymic biopsy or not. A serial follow-up with ultrasound was planned.

The first follow-up ultrasound at a 5-day interval showed a decreased size and internal echogenicity with development of some internal small cysts (Figure 4). The findings indicated partial resolution of multifocal hematomas within the thymus gland. The vascular flow was still detected within these lesions, showing a low-resistant waveform.

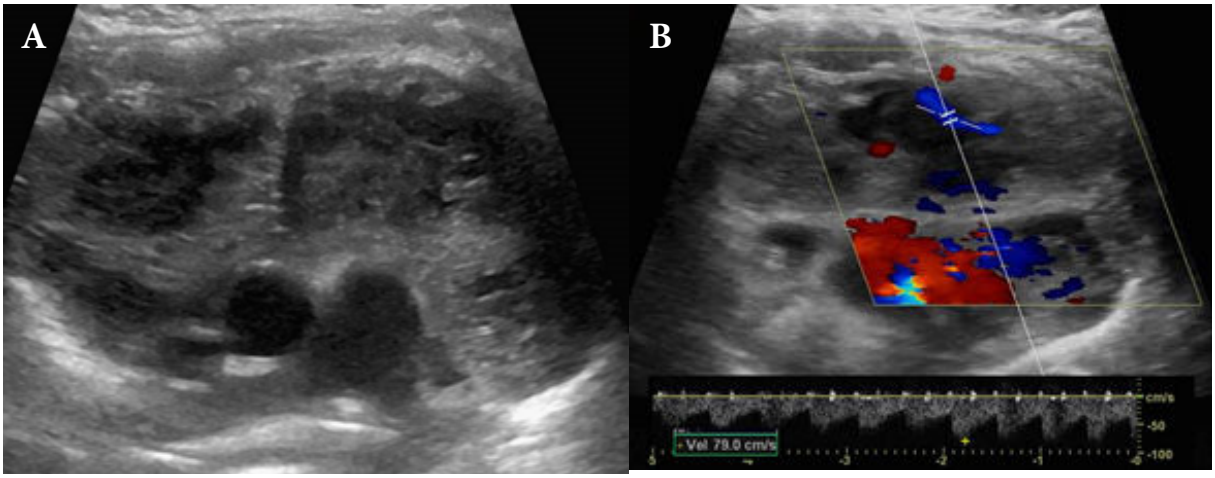

Figure 4. *The first follow-up ultrasound at 5-day interval (A) showed decreased size, less echogenicity, and more well-defined border of the multifocal thymus lesions. (B) Vascular flow within the lesion had low-resistant waveform.*

A subsequent follow-up chest ultrasound at 3-week interval showed a further decrease in size of the thymus with residual minimal heterogeneity and tiny cystic areas. His chest radiograph on the same day looked normal (Figure 5).

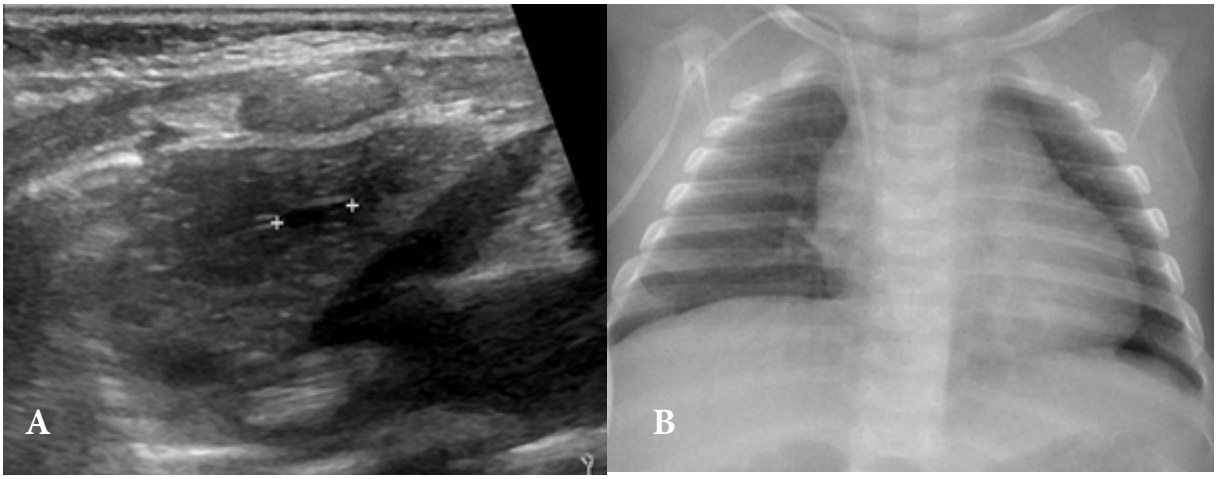

Figure 5. *The subsequent 3-week follow-up chest ultrasound (A) showed thymic gland returning to a nearly normal size with residual tiny cystic areas. His chest radiograph on the same day (B) showed normal cardiothymic shadow, complete resolution of the left pleural effusion, and well-aerated lungs.*

His clinical symptoms were resolved without other bleeding sites. Blood tests were repeated before discharge and showed normal values. The duration of his second admission was 14 days.

Discussion

Thymic hemorrhage, although rare, is an important life-threatening condition. When a spontaneous hemorrhage in a normal thymus (SHNT) occurs in the perinatal and infantile age group, the most common postulated etiology is vitamin K deficiency (formerly known as a hemorrhagic disease of the newborn) [9]. Besides clinical findings of acute respiratory distress and anemia, imaging adds an important role in supporting the diagnosis of the thymic hemorrhage.

The frontline imaging modality is usually a chest radiograph. As a normal thymus in infants can be widely variable in size and shape, it may be difficult to differentiate a normal or rebound hypertrophic thymus from pathologic thymic entities without adding other imaging investigations. The echogenicity in ultrasound or homogeneous density in CT can differentiate between rebound thymic hyperplasia and an enlarged thymic hemorrhage. The rebound thymic hyperplasia still preserves a normal 'starry sky' appearance while the thymic hemorrhage does not. Again the thymic hemorrhage shows heterogeneous hyper-attenuation on the CT scan while the rebound thymic hyperplasia does not.

The affected 4-month-old boy with congenital factor VII deficiency had the second episode of symptomatic intracranial bleeding and the first episode of thymic bleeding. His chest radiography showed widened superior mediastinum without an identified cause. The ultrasonographic findings showed a loss in 'starry sky' appearance of normal thymus and presence of a mass-like lesion in left thymic lobe, so thymic hemorrhage was considered. The possibility of hyperechoic thymic tumor was raised when the radiologist detected minimal vascular flow within the hyperechoic thymic mass. From the single venous-phased chest CT in this case, the retained thymic shape and the alternating areas of hypo- and hyper-density suggested the possibility of hematomas (57 HU) among the enhanced thymic tissue (89 HU). Performing a pre- and post-contrast enhanced chest CT would be easier to diagnose a thymic hemorrhage, but it was not recommended to perform it with infants and small children due to increased radiation exposure. The clinical context and serial follow up imaging with ultrasound is the best management. This could obviate the need for biopsy, surgery, or any further CT or MR imaging.

Imaging findings in the nine cases of SHNT in perinatal and infantile period [3-9], this report included, are summarized in Table 1-2. Four of them were presented in a very early neonatal period and the other five cases were presented in an early infantile period (between the age of 4 weeks and 4 months). All reported cases mentioned non-specific enlarged antero-superior mediastinum in chest radiographs; seven of the nine cases had associated pleural effusion, preferential

on the left side or both sides. Two had pericardial effusion detected by the ultrasound. Pleural effusion was proven to be hemothorax in patients who had the effusion drained. In the three cases having surgical thymectomy, pleural perforation was detected in two of them.

Table 1. *Demographic data and chest radiographic findings of SHNT from literature review and this case report.*

Case no.	Year reported	Author	Gender	Age	Surgery	Coagulo -pathy*	Outcome	Chest radiograph				Other imaging evaluation
								Mediastinal widening	Pleural effusion			
									Bilateral	Left only	None	
1	1974	Wooley (3)	F	2 days	Thymectomy	-	Survive	√		√		-
2	1974	Wooley (3)	M	4 weeks	Thymectomy	√	Survive	√		√		-
3	1989	Lemaitre (4)	M	2 months	-	√	Survive	√	√			US
4	1994	Urvoas (5)	M	4 weeks	-	√	Survive	√			√	US
5	1996	Walsh (6)	M	Perinatal	-	-	Die	√			√	-
6	1997	Bees (7)	F	Perinatal	Thymectomy	X	Survive	√		√		US, CT
7	2015	Gargano (8)	M	Perinatal	-	√	Survive	√	√			US, CT, MRI
8	2017	Palau (9)	M	4 weeks	(Biopsy, US guidance)	√	Survive	√	√			US, CT
9	2019	This report	M	4 months	-	√	Survive	√		√		US, CT

** Coagulopathy in case number 2,3,4,7,8 was believed to be from vitamin K deficiency, and in case number 9 is Factor VII deficiency.*

Ultrasound, from its wide availability, portability and nowadays a good resolution, is suitable to be the next imaging tool after the chest radiograph in this clinical scenario to reveal the location and the solid or cystic nature of the lesion. Vascular malformation or a teratoma may be suspected if there is a cystic component or calcification. Ultrasound findings performed in six of the nine cases of a thymic hemorrhage (table 2) showed solid lesions with heterogeneous echotexture. Focal

nodular lesion(s) of either hyper- or hypo-echogenicity, or bulls' eye appearance, were found, depending on the chronology of the hemorrhage. The presence of a few foci of vascular flow within the lesion cannot rule out the thymic hemorrhage, as evidence in this reported case. Therefore, ultrasound findings were nonspecific, and hardly possible to be differentiated from other rare thymic or anterior mediastinal tumors in this age group such as Langerhans cell histiocytosis, lymphoma, or hemorrhage of other underlying thymic lesions.

Table 2. *Findings from ultrasonography, CT, and MRI of SHNT from literature review and this case report.*

Case no.	Echotexture	Ultrasound Focal nodule(s)			Other findings	CT and MRI findings
		Hypo	Hyper	Bulls' eye		
3	Heterogeneous	√	√			-
4	Heterogeneous	√		√	Mass effect on LBCV	-
6	Heterogeneous		√			CT - Large anterior mediastinal mass, inhomogeneous attenuation, did not enhanced with contrast medium, with mass effect on left main bronchus
7	Heterogeneous		√		Small pericardial effusion	CT - Enlarged thymus, mainly left side with tracheal displacement to the right, hyperdensity areas on NECT, non-homogeneous on CECT MRI (day 10) - Very reduced size of the thymus, homogeneous structure with hyperintense signal in T1 and T2 sequences (subacute hemorrhage)
8	Not described	Solid mass, detail not described			Minimal ascites modest pericardial effusion	CT - Homogeneously enhancing anterior mediastinal mass of thymic contour, with mass effect on the vessels and airway
9	Heterogeneous		√		A few internal vascular flows in the nodule	CT - Enlarged thymus, heterogeneous enhancement (NECT not performed)

Follow-up thymic lesion(s) with the ultrasound to confirm a complete resolution in case of hemorrhage is noninvasive and simple. The thymic hemorrhage in this reported case, after control of coagulopathy, showed a partial resolution within 5 days, seen as better delineation and decreased echogenicity of an internal hemorrhage, or an early small cystic change. Vascular flow was still noted within the resolving thymic hematoma, showed a low-resistant waveform. In further follow-ups, the thymus gland gradually returned to nearly normal echogenicity, but atrophic, and the internal flow was hardly detected. After seeing this case, one of the authors performed color Doppler ultrasound on the normal thymus of the two neonates which revealed a few foci of vascular flows with a low-resistant waveform (Figure 6). So the vascular flow demonstrable in area of thymic hemorrhage could be a normal intra-thymic vessel.

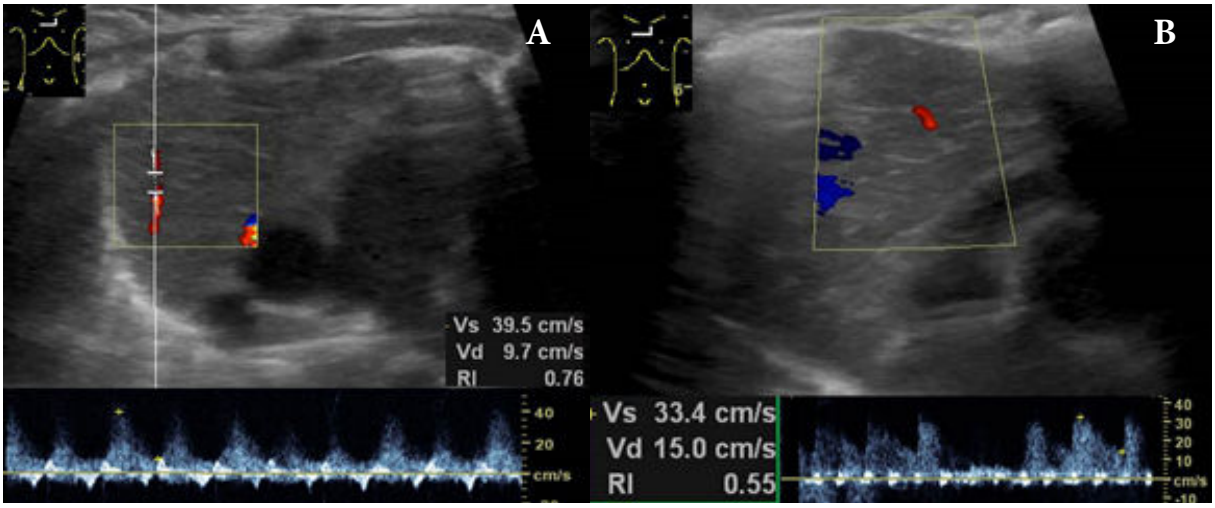

Figure 6. *Color Doppler sonography of normal thymus in a 2-month-old boy (A) and another 4-month-old boy (B) revealed a few intra-thymic artery with low-resistant waveform.*

From the literature review and this case report, the CT scan better provided the overview of the entire thymus[2]. It showed a retained thymic shape, and detected hyper-attenuatedarea of hemorrhage in a non-contrast scan that did not enhance after the contrast injection. However, it cannot rule out a thymic tumor with bleeding or may have inconclusive result if there is no hyper-attenuated area of an acute hemorrhage (probably from severe anemia or subacute hemorrhage). Although both ultrasound and CT were performed, biopsy was still required in one case to rule out underlying thymic pathology.

MRI was performed in only one case of the thymic hemorrhage[8], showing subacute hematoma within the thymus on the sixteenth day after the onset of the bleeding. MRI can be excellent in confirming and dating thymic hemorrhage, and also excluding an underlying thymic tumor. However, a long imaging time of MRI prohibits its use in emergent unstable patients.

The management of an infantile thymic hemorrhage usually started with normalization of coagulation indices by giving vitamin K and fresh frozen plasma, and adding packed red cell to the anemic ones[3-9]. The coagulopathy was usually corrected within 6-24 hours. Thymectomy was indicated when the respiratory distress was severe due to airway compression[3]. Thymectomy or biopsy under an imaging guidance was also performed when suspicious of a thymic tumor[7,9].

In conclusion, although the thymus is an uncommon target organ of bleeding in coagulopathy compared to the brain or gastrointestinal tract, this possibility should not be overlooked. Almost all of the imaging findings were abnormal widened superior mediastinum with or without pleural effusion found on the chest radiograph, heterogeneous thymus with hyper- or hypoechoic nodule(s) on ultrasound and thymic enlargement with heterogeneous densities on CT images. The presence of intralesional vascularity on color Doppler sonography could not rule out the thymic hemorrhage. An ultrasound can be used as a mainstay modality to show the abnormality, to follow up the resolution, and to avoid further unnecessary imaging or invasive procedures.

References

1. Han BK, Suh YL, Yoon HK. Thymic ultrasound. I. Intrathymic anatomy in infants. Pediatr Radiol 2001;31:474-9.

2. Webb WR. The mediastinum: mediastinal masses. In: Webb WR, Higgins CB. Thoracic imaging: pulmonary and cardiovascular radiology. 2 nd ed. Philadelphia PA: Lippincott Williams & Wilkins; 2011. p.219-85.

3. Woolley MM, Isaacs H Jr, Lindesmith G, Vollmer DM, Van Adelsberg S. Spontaneous thymic hemorrhage in the neonate: report of two cases. J Pediatr Surg 1974;9:231-3.

4. Lemaitre L, Leclerc F, Dubos JP, Marconi V, Lemaire D. Thymic hemorrhage: a cause of acute symptomatic mediastinal widening in an infant with late haemorrhagic disease. Sonographic findings. Pediatr Radiol 1989;19:128-9.

5. Urvoas E, Pariente D, Rousset A, De Victor D, Leblanc A. Ultrasound diagnosis of thymic hemorrhage in an infant with late-onset hemorrhagic disease. Pediatr Radiol 1994;24:96-7.

6. Walsh SV, Cooke R, Mortimer G, Loftus BG. Massive thymic hemorrhage in a neonate: an entity revisited. J Pediatr Surg 1996;31:1315-7.

7. Bees NR, Richards SW, Fearne C, Drake DP, Dicks-Mireaux C. Neonatal thymic haemorrhage. Br J Radiol 1997;70:210-2.

8. Gargano G, Paltrinieri AL, Gallo C, Di Pancrazio L, Roversi MF, Ferrari F. Massive thymic hemorrhage and hemothorax occurring in utero. Ital J Pediatr 2015 Nov14;41:88. doi: 10.1186/s13052-015-0196-5.

9. Palau MA, Winters A, Liang X, Nuss R, Niermeyer S, Gossling M, et al. Vitamin K deficiency presenting in an Infant with an anterior mediastinal mass: A case report and review of the literature. Case Rep Pediatr 2017;2017: 7628946. doi: 10.1155/2017/7628946.

10. Ghoshhajra K. Spontaneous thymic hemorrhage in an adult. Chest 1977;72: 666-8.

11. Sakuraba M, Tanaka A, Tsuji T, Mishina T. Spontaneous thymic hemorrhage in an adult. Ann Thorac Surg 2014 May;97(5):1800-2. doi: 10.1016/ j.athoracsur.2013.07.098.

12. de Perrot M, Bründler MA, Girardet C, Spiliopoulos A. Spontaneous hemorrhage of thymus and thymoma in adults. Eur J Cardiothorac Surg 1999;16:674-6.

13. Yekeler E, Tambag A, Tunaci A, Genchellac H, Dursun M, Gokcay G, et al. Analysis of the thymus in 151 healthy infants from 0 to 2 years of age. J Ultrasound Med 2004;23:1321-6.

Case Report

Atraumatic splenic rupture in chronic pancreatitis with successful embolization

Anooja Abdul Salam, M.D.[(1)]
Ben Pearch, M.D.[(2)]
Lisa Sorger, M.D.[(1)]
From [(1)]Department of Radiology, Royal Darwin Hospital, Australia.
[(2)]Department of Radiology, Department of Interventional Radiology, Princess Alexandra Hospital, Brisbane, Queensland, Australia.
Address correspondence to A.A.S. (e-mail: abcanu@gmail.com)

Abstract

Atraumatic splenic rupture is uncommon but it is a life threatening condition because of hypovolemic shock. Early recognition and treatment are the keys to a successful outcome. We report a case of atraumatic splenic rupture secondary to chronic pancreatitis treated successfully by splenic artery embolization.

Keywords: Atraumatic splenic rupture, Chronic pancreatitis, Embolization.

Introduction

Atraumatic splenic rupture (ASR) is an uncommon and rarely reported complication of chronic pancreatitis. It is often overlooked in a patient with known history of pancreatitis (chronic or acute), secondary to alcohol consumption. In case of splenic complications associated with pancreatitis, the morbidity rates range from 39% to 79% and mortality rates range from 3.5% to 0.8%[1]. We discuss here a case of acute exacerbation of chronic pancreatitis complicated by splenic rupture.

Case report

A 56-year-old male was admitted with 2 weeks of worsening epigastric pain that suddenly became very severe in the left upper quadrant for 24 hours.

This is on background of chronic pancreatitis, secondary to chronic alcohol abuse treated with Pancrelipase (Creon) tablets. There was no history of trauma reported. His other comorbidities included severe chronic obstructive pulmonary disease, large bilateral apical bullae, recent ICU admission for spontaneous pneumothorax secondary to burst bulla, and chronic alcoholism.

An initial examination showed normal blood pressure, mild tachycardia and a distended abdomen that was painful to palpation but with no signs of peritonitis. The laboratory results revealed an elevated lipase of 4580 U/L and the patient was assessed to have acute exacerbation of chronic pancreatitis and was admitted for conservative management under the surgical team. Few hours later, the patient became unstable (the pulse rate of 135/min, the respiratory rate of 35/min and the blood pressure at 70/40 mmHg), with a rising lactate and worsening acidosis despite intravenous therapy, and a haemoglobin drop from 130 to 87 g/L.

A Computed Tomography (CT) scan of the abdomen (Figure 1) demonstrated a splenic rupture with a large volume of perisplenic hematoma extending into the peritoneal cavity to the pelvis, without any active bleeding. It also demonstrated changes consistent with chronic pancreatitis.

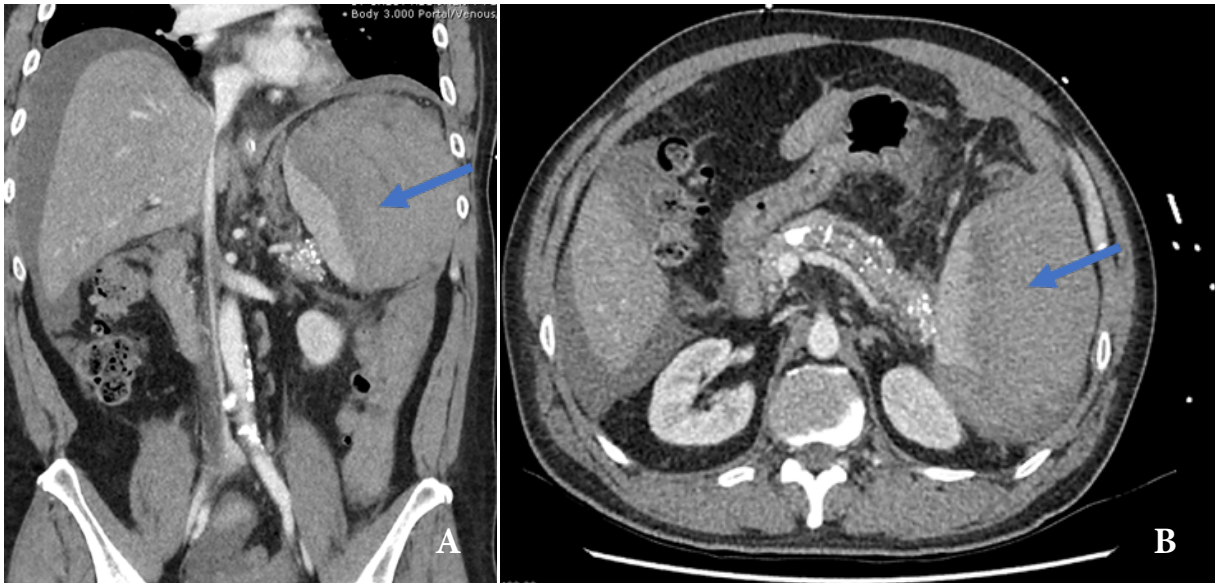

Figure 1. *Computed tomographic image (A. coronal and B. axial views) in the portovenous phase demonstrating the splenic hematoma (arrow) with hemoperitoneum.*

The patient was assessed to be unfit for laparotomy due to his multiple comorbidities. The decision was then made to proceed with splenic artery embolization after the discussion among the surgical and anaesthetic team since the patient was hemodynamically unstable and there was a likelihood of ongoing bleeding which could have been missed in the CT scan. The patient was transferred urgently to the theatre where he underwent an angiogram with a splenic artery embolization. The procedure was done under sedation and local anaesthesia. The right common femoral artery was accessed with 5 French vascular sheathes. The angiogram demonstrated an abnormal blood vessel with possible bleeding (Figure 2A). A Cobra head catheter and a progreat microcatheter were used to access splenic artery. Embolization was done with tornado and Nester microcoils and gelfoam slurry (Figure 2B). Satisfactory embolization was achieved successfully with no immediate complications noted.

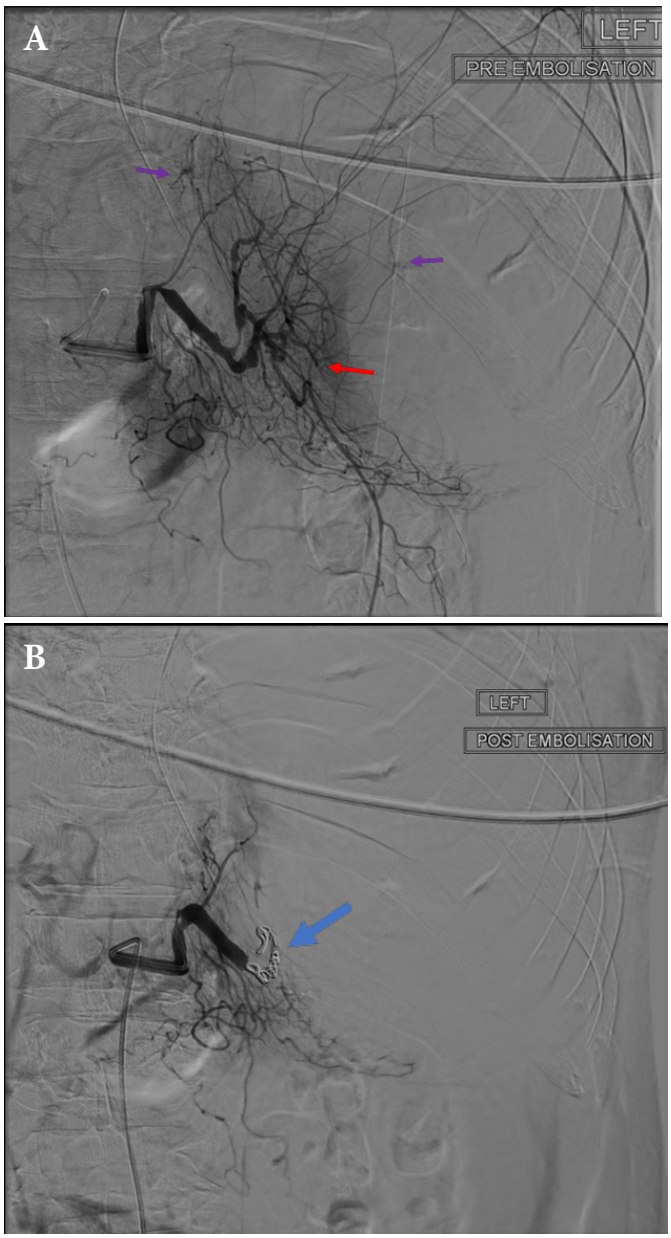

Figure 2. *Pre embolization image (A) Red arrow - shows artery disruption, dissection in keeping with acute bleeding. Purple arrow – shows minor blush - slow bleeding. Post embolization image (B) showing successful coil embolization (arrow) of the splenic artery.*

The patient was stable after the procedure and was transferred to the intensive care unit for further management. The follow-up CT scan (Figure 3) 4 days later showed no evidence of ongoing bleeding. The coil in the splenic artery was in a stable location and satisfactory perfusion of more than 50% of the splenic parenchyma was noted. The patient gradually recovered and was discharged home ten days later. He is currently being reviewed regularly as an outpatient.

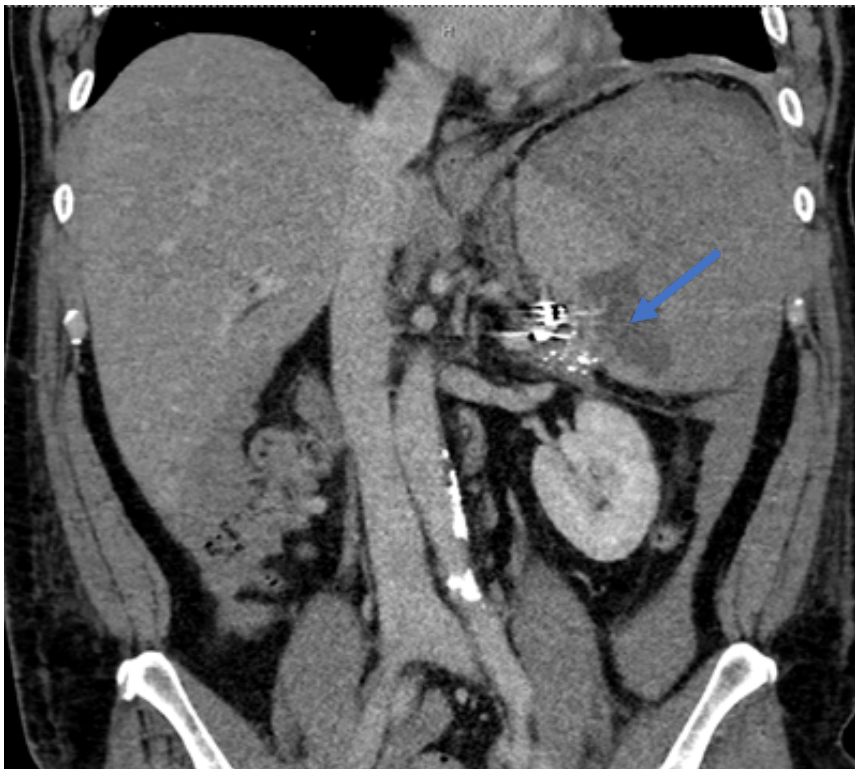

Figure 3. *Post embolization axial CT showing no evidence of ongoing bleeding. There is a reduction in the volume of perisplenic, perihepatic and intraperitoneal blood volume. The wedge shaped area of hypodensity involving the anterior aspect of the spleen is in keeping with the splenic infarct (arrow).*

Discussion

Chronic pancreatitis accounts for about 8.27% of the ASR cases, the commonest aetiology being local inflammatory processes[1, 2]. Other conditions associated with ASR are leukaemia, malaria, sarcoidosis, tuberculosis, sepsis, infectious mononucleosis and viral hepatitis[2]. The pancreas and spleen are closely related; as a result, an inflammatory process at the tail of the pancreas may disrupt the spleen resulting in several complications[1, 3].

The treatment of ASR depends upon the hemodynamic stability of the patient[1]. In case of a stable patient; a conservative treatment, angiogram with embolization or even surgery is considered[1]. However, for a hemodynamically unstable patient surgical approach is the mainstay of management[1]. The major disadvantages of splenectomy are the increased risk of susceptibility to infections which can manifest as overwhelming post splenectomy sepsis (OPSI) which has a mortality rate of >80% and also a compromised immunological function[5].

The criteria for non-operative management include being a readily stabilizable patient, a lack of rebound tenderness and guarding, blood transfusions ≤ 4 units, no loss of consciousness, age <55 years, and a radiologically confirmed splenic injury[5]. While selecting patients for conservative management, it is important to identify patients with hemorrhagic lesions that clot spontaneously[5]. For example, longitudinal lesions that parallel the long axis of the spleen might cross larger segmental vessels, thus, reducing the likelihood of spontaneous hemostasis[5]. The benefits of non-operative management are lower rates of morbidity and mortality, lower infection risk and prevention of OPSI, prevention of a non-therapeutic laparotomy and associated complications, minimal blood transfusions, decreased hospital stay, preserving an immunological function[5].

Some of the major complications (19% - 28.5%) associated with splenic artery embolization are bleeding which is the most common complication, overlooked injuries in trauma patients (diaphragmatic, pancreatic), splenic abscess, sepsis, splenic atrophy, iatrogenic arterial damage, acute renal failure after contrast administration.

Other minor complications (23%-61.9 %) include splenic infarction (significant in case of >25% of splenic parenchyma devascularization), migration of embolic material, angiographic vascular dissection, vascular damage when inserting the catheter (arterio-venous fistula), ongoing pain or hematoma at the puncture site, post-embolization syndrome (self-limiting), pulmonary complications and an allergic reaction to contrast.

Splenic injuries heal as a result of early accumulation of myofibroblasts at the lesion site[5]. This accelerated healing occurs via a regeneration process rather than collagen scarring assisting in successful management via a non-operative approach[5].

A table showing a list of publications with the outcome data of ASR managed by splenic artery embolization is given below.

Table 1. *List of publications showing the outcomes of splenic artery embolization in atraumatic splenic rupture.*

Case reports and articles on ASR and management	Outcomes
Effraemidou E, Souftas V, Kofina K, Karanikas M, Lyratzopoulos N[6].	ASR secondary to ruptured splenic artery aneurysm with haemodynamic instability treated successfully with coil embolization.
Kamalanathan KC, Barnacle AM, Holbrook C, Rees C [7].	ASR secondary to Ehler Danlos syndrome treated successfully with coil embolization.
Kim NH, Lee KH, Jeon YS, Cho SG, Kim JH [8].	ASR secondary to malaria treated successfully with Transcatheter Coil Embolization of the Splenic Artery.
Bellingham GA, Kribs S, Kornecki A, Scott L, Leaker M, Fraser DD[9].	ASR secondary to acute lymphoblastic leukemia in an 8 year old boy treated successfully with proximal splenic artery embolization.
Gaba RC, Katz JR, Parvinian A, Reich S, Omene BO, Yap FY. et al[10].	Single centre trial involving 50 patients showing splenic artery embolizations were highly successful technically with 90% procedure efficacy.

In the case discussed here, the CT scan was urgently done after hours, when patient showed signs of hemodynamic instability. This assisted in an early diagnosis of the splenic hematoma. Our patient was not fit for surgical management. Hence, we proceeded to treat him with embolization. Due to excellent teamwork and prompt recognition of the condition, we could successfully treat him by splenic artery embolization and the patient recovered well without any complications.

Conclusion

Even though there are many cases of ASR reported previously in the literature, it still remains an uncommon phenomenon; hence, this diagnosis is often overlooked.

Early recognition and prompt treatment are essential to reduce the morbidity and mortality in these patients. From this case, it is evident that we could successfully manage a hemodynamically unstable patient with embolization if a surgical option is not ideal for the patient.

References

1. Hernani BL, Silva PC, Nishio RT, Mateus HC, Assef JC, De Campos T. Acute pancreatitis complicated with splenic rupture: a case report. World J Gastrointest Surg 2015;7:219–22. doi: 10.4240/wjgs.v7.i9.219.

2. Sharada S, Olakkengil S, Rozario AP. Occult splenic rupture in a case of chronic calcific pancreatitis with a brief review of literature. Int J Surg Case Rep 2015;14:95–7. doi: 10.1016/j.ijscr.2015.06.015.

3. Gardner RJ, Preston FW. Rupture of the spleen associated with pancreatitis. JAMA 1961;177:784–5. doi: 10.1001/jama.1961.73040370016014a.

4. Moori P, Nevins EJ, Wright T, Bromley C, Rado Y. A case of a chronic pancreatic pseudocyst causing atraumatic splenic rupture without evidence of acute pancreatitis. Case Rep Surg 2016;2016:2192943. doi: 10.1155/2016/2192943.

5. Beuran M, Gheju I, Venter MD, Marian RC, Smarandache R. Non-operative management of splenic trauma. J Med Life [Internet]. 2012 Feb [cited 2020 Apr 6];5(1):47-58. Available from: https://www.ncbi.nlm.nih.gov/pmc/articles/PMC3307080/

6. Effraemidou E, Souftas V, Kofina K, Karanikas M, Lyratzopoulos N. Spontaneous rupture of a splenic artery aneurysm treated with a spleen-preserving procedure: a case report. J Surg Case Rep 2020;2020(2):rjz412. doi: 10.1093/jscr/rjz412.

7. Kamalanathan KC, Barnacle AM, Holbrook C, Rees C. Splenic rupture secondary to Vascular Ehlers-Danlos Syndrome managed by coil embolization of the splenic artery. European J Pediatr Surg Rep 2019;7(1): e83-5. doi:10.1055/s-0039-3399555.

8. Kim NH, Lee KH, Jeon YS, Cho SG, Kim JH. Spontaneous splenic rupture in a vivax malaria case treated with transcatheter coil embolization of the splenic artery. Korean J Parasitol 2015;53:215-8. doi: 10.3347/kjp.2015.53.2.215.

9. Bellingham GA, Kribs S, Kornecki A, Scott L, Leaker M, Fraser DD. Proximal splenic artery embolization in the management of splenic rupture. Pediatr Crit Care Med 2009;10(1):e1-4. doi:10.1097/PCC.0b013e31818e38fb.

10. Gaba RC, Katz JR, Parvinian A, Reich S, Omene BO, Yap FY. et al. Splenic artery embolization: a single center experience on the safety, efficacy, and clinical outcomes. Diagn Interv Radiol 2013;19:49-55. doi:10.4261/1305-3825.DIR.5895-12.1.

Case Report

COVID-19 pneumonia: The first two chest CTs in the Bamrasnaradura Infectious Disease Institute

Panyaros Kongpanya, M.D.[(1)]
Parichut Vongthawatchai, M.D.[(1)]
Priyanut Atiburanakul, M.D.[(1)]
Nayot Panitanum, M.D.[(2)]
Patama Suttha, M.D.[(2)]
From [(1)]Department of Radiology, Bamrasnaradura Infectious Disease Institute, Nonthaburi, Thailand.
[(2)]Department of Internal Medicine, Bamrasnaradura Infectious Disease Institute, Nonthaburi, Thailand.
Address correspondence to P.K. (e-mail: panyaros056@gmail.com)

Abstract

Coronavirus disease 2019 (COVID-19), caused by the severe acute respiratory syndrome coronavirus 2 (SARS-CoV-2), continues to spread rapidly around the world. We reported the first two cases of COVID-19 pneumonia who had the chest computed tomography (CT) performed at the Bamrasnaradura Infectious Disease Institute (BIDI). The chest CT findings in the two patients with COVID-19 pneumonia showed bilateral lung involvement, multifocal involvement, peripheral distribution, ground glass opacity (GGO), consolidation and GGO with interlobular septal thickening ("crazy-paving" pattern). The chest CT findings in these patients are nonspecific and overlapped with other diseases.

Keywords: COVID-19, SARS-CoV-2, Chest computed tomography, Ground glass opacity, Consolidation.

Introduction

In the late 2019, a large outbreak of pneumonia with an unknown cause was reported in Wuhan, Hubei province, China. A novel coronavirus, officially named severe acute respiratory syndrome coronavirus 2 (SARS-CoV-2), was later identified as the cause of the outbreak, named coronavirus disease 2019 (COVID-19) by the World Health Organization (WHO)[1], which is currently spreading in several countries around the world.

Case Summary

Case 1

A 35-year-old female is a health-care worker with Hemoglobin E trait. Four days before her admission to a private hospital in Bangkok, she had close contact with a COVID-19 patient at her workplace and developed a low-grade fever and a cough during the next 2 days. The result of the real-time reverse transcription polymerase chain reaction (RT-PCR) detected SARS-CoV-2 on the date of the initial symptoms. The initial chest radiograph (CXR), 2 days after the initial symptoms, was normal. She received a treatment with lopinavir/ritonavir, oseltamivir, and ganciclovir. Seven days after the initial symptoms, her CXR started to show the first abnormalities and she received treatments with chloroquine, darunavir, and ritonavir instead. Nine days after the initial symptoms, her clinical symptoms progressed and the CXR showed an increase in abnormalities. Therefore, she was referred to the Bamrasnaradura Infectious Disease Institute (BIDI) for further treatment. Her physical examination revealed the body temperature of 37.9 °C, the pulse of 110 beats per minute (bpm), a normal respiratory rate and blood pressure. The oxygen saturation was 95% under ambient air. Her complete blood count (CBC) revealed normal. The CXR made at the BIDI, 9 days after the initial symptoms, showed patchy opacities at the left perihilar region, left lower lung zone, and reticular opacities at the right perihilar region, and the right lower lung zone (Figure 1).

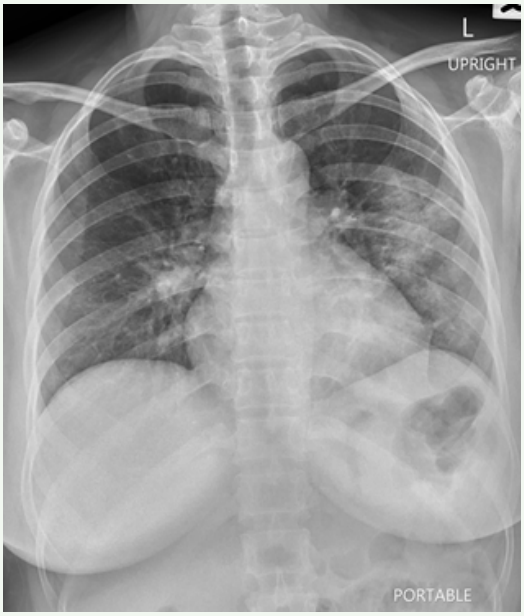

Figure 1. *Frontal anteroposterior (AP) CXR shows patchy opacities at the left perihilar region and the left lower lung zone and reticular opacities at the right perihilar region and the right lower lung zone.*

At the BIDI, she received treatments with favipiravir, darunavir, ritonavir, and chloroquine. Her fever resolved within 2 days. Seventeen days after the initial symptoms, she obtained a negative real-time RT-PCR result for SARS-CoV-2. However, the CXR showed an increase of opacities (Figure 2).

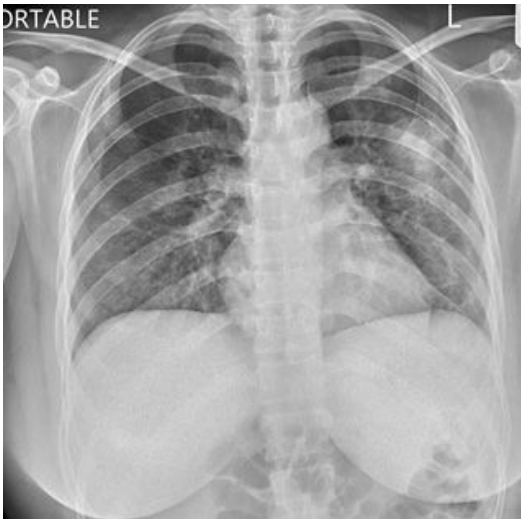

Figure 2. *Frontal AP CXR shows an increase of patchy opacities with ground glass opacities (GGO) at the left perihilar region and the left lower lung zone, and an increase of reticular opacities with GGO at the right perihilar region and the right lower lung zone.*

The non-contrast chest computed tomography (CT) was performed for evaluation, 18 days after the initial symptoms, which showed GGO with interlobular septal thickening (crazy-paving pattern) at both lungs (Figure 3). Thirty-three days after the initial symptoms, she had no symptom, and she had a follow-up non-contrast chest CT which marked resolutions of lung abnormalities (Figure 4).

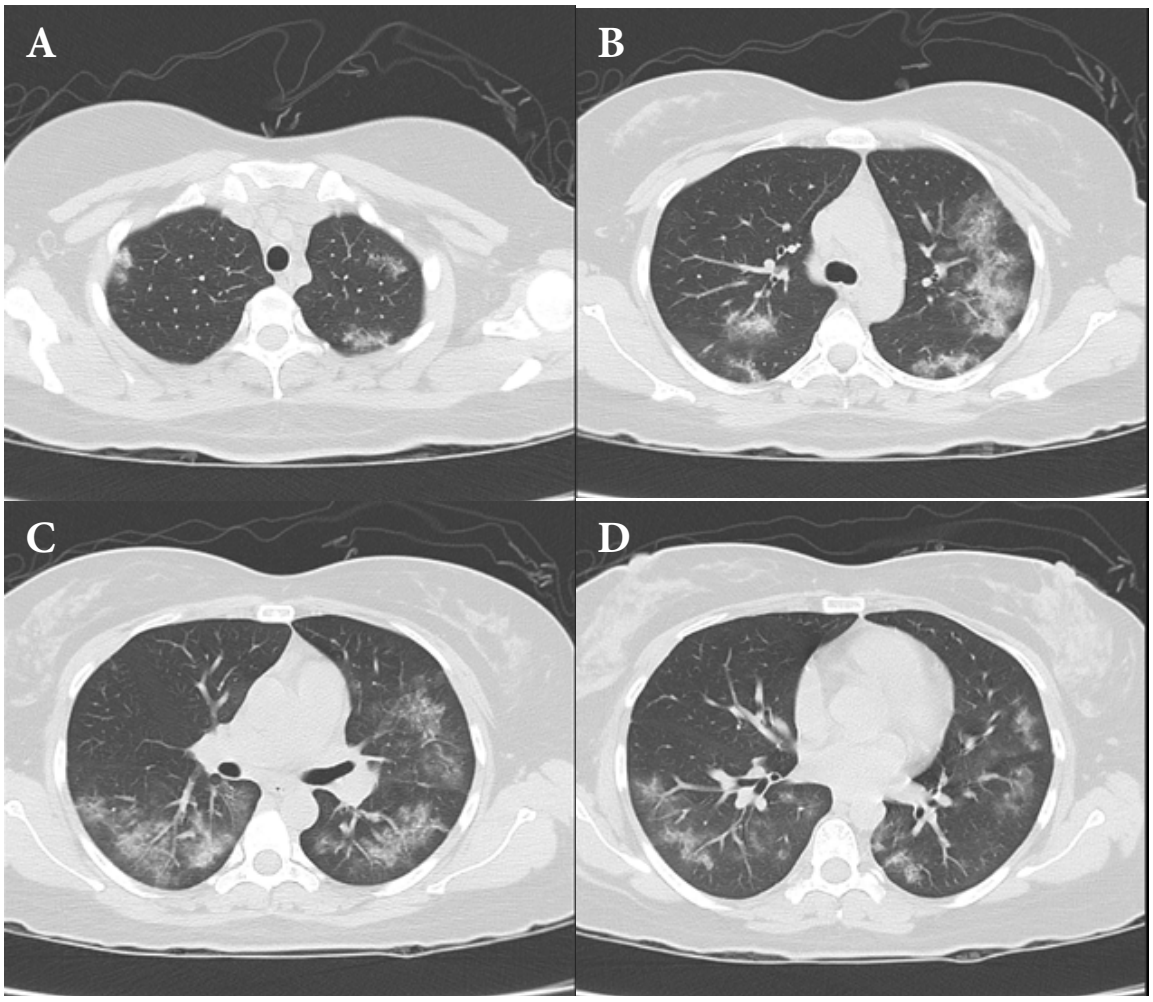

Figure 3. *Axial non-contrast chest CT (A-D) shows crazy-paving pattern at both upper lobes and both lower lobes, involving peripheral regions with presence of subpleural sparing.*

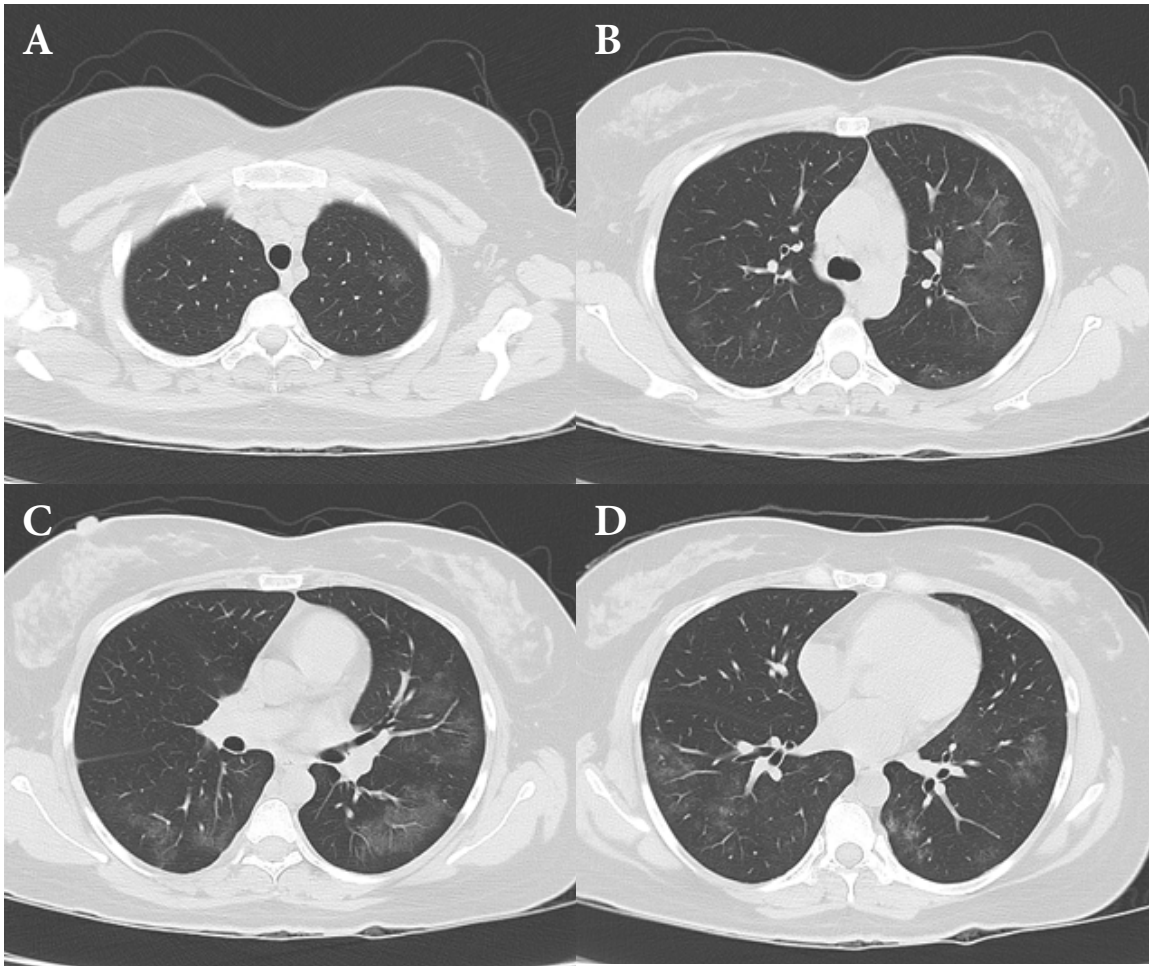

Figure 4. *Axial non-contrast chest CT (A-D) shows resolutions of crazy-paving pattern with residual GGO at both lungs.*

Case 2

A 25-year-old male presented with a sore throat and a cough for 4 days and a fever for 1 day before admission. He returned from the Republic of Korea 2 days before the initial symptoms. His physical examination revealed the body temperature of 38.2 °C, the pulse of 112 bpm, a normal respiratory rate and blood pressure. The oxygen saturation was 100% under ambient air. His CBC was normal. The result of the real-time RT-PCR detected SARS-CoV-2 and the initial CXR was a questionable abnormality at the right upper lobe, 4 days after the initial symptoms, (Figure 5).

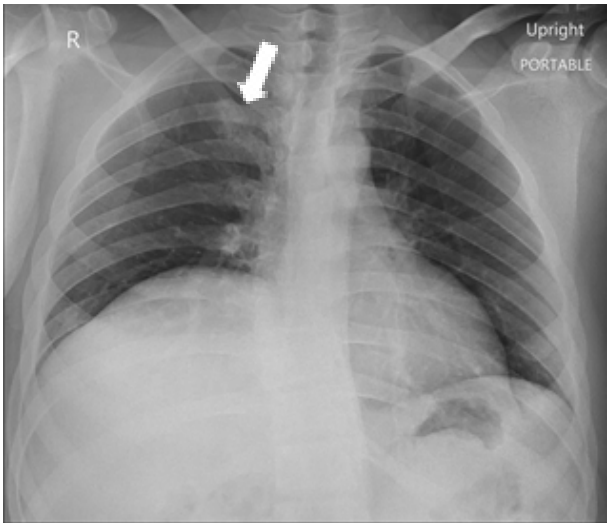

Figure 5. *Frontal AP CXR shows an opacity at the right upper lobe, superimposed on the 1st right anterior rib (arrow).*

His follow-up CXR, 7 days after the initial symptoms, showed a minimal amount of GGO at the right upper lobe (Figure 6). However, he still had a fever and more dyspnea. Therefore, a non-contrast chest CT was performed in order to evaluate the severity of the disease. The non-contrast chest CT, 7 days after the initial symptoms, showed GGO at both upper lobes and both lower lobes and consolidation was visible at the right lower lobe which could not be seen on the CXR (Figure7).

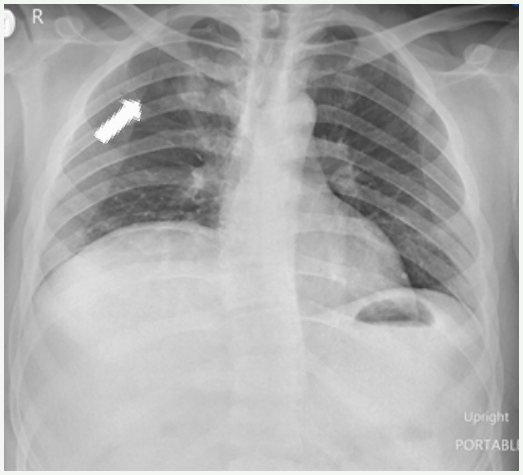

Figure 6. *Frontal AP CXR shows an increase of GGO at the right upper lobe (arrow).*

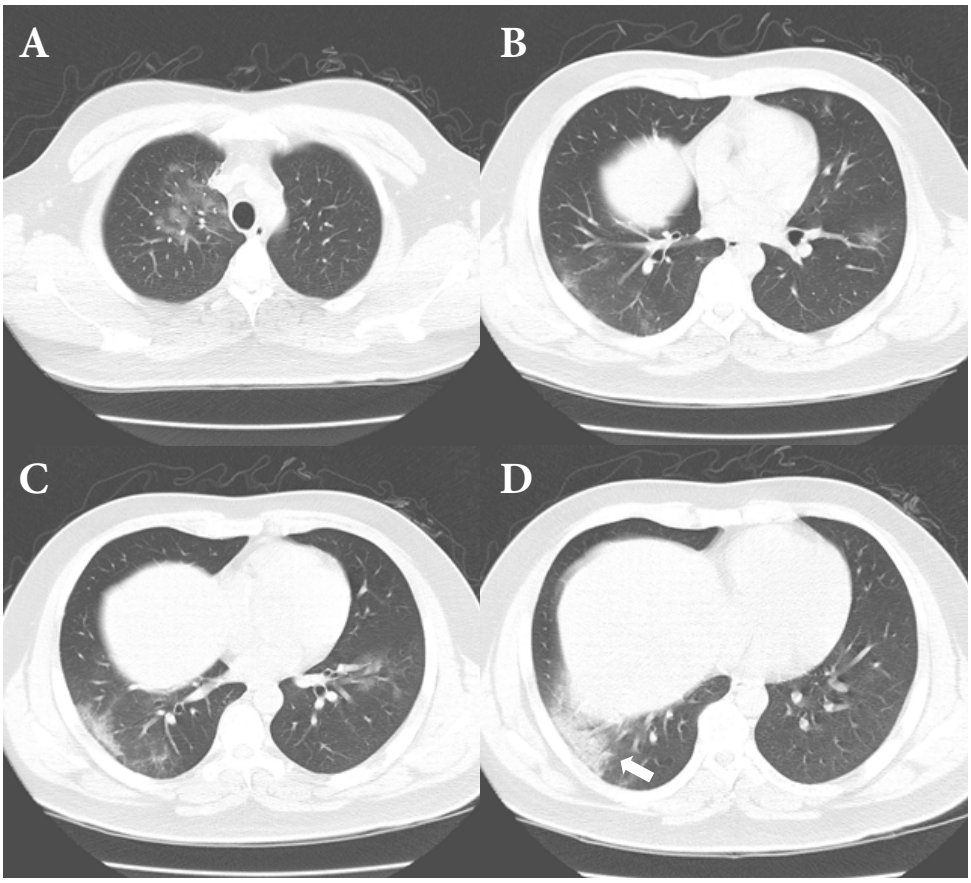

Figure 7. *The axial non-contrast chest CT (A-D) shows GGO at both upper lobes and both lower lobes with subpleural consolidation (arrow) at the right lower lobe.*

After the chest CT, he received treatments with lopinavir/ritonavir, favipiravir, darunavir, ritonavir, and chloroquine and the following day, a fever was absent. The real-time RT-PCR did not detect SARS-CoV-2, 15 days after the initial symptoms. Seventeen days after the initial symptom, he had no symptom, and he was given a follow-up non-contrast chest CT, which marked resolutions of GGO at both lungs and changes of the subpleural consolidation to GGO at the right lower lobe (Figure 8).

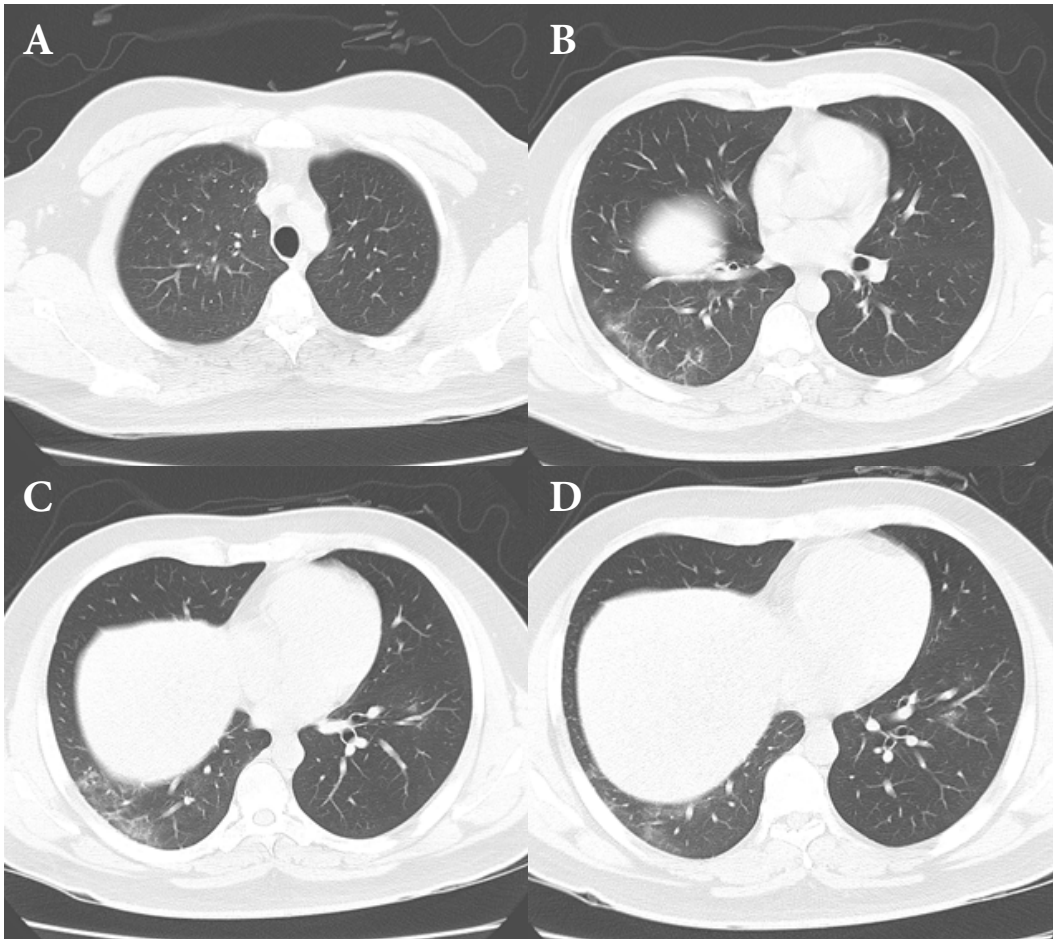

Figure 8. *The axial non-contrast chest CT (A-D) shows partial resolutions of GGO at both upper lobes and both lower lobes. The previously seen subpleural consolidation at the right lower lobe has turned into GGO.*

Discussion

The outbreak of the COVID-19 caused by SARS-CoV-2 rapidly spreads around the world. On the 11th of March 2020, the WHO made the assessment that the COVID-19 could be characterized as a pandemic[2]. The virus can be transmitted from person to person via droplets and close contact[3, 4]. The patients may be asymptomatic to critical and even fatal, most patients experience mild symptoms[5]. The most common symptoms of COVID-19 are fever and cough[5-7].

The CXR is a low sensitivity modality, 69%, in the detection of COVID-19 pneumonia in the early state[8]. The initial CXR may be normal and developed abnormalities on the follow-up CXR[8], similar to our case 1.

The chest CT findings of COVID-19 pneumonia in our cases showed bilateral and multifocal pulmonary involvements, peripheral distribution, GGO, crazy-paving pattern, absent pleural effusion and mediastinal lymphadenopathy, which are consistent with the previous studies[5, 6, 9-11]. However, the GGO and consolidation are also commonly seen in other diseases such as influenza pneumonia, adenovirus pneumonia and organizing pneumonia[12-15].

CT imaging patterns of viral pneumonia are related to the pathogenesis of viral infections. Most viral pneumonia share similar CT imaging patterns in the same families because viruses have a similar pathogenesis[12]. The outbreaks of the severe acute respiratory syndrome (SARS) in 2002-2003 and Middle East respiratory syndrome (MERS) in 2012 were caused by other strains of the coronavirus family. Therefore, chest CT findings of COVID-19 pneumonia resemble SARS and MERS, however, unilateral involvement is more common in the early acute phase of SARS and MERS[17, 18].

The follow up chest CT, 33 days and 17 days after the initial symptoms for the first case and second case respectively, showed partial resolutions of lung abnormalities. The crazy-paving pattern was no longer observed in case 1 and

the consolidation was absorbed and turned into the GGO in case 2 which are consistent with the absorption stage in the previous study[19]. Sequelae of pulmonary fibrosis, which is likely with SARS and MERS[12, 17, 20], may in our two cases be less likely to occur, because both cases were mild cases of COVID-19 pneumonia and received early treatment with antiviral medications. There were no signs of the acute respiratory distress syndrome (ARDS) and no symptoms on the day of the follow up chest CT. Neither the crazy-paving pattern was found, probably due to the recovering stage[19]. However, detection of pulmonary fibrosis should still be followed up in the long term.

Many patients of COVID-19 were admitted at the BIDI. There were a few cases of COVID-19 pneumonia which the chest CT was performed. Although the chest CT has a high sensitivity to detect lung abnormalities and the previous studies[5, 6, 10] suggested that the chest CT may be useful for screening or initial diagnosis of COVID-19, we do not use the chest CT screening for diagnosis of COVID-19 pneumonia, because the clinicians usually use clinical which correlates with the CXR. Therefore, it is sufficient for the diagnosis and treatment. The chest CT is mostly performed in case of a questionable abnormal CXR for an early diagnosis and treatment.

Conclusion

The chest CT findings of COVID-19 pneumonia are nonspecific and are overlapped with other viral infections and other diseases. Although the chest CT has a high sensitivity in the detection of lung abnormalities and is very useful for early diagnosis and treatment, it is not recommended as a first-choice modality to diagnose COVID-19 pneumonia.

References

1. World Health Organization [Internet]. Geneva: WHO; c2020 [cited 2020 Mar 20]. Naming the coronavirus disease (COVID-2019) and the virus that causes it; [about 2 screens]. Available from: https://www.who.int/emergencies/diseases/novel-coronavirus-2019/technical-guidance/naming-the-coronavirus-disease-(covid-2019)-and-the-virus-that-causes-it.

2. World Health Organization [Internet]. Geneva: WHO; 2020 [cited 2020 Mar 20]. Coronavirus disease 2019 (COVID-19) situation report – 51; [about 9 p.]. Available from: https://www.who.int/docs/default-source/coronaviruse/situation-reports/20200311-sitrep-51-covid-19.pdf?sfvrsn=1ba62e57_10.

3. Carlos WG, Dela Cruz CS, Cao B, Pasnick S, Jamil S. Novel Wuhan (2019-nCoV) coronavirus. Am J Respir Crit Care Med. 2020 Feb 15;201(4):P7-8. doi: 10.1164/rccm.2014P7.

4. Li Q, Guan X, Wu P, Wang X, Zhou L, Tong Y, et al. Early transmission dynamics in Wuhan, China, of novel coronavirus-infected pneumonia. N Engl J Med 2020;382:1199-207. doi: 10.1056/NEJMoa2001316.

5. Zhao S, Zhong Z, Xie X, Yu Q, Liu J. Relation between chest CT findings and clinical conditions of coronavirus disease (COVID-19) pneumonia: a multi center study. AJR Am J Roentgenol 2020 ;214:1072-7. doi: 10.2214/AJR.20.22976.

6. Xu X, Yu C, Qu J, Zhang L, Jiang S, Huang D, et al. Imaging and clinical features of patients with 2019 novel coronavirus SARS-CoV-2. Eur J Nucl Med Mol Imaging 2020;47:1275-80. doi: 10.1007/s00259-020-04735-9.

7. Lai CC, Shih TP, Ko WC, Tang HJ, Hsueh PR. Severe acute respiratory syndrome coronavirus 2 (SARS-CoV-2) and coronavirus disease-2019 (COVID-19): the epidemic and the challenges. Int J Antimicrob Agents 2020 Mar;55(3):105924. doi: 10.1016/j.ijantimicag.2020.105924.

8. Wong HYF, Lam HYS, Fong AH, Leung ST, Chin TW, Lo CSY, et al. Frequency and distribution of chest radiographic findings in COVID-19 positive patients. Radiology 2020;296(2):E72-8. doi: 10.1148/radiol.2020201160.

9. Shi H, Han X, Jiang N, Cao Y, Alwalid O, Gu J, et al. Radiological findings from 81 patients with COVID-19 pneumonia in Wuhan, China: a descriptive study. Lancet Infect Dis 2020;20:425-34. doi: 10.1016/S1473-3099(20)30086-4.

10. Li Y, Xia L. Coronavirus disease 2019 (COVID-19): role of chest CT in diagnosis and management. AJR Am J Roentgenol 2020;214:1280-6. doi: 10.2214/AJR.20.22954.

11. Zhou S, Wang Y, Zhu T, Xia L. CT features of coronavirus disease 2019 (COVID-19) pneumonia in 62 patients in Wuhan, China. AJR Am J Roentgenol 2020;214:1287-94. doi: 10.2214/AJR.20.22975.

12. Koo HJ, Lim S, Choe J, Choi SH, Sung H, Do KH. Radiographic and CT features of viral pneumonia. Radiographics 2018;38:719-39. doi: 10.1148/rg.2018170048.

13. Franquet T. Imaging of pulmonary viral pneumonia. Radiology 2011;260:18-39. doi: 10.1148/radiol.11092149.

14. Samir A, El-Nekiedy AAM, Baess AI, Rizk AM. H1N1 viral pneumonia: spectrum of chest HRCT findings. Egypt J Radiol Nucl Med 2016;47:1293-301.

15. Faria IM, Zanetti G, Barreto MM, Rodrigues RS, Araujo-Neto CA, Silva JL, et al. Organizing pneumonia: chest HRCT findings. J Bras Pneumol 2015;41:231-7.

16. Hosseiny M, Kooraki S, Gholamrezanezhad A, Reddy S, Myers L. Radiology perspective of coronavirus disease 2019 (COVID-19): lessons from severe acute respiratory syndrome and Middle East Respiratory Syndrome. AJR Am J Roentgenol 2020;214:1078-82. doi: 10.2214/AJR.20.22969.

17. Ooi GC, Daqing M. SARS: radiological features. Respirology 2003;8 Suppl (Suppl 1):S15-9. doi: 10.1046/j.1440-1843.2003.00519.x.

18. Das KM, Lee EY, Langer RD, Larsson SG. Middle East respiratory syndrome coronavirus: What does a radiologist need to know? AJR Am J Roentgenol 2016;206:1193-201. doi: 10.2214/AJR.15.15363.

19. Pan F, Ye T, Sun P, Gui S, Liang B, Li L, et al. Time course of lung changes at chest CT during recovery from coronavirus disease 2019 (COVID-19). Radiology 2020;295:715-21. doi: 10.1148/radiol.2020200370.

20. Memish ZA, Perlman S, Van Kerkhove MD, Zumla A. Middle East respiratory syndrome. Lancet 2020;395:1063-77. doi: 10.1016/S0140-6736(19)33221-0.

Clinico-Radiologic-Pathologic Correlation

Distal common bile duct adenoma

Khanin Khanungwanitkul, M.D.[(1)]
Tanawat Pattarapuntakul, M.D.[(2)]
Naruemon Wisedopas, M.D.[(3)]
From [(1)]Department of Radiology, Faculty of Medicine, Prince of Songkla University, Songkhla, Thailand.
[(2)]Department of Internal Medicine, Faculty of Medicine, Prince of Songkla University, Songkhla, Thailand.
[(3)] Department of Pathology, Faculty of Medicine, Chulalongkorn University, Bangkok, Thailand.
Address correspondence to K.K. (e-mail: khanin14@gmail.com)

Keywords: Common bile duct adenoma, Benign tumor, Bile duct, Imaging findings, Clinical presentation.

Introduction

Adenoma is a benign tumor usually found in the gastrointestinal tract[1, 2]. However, it is rarely found in the extrahepatic bile duct. Although it is a benign tumor, it may cause an aggressive clinical course like a malignant disease which is more common[2]. Furthermore, there is still limited understanding of its nature, imaging finding and management of the disease. We reported a case of distal common bile duct adenoma which includes its clinical course, imaging finding and pathologic result.

case summary

An 86-year-old man presented with intermittent abdominal pain for 2 months. He had an underlying malignant gastric stromal tumor with hepatic metastasis diagnosed for 7 years, having been treated with Imatinib. The physical examination reveals low-grade fever, no pale or icteric sclera, a normal liver span, a normal active bowel sound, and no ascites. A complete blood count shows mild anemia, a normal white blood count and platelets. The liver function test shows slightly elevated serum alanine transaminase and aspartate aminotransferase of 289 and 815 U/L, respectively.

Imaging, endoscopic, and pathologic findings

Magnetic Resonance Imaging (MRI) with a hepatocyte specific contrast agent was performed (Figure 1). The study shows gastric mass and multiple cystic lesions in the liver which are decreased in size from the prior study (not shown). The diagnosis of these lesions reveals an improvement of his underlying gastrointestinal stromal tumor (GIST). Furthermore, the MRI also shows diffused dilatation of the bilateral IHDs and CBD with a round-shaped filling defect in the distal CBD. Regardless of its enhancement, the interpreted radiologist made the impression of CBD stone. The patient was then referred to perform ERCP for a stone removal.

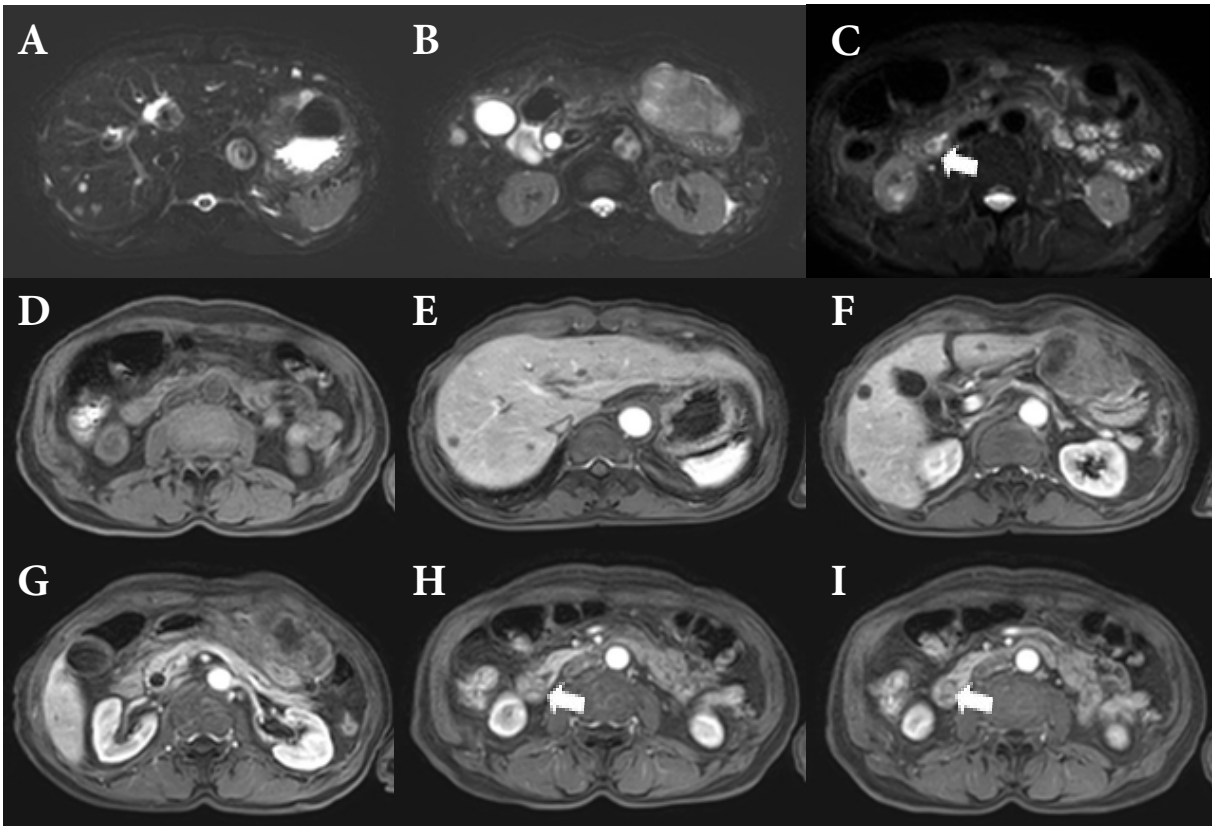

Figure 1. *Magnetic Resonance Imaging (MRI) with a hepatocyte specific contrast agent. Axial T2-weighted fat-suppressed fast spin-echo images (A-C) showing moderate dilation of extra- and intrahepatic bile ducts with an oval-shaped intra-luminal filling defect (arrow). Pre (D) and arterial-phase post-contrast axial T1w-3Dfs SGR images (E-I) demonstrating a small smoothly well-defined mildly enhancing nodule in the distal part of a common bile duct (arrow).*

The endoscopic retrograde cholangiography shows a small well-demarcated intraluminal nodule at the distal common bile duct (Figure 2A). The lesion shows no definite stalk, so the stone was diagnosed, and balloon extraction is performed. The soft tissue lesion was accidentally obtained instead of the stone. The real time endoscopy shows a yellowish soft tissue with a lobulated surface (Figure 2B). The tissue was sent for a pathologic evaluation. After the balloon extraction with the presumed total removal of the lesion, a biliary double pigtail stent was inserted in the biliary tract. Three months later, ERCP was repeated, and the stent was removed. Complete occlusion cholangiogram was done in order to expand the CBD lumen for good visualization, which confirmed that there was no recurrence of the tumor.

Tissue pathology shows bile duct adenoma, a tubular pattern. It comprises groups of glands lined with cuboidal cells, possessing low-grade dysplastic nuclei and eosinophilic cytoplasm without an obvious high-grade dysplastic change or malignant transformation. Invasion is not identified (Figure 3).

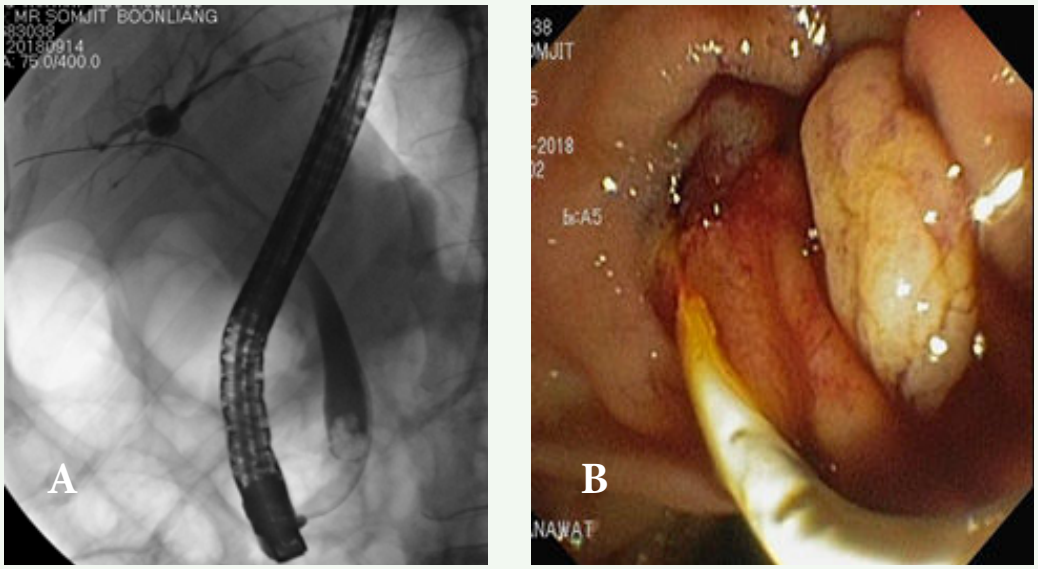

Figure 2. *Endoscopic retrograde cholangiography (A) shows a small well-demarcated intraluminal nodule in the distal part of the common bile duct. A stone was diagnosed. Endoscopic photograph (B) at ampulla exhibits that the extracted nodule from the distal part of the common bile duct was a yellowish soft tissue and a smoothly lobulated surface.*

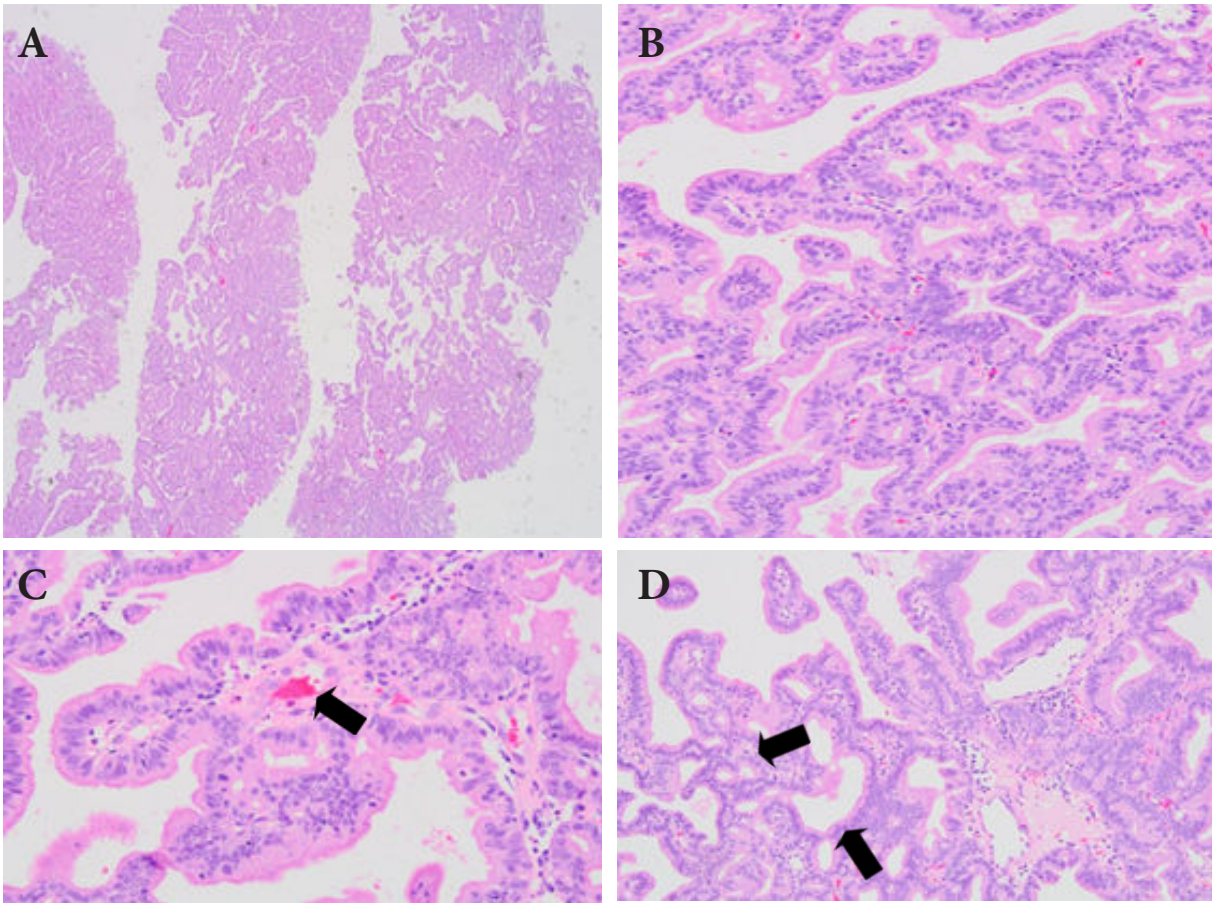

Figure 3. *Tissue pathology obtained from a distal common bile duct. Low power field microscopy (A) shows a polypoid lesion High power filed (HPF) (B) image shows a mixed tubulopapillary pattern with cuboidal cell linings, morphologically similar to gallbladder epithelium. HPF image (C) shows a papillary structure with a fibrovascular core (arrow). HPF image (D) shows a complex tubular pattern (arrow).*

Discussion

Adenoma is a benign tumor of glandular tissue. Gastrointestinal adenoma is usually located in the colon, the rectum, and less frequently, the small bowel[1]. All benign extrahepatic bile duct tumors, including adenoma, are rare[2]. Biliary adenoma are usually found in a surgically removed gallbladder, but can occur in the extrahepatic biliary tree[3]. The World Health Organization Classification of common bile duct adenomas includes tubular adenoma, papillary and tubulopapillary adenoma, biliary cystadenoma, and papillomatosis (or adenomatosis)[1].

Clinical presentations of extrahepatic biliary adenoma are obstructive jaundice, right upper quadrant abdominal pain (biliary colic), ascending cholangitis, biliary pancreatitis and an abnormal liver function test[2]. Cholangiography usually demonstrates adenomas as intraluminal mucosal polypoid lesions similar to gastrointestinal adenoma or polyp. Without demonstration of their stalks, differentiation from a stone is difficult. Densities on computed tomography, signals on Magnetic Resonance Imaging and internal enhancement on either computed tomography or Magnetic Resonance Imaging could confirm their neoplastic nature. However, differentiation from the more common malignant tumors such as extrahepatic polypoid cholangiocarcinoma or ampullary adenocarcinoma is difficult[4].

A surgical resection is the first choice of treatment, an endoscopic resection in an inoperable status by snare polypectomy or forceps has been reported[3, 5]. There are no reports of the use of an ablative therapy with radiofrequency ablation. There is limited understanding of the malignant potential of biliary adenomas, and no definite guideline for management. However, malignant transformation has also been reported[6]. So prior studies recommended aggressive surgical intervention and close postoperative surveillance when diagnosis of an extrahepatic biliary adenoma[3, 6].

In our case, we used balloon extraction and accidentally removed the tumor. We decided to follow up the patient without a surgical resection but also showed no recurrence within 3 months. A few prior studies also show no recurrence after the local resection, but all reports had a follow-up period of less than 1-2 years[6, 7].

Conclusion

Common bile duct adenoma is a rare benign tumor of the extrahepatic biliary tree. Both clinical presentation and imaging finding have limited potential to rule out malignancy. A pathological report is essential for definite diagnosis. Due to report of malignant transformation, surgical resection is the first choice of treatment. However, there were reported cases of endoscopic resection as well as balloon extraction in our report which showed no local recurrence.

Acknowledgement: This case is one of the cases presented in the clinic-radio-pathologic session of Nanthana-Kriangkrai-Chotiwattanaphan (NKC) 13th annual meeting which was held on 2nd May 2019 in Phuket, Thailand. We would like to express our sincere gratitude to the NKC Institute for giving us the opportunity to distribute this interesting case.

References

1. Albores-Saavedra J, Scoazec JC, Wittekind C, Sripa B, Menck HR, Soehendra N, et al. Carcinoma of the gallbladder and extrahepatic bile ducts. In: Hamilton SR, Aaltonen LA,editors. World Health Organization classification of tumours: pathology and genetics of tumours of the digestive system. Lyon, France: IARC Press; 2000. p. 204-14.

2. Xu HX, Chen LD. Villous adenoma of extrahepatic bile duct: contrast-enhanced sonography findings. J Clin Ultrasound 2008;36:39-41. doi: 10.1002/jcu.20361.

3. Loh KP, Nautsch D, Mueller J, Desilets D, Mehendiratta V. Adenomas involving the extrahepatic biliary tree are rare but have a aggressive clinical course. Endosc Int Open 2016;4: E112-7. doi: 10.1055/s-0041-107897.

4. Aparajita R, Gomez D, Verbeke CS, Menon KV. Papillary adenoma of the distal common bile duct associated with a synchronous carcinoma of the peri-ampullary duodenum JOP 2008;9:212-5.

5. Pracchayakul V, Aswakul P, Kachintorn U. Incidental removal of distal common bile duct adenoma after plastic stent placement. Endoscopy 2012;44 Suppl 2 UCTN:E11-2. doi: 10.1055/s-0031-1291497.

6. Ariche A, Shelef I, Hilzenrat N, Dreznik Z. Villous adenoma of the common bile duct transforming into a cholangiocarcinoma. Isr Med Assoc J 2002;4:1149-50.

7. Bahuth JJ, Winkley JH. Benign tumor of the common bile duct. Calif Med 1966;307-9.

Pictorial Essay

Ultrasound imaging of acute scrotum: Pictorial review with etiological correlation

Anitha Mandava, M.B.B.S., D.M.R.D., D.N.B.
Veeraiah Koppula, M.B.B.S., D.N.B.
Rohit Yalamanchili, M.B.B.S, M.D.
Dilip Yadav, MBBS, D.N.B.
Juluri Rakesh, M.B.B.S, M.D.
From Department of Radiodiagnosis, Basavatarakam Indo American Cancer Hospital & Research Institute, Telangana, India.
Address correspondence to A.M. (e-mail: kanisri@gmail.com)

Abstract

High resolution ultrasound with color Doppler is the first-line imaging investigation in the evaluation of acute scrotum. It plays a crucial role in distinguishing urological emergencies necessitating immediate surgical exploration from those that can be managed conservatively. Acute scrotal pathologies can involve the scrotal sac or its contents like testis, epididymis and testicular appendages and could range from benign, self-limiting conditions to emergencies. In this pictorial essay, we briefly review the ultrasonographic technique, scrotal anatomy and characteristic imaging features of various pathologies presented as acute scrotum.

Keywords: Acute scrotum, Testis, High resolution ultrasound, Color doppler.

Introduction

Acute scrotum is defined as scrotal pain, with or without swelling and redness, of acute onset[1,2]. Ultrasonography (US) with high resolution ultrasound probe and color Doppler is the primary imaging modality in the evaluation of acute scrotal pathology. In this article, we review and discuss sonographic appearances of both common and uncommon conditions presenting with acute scrotum.

The etiology of acute painful scrotum is varied, ranging from benign and self-limiting conditions to those that are medical and surgical emergencies (Table 1). The commonly encountered cases of acute scrotum in clinical practices are acute epididymo-orchitis, torsion of testis or testicular appendages and traumatic injuries[3]. Prompt imaging workup and rapid diagnosis are essential to avoid adverse outcomes as few of these conditions need immediate surgical and urologic intervention[4]. US imaging of acute scrotum is quick, cost effective and accurate with almost 100% sensitivity in the detection and differentiation of intra- and extratesticular diseases[3-7].

US of scrotum is performed with the patient lying down in the supine position while supporting the scrotum by positioning a folded towel or sheet between the legs. Linear array (4-13 MHz) and convex curved array (1-8 MHz) transducers are used for scrotal and abdominal ultrasonography, respectively. Transverse and sagittal images of bilateral testis and epididymis are obtained in gray-scale and color Doppler modes. The size, echogenicity, and blood flow of each testis and epididymis are compared to the contralateral side [8,9]. The spermatic cord and the relevant extratesticular structures are also evaluated in suspicious cases of testicular torsion[6,8]. Doppler sonography (spectral and color/power Doppler imaging) is used with low-flow detection settings in all cases of acute scrotal pain[7].

Table 1. *Differential diagnosis of acute scrotum according to etiology.*

Etiology	Possible diagnoses
Inflammation, Infections	Scrotum: Scrotal wall cellulitis, Pyocele Perineum: Fournier's gangrene Testis and epididymis: Acute epididymo-orchitis, Acute epididymitis, Acute orchitis, Emphysematous epididymo- orchitis, Testicular abscess
Vascular Causes	Testis: Testicular torsion, Testicular appendages: Torsion of testicular appendages. Venous plexus: Varicocele
Trauma	Testis: Contusion, laceration, Testicular fracture, Testicular rupture, hematocele, hematoma. Scrotum: Acute hydrocele, hematocele, hematoma.
Tumors	Testis: Primary: Germ cell tumor (seminoma), Nonseminomatous germ cell tumor, Lymphoma Secondary: Lymphoma, Leukaemia, Metastases Scrotum: Extratesticular malignancy
Miscellaneous	Obstructed/ strangulated inguinoscrotal hernias, Spermatic cord hydrocele or cyst

Normal sonographic scrotal anatomy: The scrotum has two testes, one in each hemiscrotum separated by a septum. The scrotal wall is 2-8 mm in thickness[10]. Tunica vaginalis is derived from the processus vaginalis of the peritoneum with the inner visceral layer enveloping most of the testis and epididymis, and the outer parietal layer lining the internal spermatic fascia of the scrotal wall. Hydroceles or other fluid collections (eg, blood or pus) may accumulate in the potential space between these layers. The normal adult testis is ovoid and approximately measures 5x3x3 cm with homogeneous, intermediate echotexture[11]. Epididymal head and tail are at the superior and inferior poles of the testis, respectively and are isoechoic to testis. The testicular appendages are the remnants of embryonic ducts and the only testicular appendages seen on ultrasound are the appendix testis and the appendix epididymis. The scrotum is supplied by the external pudendal, internal pudendal and the cremasteric arteries and the venous drainage follows the arterial supply. The testes are supplied by the testicular arteries, branches of

the abdominal aorta and the venous drainage is via the pampiniform plexus of draining veins into the testicular veins that drain into the inferior vena cava on the right side and the renal vein on the left side[12].

Inflammation and infections: Scrotal wall cellulitis is due to an acute bacterial infection of the skin and subcutaneous tissues. It can spread quickly and in untreated or incompletely treated cases it may progress to form scrotal abscess. HRUS in cellulitis shows an increase in the thickness of the scrotal wall with anechoic to hypoechoic areas in the skin and subcutaneous tissues of scrotal wall (Figure 1A) [13].

Fournier's gangrene is a life-threatening necrotizing fasciitis of the perineal, genital and perianal regions with a high mortality rate. It occurs more commonly in males, especially in diabetics, alcoholics and those who are immunocompromised. US may show the thickening of the subcutaneous tissues and fascia of the perineum with abnormal fluid and air collections within these tissues (Figure 1B). Castleberg et al have proposed a mnemonic "STAFF" for rapidly diagnosing Fournier's gangrene by using bedside ultrasound evaluation for Subcutaneous thickening, Air, and Fascial Fluid (STAFF)[14].

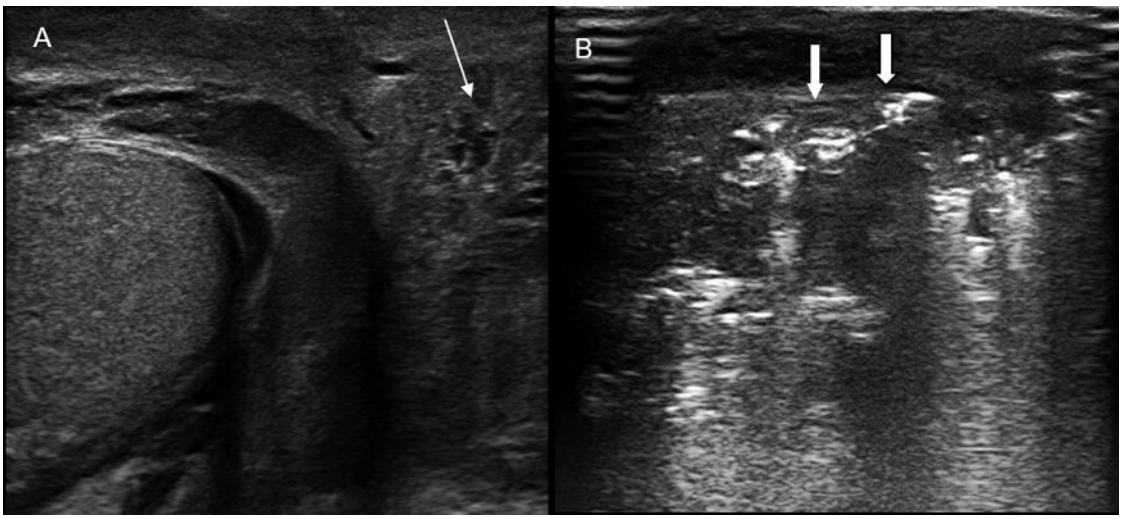

Figure 1. (*A) Scrotal wall cellulitis: Scrotal wall thickening with anechoic to hypoechoic areas (thin arrow). (B) Fournier's gangrene: Subcutaneous gas within the scrotal wall seen as numerous discrete hyperechoic foci with reverberation artefacts (thick arrows), the sonographic hallmark.*

Epididymo-orchitis is the most common cause of acute scrotum in boys and adults and, if left untreated, may lead to abscess formation and testicular infarction[4,7,13]. US features include enlargement of the epididymis, testis or both with decreased echogenicity, reactive hydrocele and scrotal wall thickening. The sonographic hallmark of epididymo-orchitis is the highly increased vascularity of epididymis and testis seen on color Doppler imaging (Figure 2A,B). Retrograde bacterial infection from a lower urinary tract infection is the usual cause of epididymo-orchitis, but rarely, it could also be from a viral infection. Infections can be limited to only epididymis leading to acute epididymitis, the epididymal head being the most commonly affected region (Figure 3). Isolated orchitis without epididymitis is rare, but can occur in mumps infection.

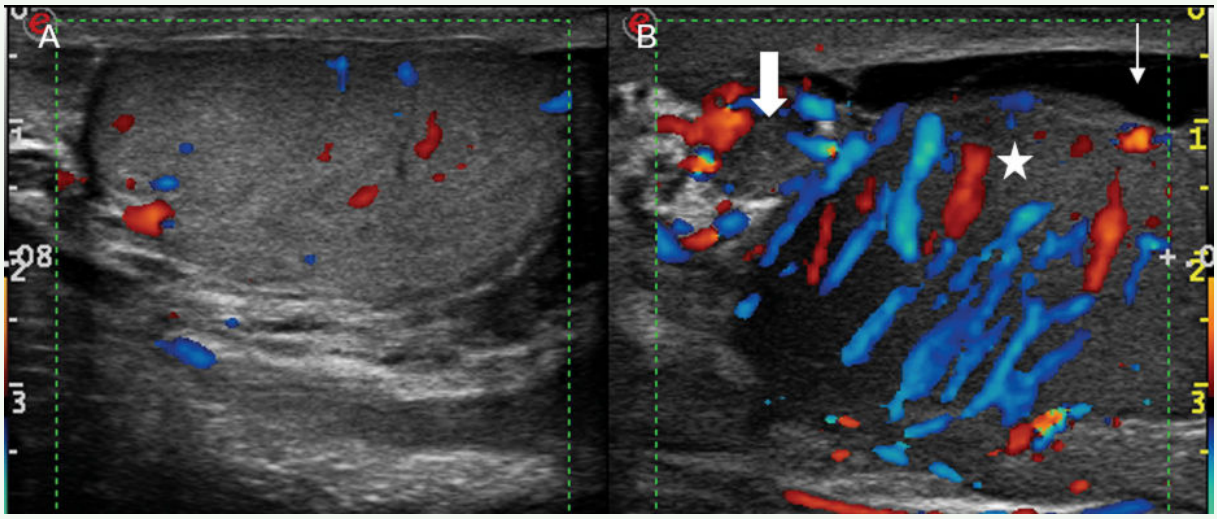

Figure 2. *Acute epididymo-orchitis: Split screen US shows (A) normal right testis (B) enlarged hypoechoic left testis (*) and epididymis (thick arrow) with marked hyperemia and reactive hydrocele (thin arrow).*

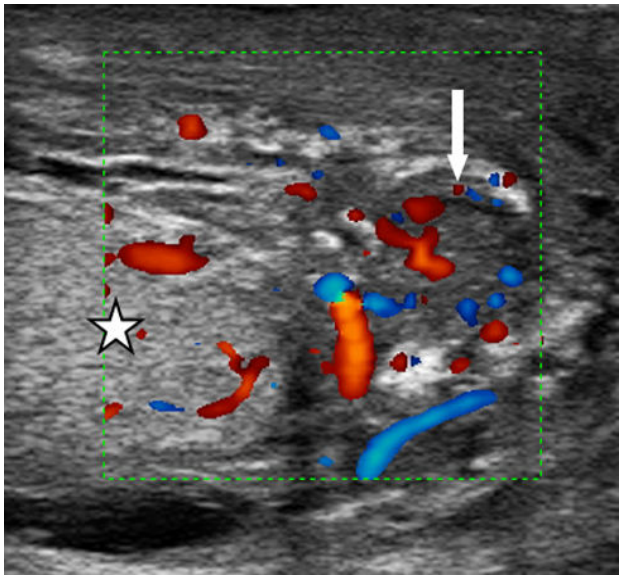

Figure 3. *Acute epididymitis: Enlarged epididymis (thick arrow) with variable echotexture and increased blood flow.*

Emphysematous epididymo-orchitis is an uncommon, acute inflammatory process of epididymis and testis, characterized by the presence of air within the tissue. It is a rare urologic emergency that needs prompt diagnosis and treatment. US shows intratesticular air as focal bright hyperechoic areas with distal acoustic shadowing that can be moved or displaced by transducer pressure (Figure 4)[15]. Intratesticular abscess and pyocele develop secondary to trauma and testicular infarction or can occur in advanced or untreated cases of epididymo-orchitis[13,16] US features of testicular abscess include intratesticular areas of complex hypoechogenicity showing low-level internal echoes, shaggy irregular walls and peripheral hyperaemic margins on color Doppler (Figure 5A). Focal orchitis or abscess may be difficult to differentiate from testicular tumour but associated epididymal involvement and scrotal skin thickening are suggestive of infection rather than tumour[16]. Rupture of an intratesticular abscess into the space between the layers of the tunica vaginalis results in pyocele. Pyocele is a surgical emergency as it can progress rapidly causing testicular damage, sepsis or complications like Fournier's gangrene. Early diagnosis, broad spectrum antibiotics, surgical drainage and in a few cases orchidectomy are indicated in the management. Pyoceles on US may be seen as complex anechoic intrascrotal collections with internal echoes, septations, loculations and skin thickening (Figure 5B).

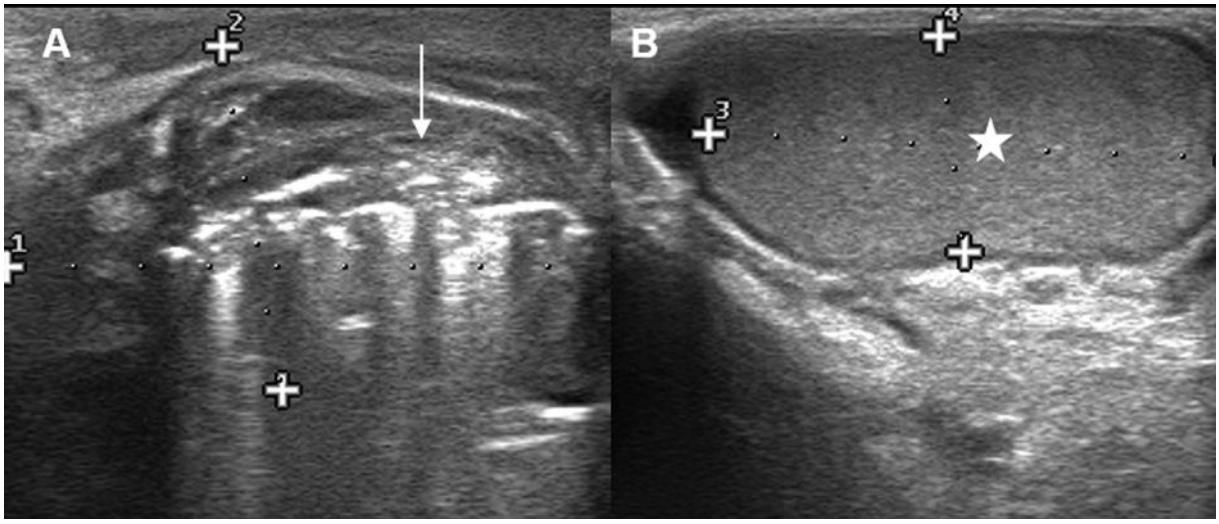

Figure 4. *Emphysematous epididymo orchitis: Split screen US shows (A) normal left testis (*) (B) enlarged, ill-defined right testis with multiple linear and punctate bright, highly reflective hyperechoic foci (arrow).*

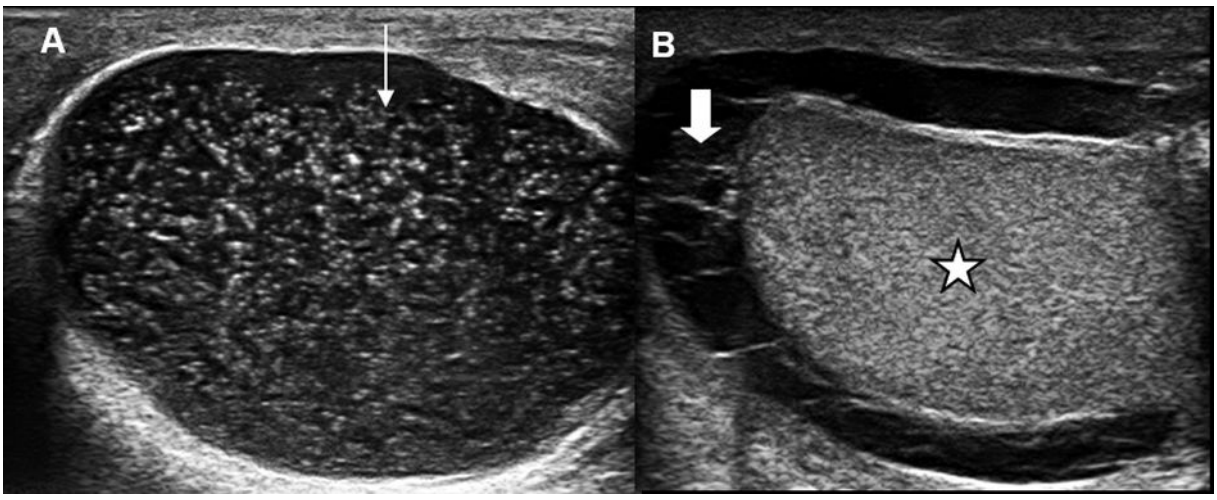

Figure 5. (*A) Intratesticular abscess: Enlarged testis with low-level intratesticular internal echoes (thin arrow). (B) Pyocele: Free fluid in the scrotum with newly developed septations, echogenic debris and thickened scrotal skin (thick arrow) and normal testis (*).*

Vascular Causes: Testicular torsion can occur at any age, but is most common in young adolescents and it is an emergency that needs immediate surgical exploration to salvage the testis[2,6]. US features and the testicular salvage rate depend on the duration of ischemia and the degree of torsion that can range from 180° to 720° or more[9]. Acute testicular torsion with a viable testis can be normal on HRUS; hence, absence of detectable blood flow in the testis on colour Doppler US is essential to confirm testicular torsion (Figure 6A)[9]. As ischemia progresses, the testis becomes enlarged and hypoechoic. Later, the testis may develop heterogeneous echotexture secondary to haemorrhage and infarction and these findings may suggest nonviability[4]. US of spermatic cord cranial to the testis at the site of torsion can show an oedematous round or ovoid intrascrotal cord with the epididymal head wrapped around it, appearing as a whirlpool, or a doughnut[6]. The real-time whirlpool sign is seen on gray scale as well as color Doppler imaging (Figure 6B,C) in both complete and incomplete torsions and it is the most definitive sign of torsion with 100% specificity and sensitivity[6].

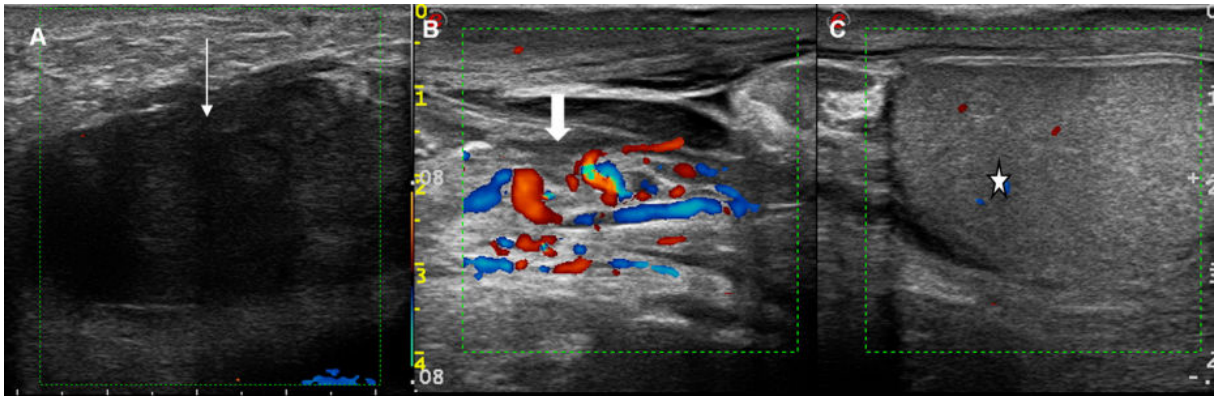

Figure 6. (*A) Acute torsion: Hypoechoic testis with completely absent vascularity on color Doppler (thin arrow). (B,C) Split screen color Doppler US shows "Whirl pool" sign of testicular torsion due to the twisting of spermatic cord (thick arrow) and avascular testis (*).*

Torsion of testicular appendages can present as the acute scrotum and the role of US in this condition is to exclude testicular torsion and acute epididymo-orchitis[9]. US appearance of torsion of the appendages of the testes is variable. The twisted appendage may be isoechoic, hypoechoic, or hyperechoic to the testis and epididymis with increased vascular flow around it while the adjacent testis or epididymis show normal vascularity (Figure 7)[3,9].

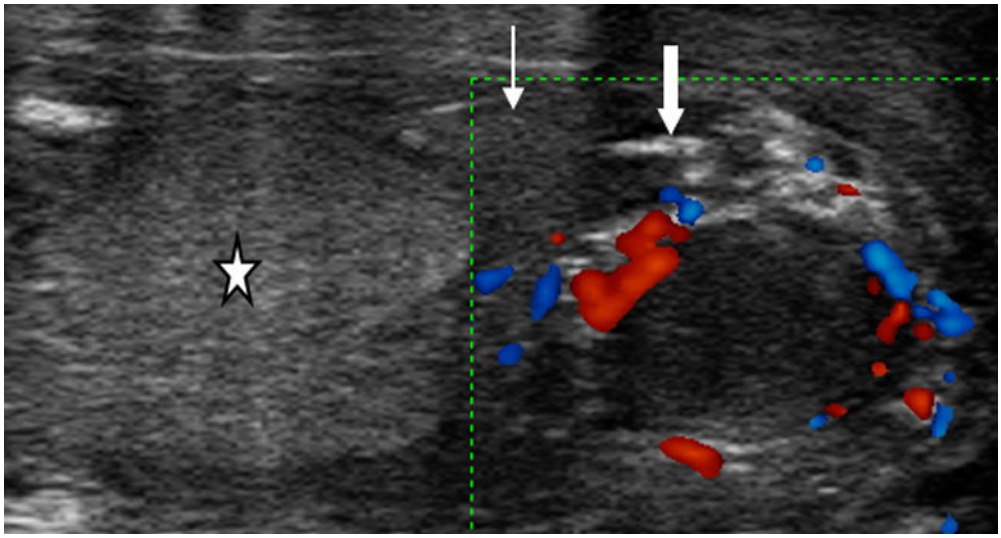

Figure 7. *Appendiceal torsion: Torsed testicular appendage seen as a circular mass of variable echogenicity with increased peripheral flow around it (thick arrow). Normal testis(*) and epididymis (thin arrow).*

Varicoceles are abnormally dilated, tortuous veins of the pampiniform plexus. Most often they are asymptomatic or cause dull pain and discomfort but rarely can they mimic the pain of acute testicular torsion. Color Doppler US is nearly 100% sensitive and specific in the diagnosis of varicoceles[3,9,13]. US features include dilated venous plexus (>2-3 mm diameter) with serpiginous appearance posterior and lateral to the testis within the spermatic cord (Figure 8). Varicoceles increase in size on standing and show a flow reversal with valsalva maneuver; hence, scanning in the upright position and valsalva maneuver should be performed while evaluating for varicoceles[9].

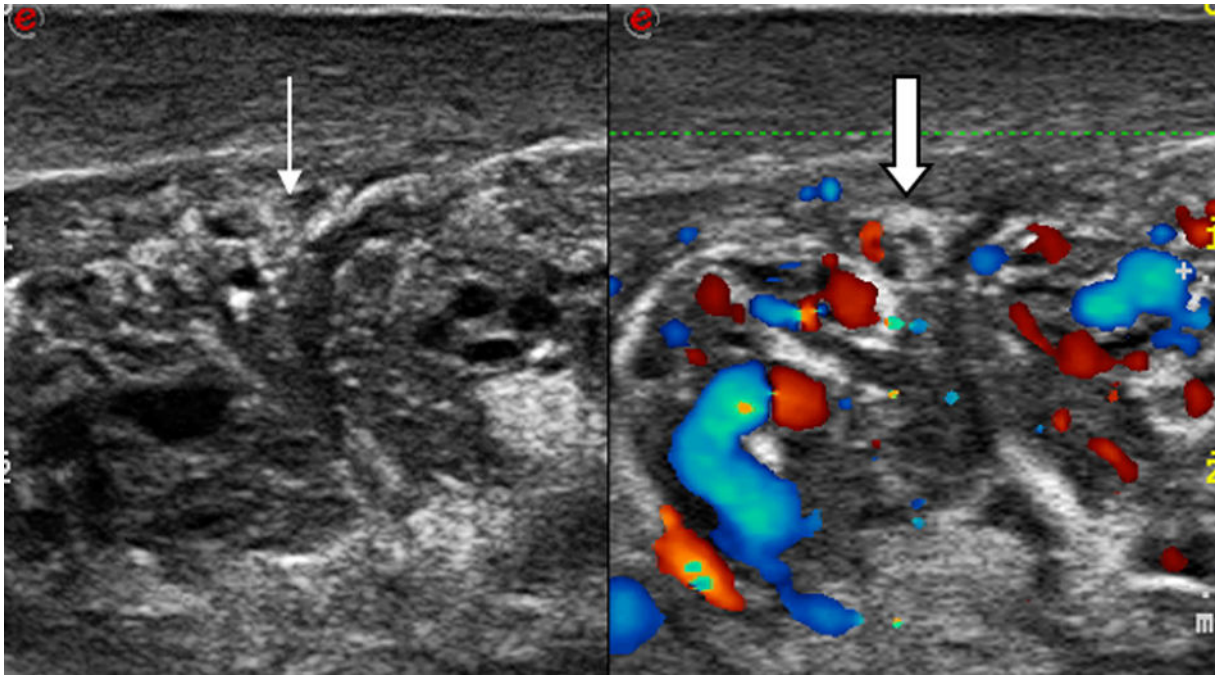

Figure 8. *Varicocele: Split screen gray scale and color Doppler US show multiple tortuous, dilated veins of pampiniform plexus.*

Trauma: Testicular trauma is the third most common cause of acute scrotal pain and can be blunt or penetrating[13,18]. Scrotal trauma can result in contusions, lacerations, fracture, or rupture of the testis. On US, contusions are seen as areas of heterogeneous appearance in the testis due to focal intratesticular bleeding (Figure 9A). Testicular fracture is seen as a break in the normal testis, while the testicular shape and contour are maintained (Figure 9B). Testicular rupture is seen as the discontinuity of tunica albuginea with hemorrhage and extrusion of the testicular contents into the scrotal sac (Figure 9C)[17,18]. Immediate surgical exploration and/or orchidectomy is needed in testicular rupture and in all the cases of scrotal trauma with impaired perfusion. Diagnostic delays or errors can lead to ischemia, infarction, necrosis and even testicular atrophy with the risk of reduced fertility and infection[17,18].

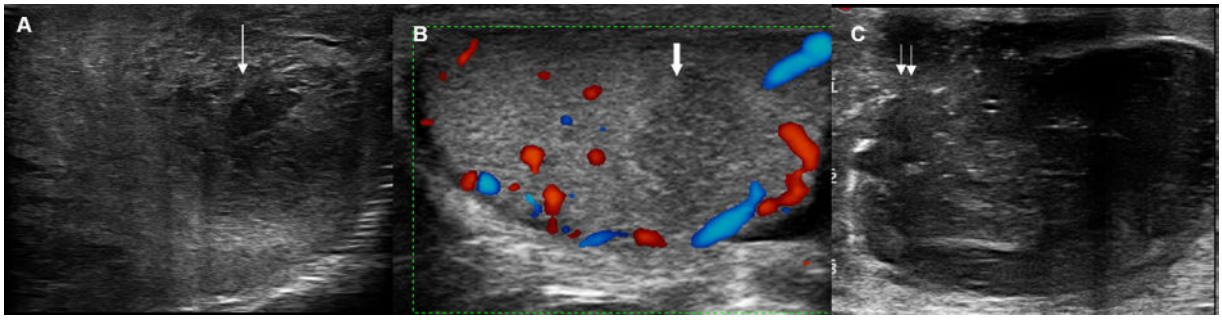

Figure 9. (*A) Testicular Contusion: Focal hypoechoic, heterogenous areas in a case of blunt trauma to the testis (thin arrow). (B) Testicular fracture: Hypoechoic band extending across the testicular parenchyma (thick arrow). (C) Testicular rupture: Contour abnormality of the testis with disruption of the tunica albuginea and extrusion of testicular parenchyma through a defect in the superior pole (double arrows).*

Scrotal trauma can also produce intra or extratesticular fluid collections like acute hydroceles, hematoceles, and hematomas. Hydrocele is an abnormal collection of serous fluid accumulating between the visceral and parietal layers of the tunica vaginalis. It occurs in up to 25% of all major cases of trauma and hydrocele can also be seen in acute scrotal pathologies like epididymo-orchitis, torsion and neoplasms[5]. On US, hydrocele appears as an anechoic fluid collection surrounding the anterolateral aspects of the testis. Traumatic hematoceles and hematomas occur as a collection within the tunica vaginalis or testis due to extra or intra testicular bleeding, respectively and have variable presentations on US[5]. Acute hematoceles are anechoic to echogenic (Figure 10A), whereas older hematoceles appear as a fluid collection with low-level internal echoes, fluid-fluid levels and septations [13,18]. Acute hematomas appear hyperechoic, and later become complex and are avascular on color Doppler (Figure 10B).

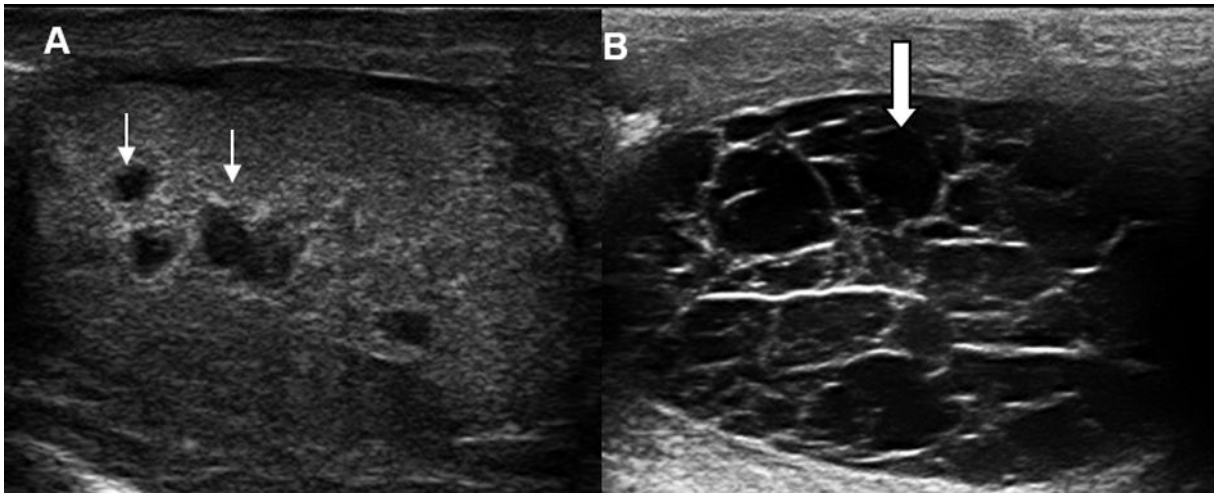

Figure 10. (*A) Intratesticular hematocele: Small fluid collections seen as anechoic foci (thin arrows) within the testis in a case of blunt trauma to scrotum. (B) Intratesticular hematoma: Complex fluid collection with low-level internal echoes, fluid-fluid levels and septations seen within the testis (thick arrow) in a case of trauma.*

Testicular tumors: Testicular tumors are generally painless but acute pain may occur secondary to epididymo-orchitis or aemorrhage within the tumor. US appearance of intratesticular tumors is non-specific and most tumors are homogenously hypoechoic in echotexture[19]. The commonest germ cell tumor is seminoma, and on gray-scale US, it appears as a homogeneous hypoechoic lesion (Figure 11)[13,19]. Testicular tumors may also sometimes be hyperechoic in echotexture. Nonseminomatous germ cell tumors and extratesticular tumors can be irregular with ill-defined margins and appear heterogenous in echotexture with echogenic foci due to internal calcification and hemorrhage (Figure 12)[3,19]. Testicular lymphomas can be primary or secondary non-Hodgkin lymphomas, bilateral in 40% and are the most common testicular tumours after the age of 60[13,19]. US may show a homogeneously hypoechoic testis with diffuse enlargement (Figure 13) or multiple focal hypoechoic masses[13,19]. Metastases to the testes are rare and occur most commonly from the cancers of the prostate, lung, kidney, colon, melanoma and leukaemia (Figure 14)[19].

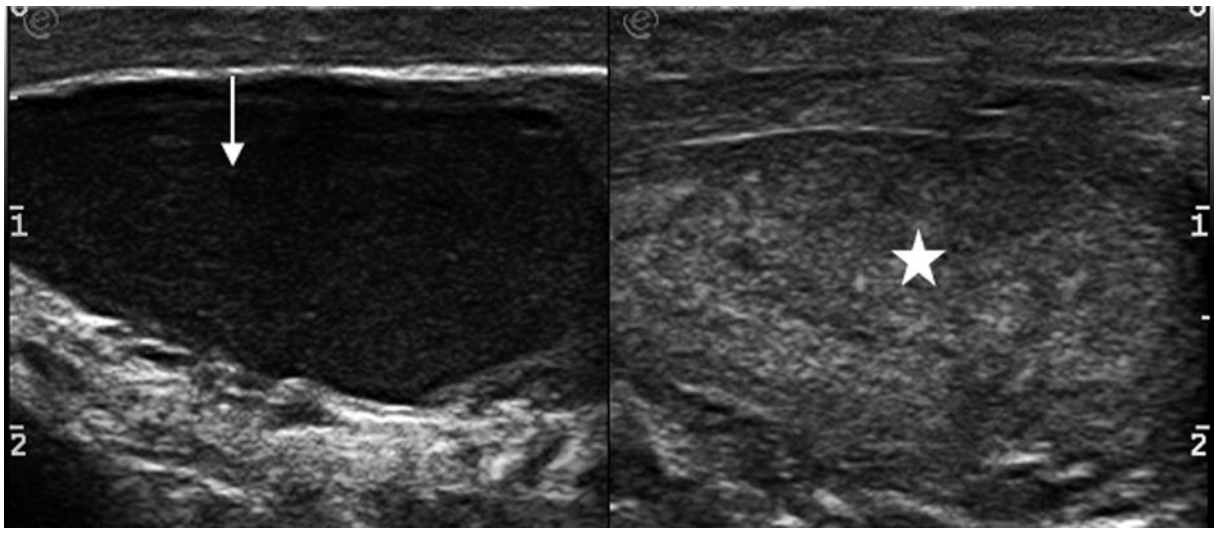

Figure 11. *Seminoma: Split screen US shows diffusely hypoechoic right testis (thin arrow) compared to the normal left testis (*) in a case of seminoma.*

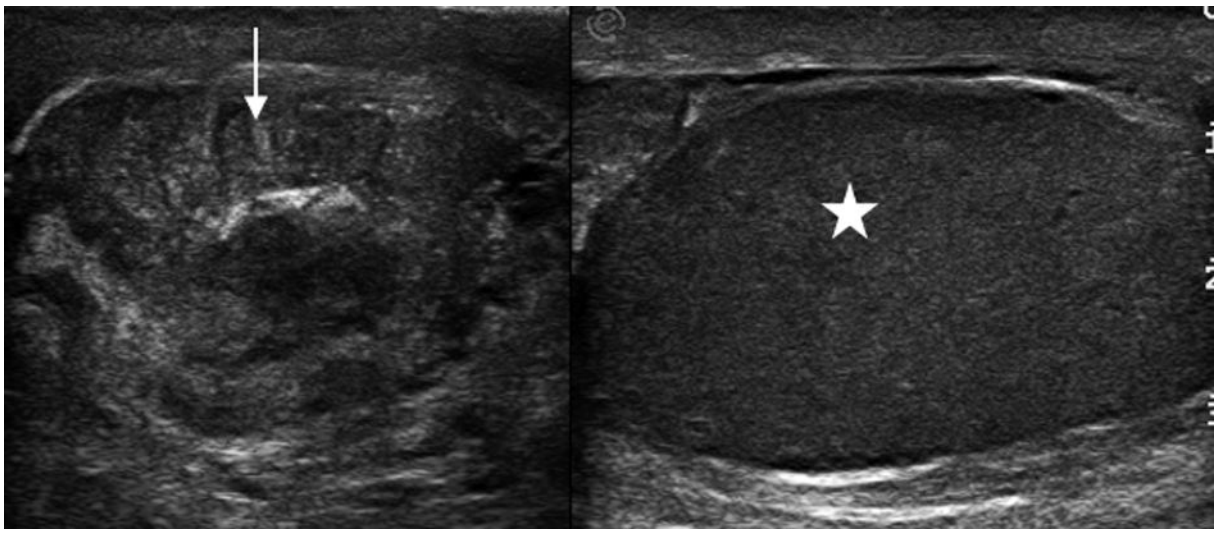

Figure 12. *Germ cell tumor: Split screen US shows hypoechoic heterogenous mass with hyperechoic foci in the right testis (thin arrow) compared to the normal left testis (*) in a case of nonseminomatous germ cell tumor of testis.*

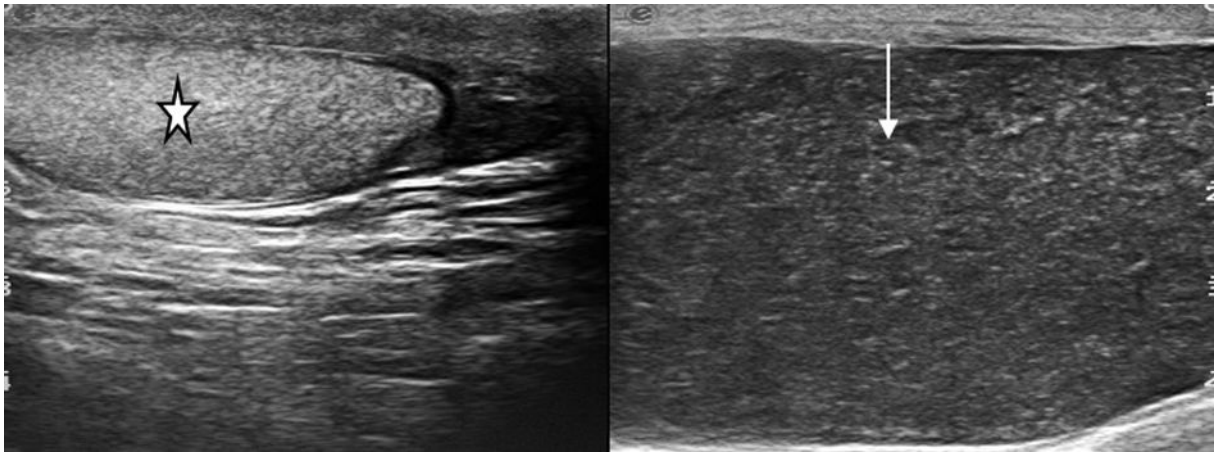

Figure 13. *Lymphoma: Split screen US shows enlarged hypoechoic left testis (thin arrow) and the normal right testis (*) in a case of Non Hodgkin's lymphoma.*

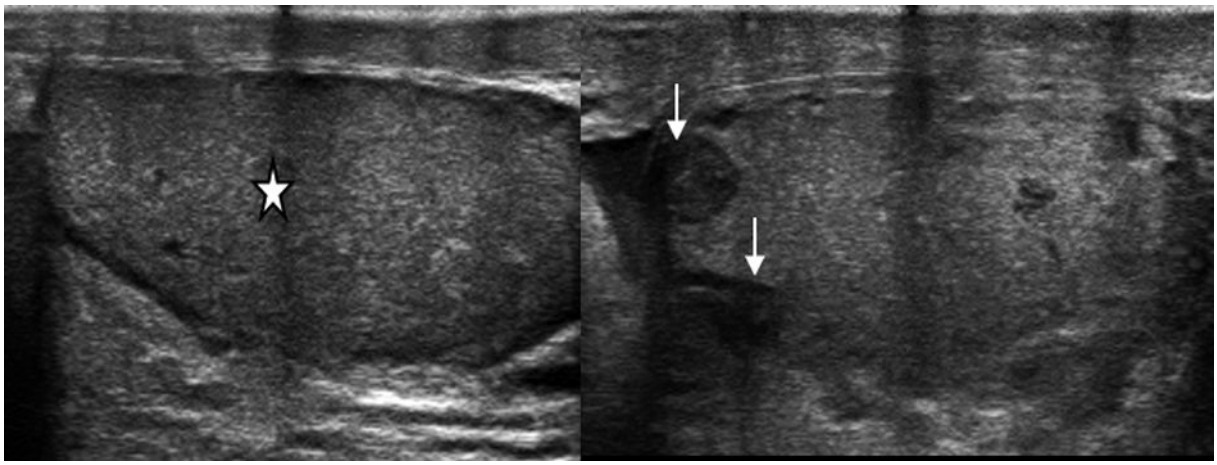

Figure 14. *Leukemia: Split screen US shows small hypoechoic deposits (thin arrows) in right testis and normal left testis (*) in a child with leukemia.*

Miscellaneous: Inguinoscrotal hernias with incarcerated and strangulated bowel loops can present as an acute scrotum (Figure 15). A case of spermatic cord hydrocele presented as an acute scrotum was observed during our evaluation. A spermatic cord hydrocele or a cyst is a rare condition and is seen as a loculated fluid collection along the spermatic cord (Figure 16).

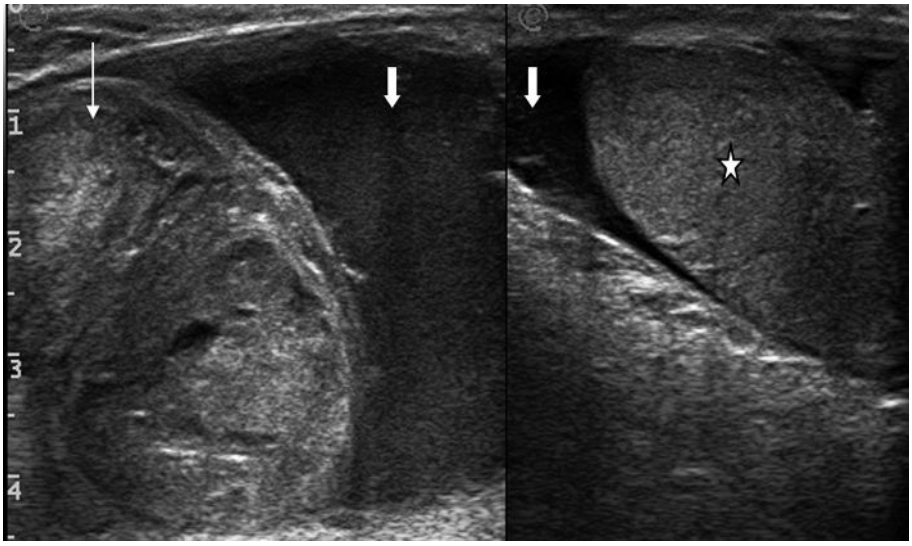

Figure 15. *Intrascrotal inguinal hernia: Split screen US shows omentum and bowel loops in the scrotal sac (thin arrow), hydrocele with low level internal echoes (thick arrows) and displaced normal testis (*).*

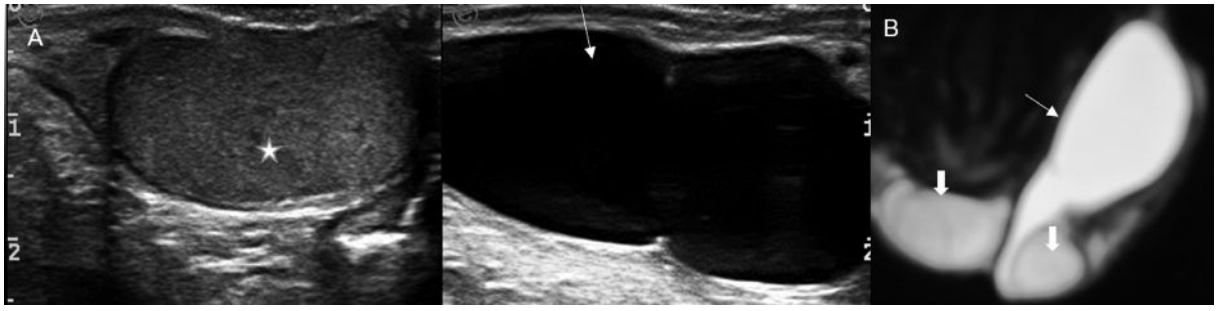

Figure 16. *(A) Spermatic cord cyst: Split screen gray scale US shows the normal testis (*) and an oblong cystic lesion (thin arrow) along the course of the left spermatic cord. (B) Coronal T2W MRI image shows hyperintense left spermatic cord cyst (thin arrow) arising from the lower pole of the left testis, extending superiorly between the two normal testes (thick arrows).*

Incidental lesions in acute scrotum: A few common and uncommon lesions that are seen during the evaluation of an acute scrotum are epididymal cysts (Figure 17A), intra- or extra testicular calcifications i.e scrotoliths (Figure 17B) and testicular microlithiasis (Figure 18). They are mostly incidental findings without any clinical significance but testicular microlithiasis has a reported association with testicular neoplasia and annual US follow-up is recommended for at least several years after the diagnosis[9,20].

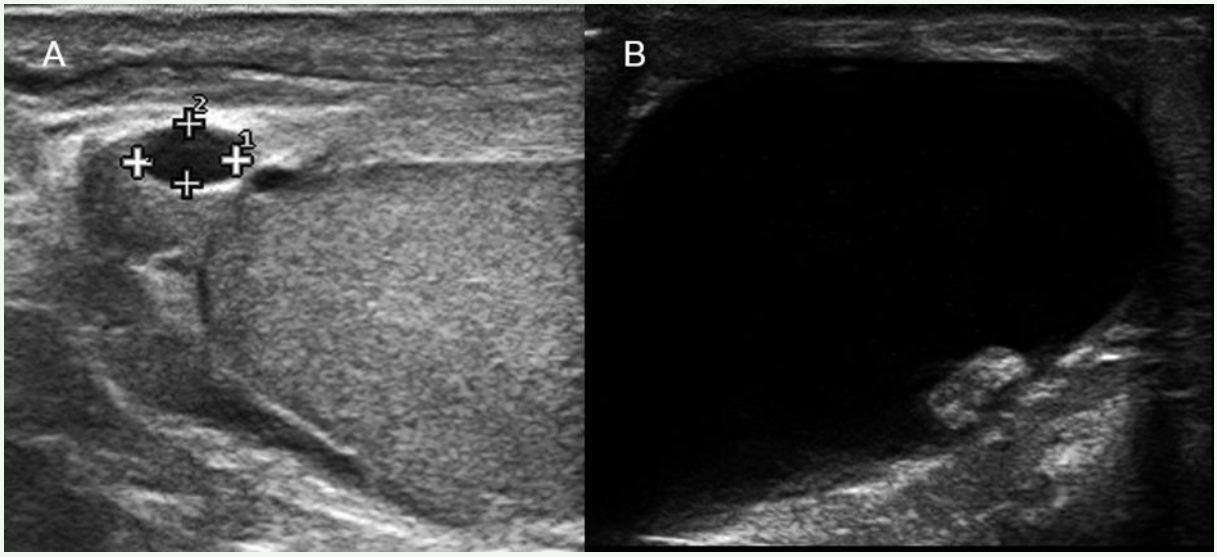

Figure 17. (*A) Epididymal cyst: Well defined anechoic lesion (arrow) in the head of the epididymis. (B) Scrotolith or scrotal pearl: Extra testicular macro-calcification within the scrotum (arrow).*

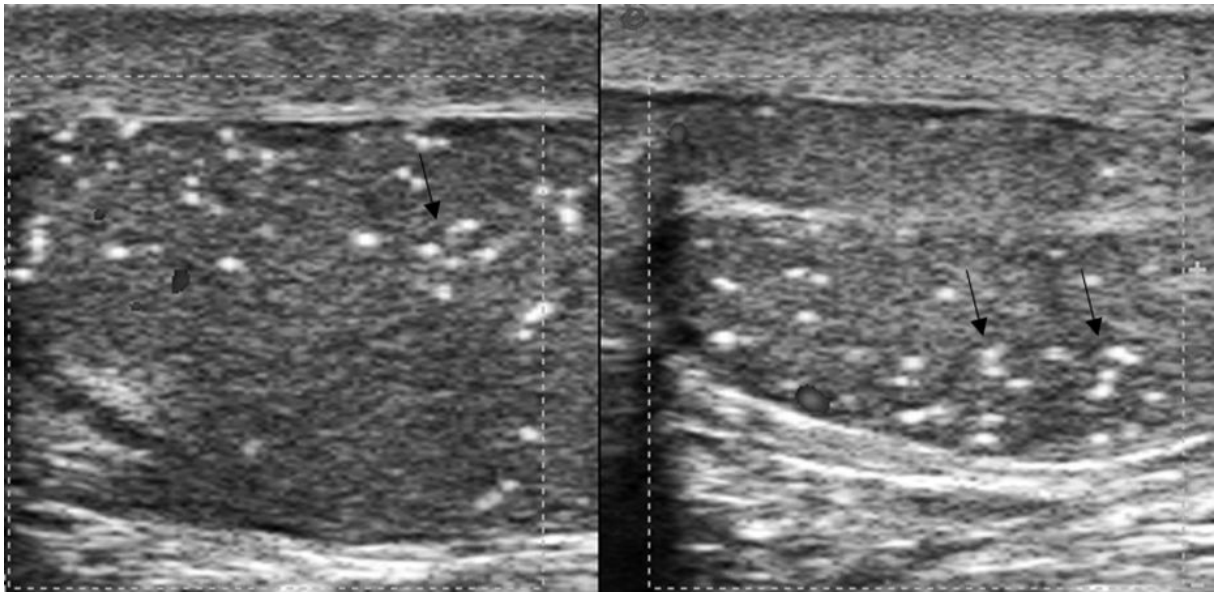

Figure 18. *Testicular microlithiasis: Multiple 2-3 mm nonshadowing echogenic foci seen in the testis (arrows).*

Conclusion

The correlation of ultrasound findings with appropriate clinical history and background can give accurate diagnosis in cases presenting with an acutely painful scrotum. In an emergency setting, US enables us to differentiate surgical emergencies like testicular torsion, scrotal abscess from acute nonsurgical causes like epididymo-orchitis. Familiarity with the imaging features of each entity including incidental lesions can avoid diagnostic errors that can significantly alter the management and outcome.

References

1. McAndrew HF, Pemberton R, Kikiros CS, Gollow I. The incidence and investigation of acute scrotal problems in children. Pediatr Surg Int 2002;18:435-7. doi: 10.1007/s00383-002-0806-3.

2. Günther P, Rübben I. The acute scrotum in childhood and adolescence. Dtsch Arztebl Int 2012;109:449-57;quiz 458. doi: 10.3238/arztebl.2012.0449.

3. Patiala B. Role of color doppler in scrotal lesions. Indian J Radiol Imaging 2009;19:187-90. doi: 10.4103/0971-3026.54874.

4. Avery LL, Scheinfeld MH. Imaging of penile and scrotal emergencies. Radiographics 2013;33:721-40. doi: 10.1148/rg.333125158.

5. Resende DAQP, Souza LRMF, Monteiro IO, Caldas MHS. Scrotal collections: pictorial essay correlating sonographic with magnetic resonance imaging findings. Radiol Bras 2014;47:43-8.

6. Vijayaraghavan SB. Sonographic differential diagnosis of acute scrotum: real-time whirlpool sign, a key sign of torsion. J Ultrasound Med 2006;25:563-74. doi: 10.7863/jum.2006.25.5.563.

7. Ragheb D, Higgins JL Jr. Ultrasonography of the scrotum: technique, anatomy, and pathologic entities. J Ultrasound Med 2002;21:171-85. doi: 10.7863/jum.2002.21.2.171.

8. Guideline developed in collaboration with the American College of Radiology; Society for Pediatric Radiology; Society of Radiologists in Ultrasound. AIUM practice guideline for the performance of scrotal ultrasound examinations. J Ultrasound Med 2015;34:1-5. doi: 10.7863/ultra.34.8.15.13.0006.

9. Dogra VS, Bhatt S, Rubens DJ. Sonographic evaluation of testicular torsion. Ultrasound Clin 2006;1:55-66. doi: 10.1016/j.cult.2005.09.006.

10. Dogra VS, Gottlieb RH, Oka M, Rubens DJ. Sonography of the scrotum. Ra diology 2003;227:18-36. doi: 10.1148/radiol.2271001744.

11. Doherty, FJ. Ultrasound of the nonacute scrotum. Semin Ultrasound CT MR 1991;12:131-56.

12. Healy JC. Spermatic cords and scrotum. In: Standring S, editor. Gray's anatomy: the anatomical basis of clinical practice. 39th ed. Edinburgh: Chur chill Livingstone; 2005. p.1313-4.

13. Bhaskar MV, Pramod JS. Pictorial essay of high resolution and colour doppler sonography of scrotal pathologies. The Internet Journal of Radiology [Internet] 2009[cited 2020 Jan 2];12(2):[about 15 p.]. Avalable from: https:// print.ispub.com/api/0/ispub-article/13505.

14. Castleberg E, Jenson N, Dinh VA. Diagnosis of necrotizing faciitis with bed side ultrasound: the STAFF exam. West J Emerg Med 2014;15:111-3. doi: 10.5811/westjem.2013.8.18303.

15. Mandava A, Rao RP, Kumar DA, Naga Prasad IS. Imaging in emphysematous epididymo-orchitis: a rare cause of acute scrotum. Indian J Radiol Imaging 2014;24:306-9. doi: 10.4103/0971-3026.137067.

16. Muttarak M, Lojanapiwat B. The painful scrotum: an ultrasonographical ap proach to diagnosis. Singapore Med J 2005;46:352-7; quiz 358.

17. Lobianco R, Regine R, De Siero M, Catalano O, Caiazzo C, Ragozzino A. Contrast-enhanced sonography in blunt scrotal trauma(). J Ultrasound 2011;14:188-95. doi: 10.1016/j.jus.2011.09.003.

18. Deurdulian C, Mittelstaedt CA, Chong WK, Fielding JR. US of acute scrotal trauma: optimal technique, imaging findings, and management. Radiographics 2007;27:357-69. doi: 10.1148/rg.272065117.

19. Coursey Moreno C, Small WC, Camacho JC, Master V, Kokabi N, Lewis M, et al. Testicular tumors: what radiologists need to know--differential diagnosis, staging, and management. Radiographics 2015;35:400-15. doi: 10.1148/rg.352140097.

20. Bhatt S, Rubens DJ, Dogra VS. Sonography of benign intrascrotal lesions. Ultrasound Q 2006;22:121-36. doi: 10.1097/00013644-200606000-00025. side ultrasound: the STAFF exam. West J Emerg Med 2014;15:111-3. doi: 10.5811/westjem.2013.8.18303.

ASEAN Movement in Radiology

Summary of discussions and brainstorming session on imaging guidelines and recommendations on Thailand's COVID-19 situation

By experts in chest medicine and chest imaging

Chayanin Nitiwarangkul, M.D.[(1)]
Nitra Piyavisetpat, M.D.[(2)]
From [(1)]Department of Diagnostic and Therapeutic Radiology, Faculty of Medicine, Ramathibodi Hospital, Mahidol University, Bangkok, Thailand.
[(2)]Department of Radiology, King Chulalongkorn Memorial Hospital, Chulalongkorn University, Bangkok, Thailand.
Address correspondence to C.N. (e-mail: chayanin.ntw@gmail.com)

Keywords: Coronavirus 2 (SARS-CoV-2), COVID-19, Computed tomography (CT).

On Monday 25 May 2020, during the time of Severe Acute Respiratory Syndrome Coronavirus 2 (SARS-CoV-2) or the Coronavirus disease 2019 (COVID-19) pandemic, we arranged a panel discussion via Microsoft Teams online meeting among several experts in the field of respiratory system, including a pulmonologist who leads the Thoracic Society of Thailand, 8 thoracic radiologists responsible for the radiological workflow management of COVID-19 in university hospitals from several parts of the country, World Health Organization (WHO)-Thailand officers, and a representative from Siemens Healthineers, Thailand. We discussed three frequently-asked questions/topics as followed:

Topic 1: The current situation and guidelines on the use of chest computed tomography (CT) for COVID-19 in Thailand.

All experts unanimously agreed that a chest CT should not be used for screening in cases in which COVID-19 infection or COVID-19 pneumonia is suspected, due to the fact that the outbreak incidence in Thailand was not widespread yet. There were only around 50 patients per million people, and the abnormalities of COVID-19 pneumonia found by CT did not have specific characteristics, and were similar to those that could be found in other viral pneumonia and other diseases. Nevertheless, a chest CT might be used to aid diagnosis and treatment in the following cases:

- RT-PCR test shows a negative result but clinical symptoms raise suspicion for COVID-19.
- In COVID-19 cases already confirmed by RT-PCR testing, CT may be considered to acquire baseline images, and serve as a guide for management and follow-up.
- The patient has moderate to severe pneumonia and the physician determines that a chest CT is useful in treatment planning.
- There is suspicion of complications such as pulmonary embolism.

Topic 2: What are the standard preventive measures in Thailand's hospitals in general for a chest CT examination in COVID-19 patients and during epidemic situations?

Preventive measures should utilize the universal precaution principles so as to prevent new outbreaks. This included preparation for incidences of new diseases that may occur in the future. The Royal College of Radiologists in collaboration with the Society of Radiological Technologists will jointly create the guideline, for hospitals to apply according to their particular locations and different limitations, including considering the use of a mobile capsule (if applicable), especially if the hospital has only one CT scanner.

Topic 3: What are the appropriate recommendations for a chest CT in case of suspected COVID-19 infection or suspected COVID-19 pneumonia? Can a CT screening protocol (low dose) be used?

The meeting consensus recommended that CT examination for suspected COVID-19 infection or suspected COVID-19 pneumonia be done using thin-slice images (≤1.5 mm) and with a diagnostic image quality*.

The consensus did not recommend the use of a low dose chest CT or a CT screening protocol because some lesions such as ground-glass opacity, a common finding in this disease, may not be invisible.

Note *Diagnostic image quality may not expose each patient to the same radiation dose, depending on the size of the patient, examination techniques, and capabilities of the CT machine.

Additional recommendations:

The expert panel unanimously agreed that in the future, there should be changes in the CT examination process, to accommodate the prolonged COVID-19 epidemic situation. This could be another "new normal". The examples of such changes may include: mandatory wearing of a surgical mask for every patient and employee, regular cleaning of the CT machine, touchpoints, and examination rooms, etc.

Supplemental detail and document:

- Publication can be accessed here along with web annexes:
  https://www.who.int/publications/i/item/use-of-chest-imaging-in-covid-19
  - Web Annex A. Imaging for COVID-19: a rapid review
  - Web Annex B. GRADE evidence-to-decision tables

Acknowledgement: Nitipatana Chierakul, M.D., Wiwatana Tanomkiat, M.D., Thitiporn Suwatanapongched, M.D., Juntima Euathrongchit, M.D., Yutthaphan Wannasopha, M.D., Phakpoom Thiravit, M.D., Thanisa Tongbai, M.D., Deyer Gopinath, M.D., Mark Simmerman, and Philipp Wolber.

ASEAN

This journal provide 4 areas of editorial services: language editing, statistical editing, content editing, and complete reference-citation check in 8 steps:

Step	Services to authors	Services providers
I	Manuscript submitted	Editor
II	Language editing/ A reference-citation check	Language consultant/Bibliographer
III	First revision to ensure that all information remains correct after language editing	Editor
IV	Statistical editing	Statistical consultant
V	Content editing*	Two reviewers
VI	Second revision	Editor
VII	Manuscript accepted/ rejected	Editor/Editorial board
VIII	Manuscript published	Editorial office

*Content editing follows a double-blind reviewing procedure

JOURNAL OF RADIOLOGY